Structural and molecular determinants of prion pathogenesis

DISSERTATION

Zur

Erlangung der naturwissenschaftlichen Doktorwürde

(Dr. sc. Nat.)

vorgelegt der

Mathematisch-naturwissenschaftlichen Fakultät

der

Universität Zürich

von

Tiziana Sonati

Aus

Italien

Promotionskommitee

Prof. Dr. med. Dr. sc. Adriano Aguzzi

Prof. Dr. Lawrence Rajendran

Prof. Dr. Christian Münz

Zürich, 2013

TABLE OF CONTENTS

SUMMARY **6**

ZUSAMMENFASSUNG **9**

ABBREVIATIONS **12**

CHAPTER I **16**

INTRODUCTION TO PRION DISEASES **16**

Prion diseases **16**

Prion diseases in humans 17

Prion diseases in animals 19

Prion conversion 20

Prion pathogenesis 21

The cellular prion protein PrP^C **22**

The physiological function of PrP^C 22

PrP^C structure 22

PrP post-translational modifications and their significance 24

CHAPTER II **26**

ANTI-PRP ANTIBODY-MEDIATED NEURONAL DEATH **26**

Introduction **27**

A novel in vitro model to investigate prion pathogenesis 27

Safety of PrP immunization therapies 27

Outline of this work **29**

Results **30**

Anti-PrP antibodies are neurotoxic in a PrP-dependent manner 30
Anti-PrP antibody toxicity is time-, dose-, and gene dosage-dependent 33
Neuronal loss is neither Fc receptor- nor crosslinking-mediated 36
Neuronal expression of PrP^C is necessary and sufficient for PrP antibody-induced neurotoxicity 40
Microglia depletion neither ameliorates nor worsens POM1 toxicity 42

Discussion and outlook 44

CHAPTER III 45

STRUCTURAL DETERMINANTS OF PRION-MEDIATED NEURONAL DEATH 45

Introduction 46
Functional domains of the prion protein 46

Outline of this work 49

Results 50
Antibody toxicity is epitope-specific 50
Differential toxicity relates poorly with affinity binding 53
Antibody toxicity is not mediated by a conformational change: X-ray and NMR analyses 56
Engineering new molecules: light chain and heavy chain, cyclic peptides 59
Peptide 106-126 does not exacerbate POM1 toxicity 60
The N-terminus is the effector domain of toxicity 61
Copper involvement in antibody-mediated toxicity remains unclear 69

Discussion and outlook 72
The FT as a neurotoxic transducer moiety? 72
Differential toxicity of antibodies 74

CHAPTER IV 75

SIGNALLING PATHWAYS INVOLVED IN PRION-MEDIATED NEURONAL DEATH 75

INTRODUCTION 76

PrP in cellular signaling ... 76
Caspase involvement in prion pathology ... 77
Emerging role of calpains in neurodegenerative disorders ... 78

OUTLINE OF THIS WORK ... 79

RESULTS ... 80
Ultrastructural analyses of antibody-treated COCS ... 80
Calpains and not caspases are the main effectors of GD ligand-mediated cell death as in prion infections ... 81
Pharmacological screening did not identify the source of prion-induced Ca^{+2} influx ... 85
Superoxide species play a major role in prion-mediated neurodegeneration ... 87
ERK is activated upon POM1 treatment ... 90
Other cellular targets investigated ... 93

DISCUSSION AND OUTLOOK ... 97
Molecular players of PrP-mediated neuronal death: ... 97
ROS play a pivotal role in PrP-dependent neuronal loss ... 97
Calpain as effectors of prion-mediated neuronal death ... 97
The Contribution of Autophagy remains to be elucidated ... 98
MAPK signalling molecules as mediators of cell death ... 99
Signaling cascade remains to be uncovered ... 99

CONCLUDING REMARKS ... 101

CHAPTER V ... 103

MATERIAL AND METHODS ... 103
Mice ... 104
Chemicals ... 104
Newborn injections ... 104
Organotypic cerebellar culture preparation ... 104
Low calcium medium experiments ... 105
Antibody treatment of COCS ... 105
Pharmacological treatment of COCS ... 106
Protein analysis ... 107
Immunocytochemistry ... 108
Proteolytic assays ... 108

Electron microscopy 109
Viability and ROS assays 109
Statistical analysis of COCS 109
$F(ab)_1$POM1 and $F(ab)_2$POM1 generation 110
$F(ab)_1$POM fragments generation 110
Periplasmic expression and purification of scFvPOM1 and scFvPOM2 110
Expression and purification of scFvPOM1, VH and VL from inclusion bodies 111
Periplasmic expression and purification of $rmPrP_{23-230}$ and $rmPrP_{90-230}$: 112
Peptides 1, 2 and 3 112
SPR measurements and binding affinity determination 113
BIAcore measurements in solution 113
Protein expression 114
NMR experiments 114
Data collection and structure determination 114
Illustrations 116
Scrapie cell assay in endpoint format (SCEPA) 116

REFERENCES 117

ACKNOWLEDGEMENTS 142

CURRICULUM VITAE 144

SUMMARY

The cellular prion protein (PrP^C) is an extracellular and glycosylphosphatidyl-inositol (GPI)-linked protein that is ubiquitously expressed, and is highly abundant in the nervous system. It is highly conserved among species, and consists of two domains, an N-terminal flexible tail (FT) and a C-terminal globular domain (GD).

Widespread deposition of an aggregated misfolded isoform of PrP^C, denoted as PrP^{Sc}, is a distinctive hallmark of fatal infectious prion diseases and is accompanied by dramatic neuronal loss. Whereas it is well established that PrP^C is required for PrP^{Sc}-mediated toxicity in prion infections (Brandner et al., 1996; Bueler et al., 1993), suggesting a crucial interaction between PrP^{Sc} and PrP^C, the mechanisms by which aggregated prions are lethal to neurons remain a mystery.

Progress in understanding molecular mechanisms leading to neuronal death has been hampered by the lack of *in vitro* models representative of the disease since prion-infected cell lines replicate prions, but do not show signs of toxicity. Remarkably, prion-infected cerebellar organotypic cultured slices (COCS), which were recently established in or laboratory, represent the first *in vitro* model recapitulating all of the main characteristics of prion diseases such as prion replication, astrogliosis, neuronal cell loss, inflammation, and spongiform changes (Falsig and Aguzzi, 2008; Falsig et al., 2008; Falsig et al., 2012). Organotypic slice culture-based assays offer numerous advantages, as they are versatile, easy to manipulate with drugs and antibodies, and display an intact morphology for several months; hence, they became a fundamental tool to explore prion pathogenesis in our research.

The work presented in this thesis focuses on elucidating the mechanisms that trigger neuronal loss upon anti-PrP antibody binding to PrP and their similarities to genuine prion infections.

Chapter I of this thesis presents a broader introduction to prion diseases.

Chapter II presents our studies performed in COCS demonstrating that select antibodies against PrP^C trigger dramatic neuronal death in a very short timeframe and this approach will be referred to as the “antibody model”. Antibody-mediated neuronal death was not Fc receptor-mediated or induced by PrP-crosslinking, as divalent $F(ab)_2$-, monovalent $F(ab)_1$-, and single chain (scFv)- fragments of select anti-PrP antibodies were also neurotoxic (Sonati et al., 2013), which was in contrast to previous claims (Solforosi et al., 2004). As in genuine

prion infections, we demonstrated that anti-PrP antibody-mediated neuronal death was gene dosage-dependent and occurred via neuronal PrP^C (Falsig et al., 2012; Fischer et al., 1996; Mallucci et al., 2003; Sonati et al., 2013).

Chapter III reports structural determinants of prion-mediated neurotoxicity uncovered *via* the antibody model. After treatment of COCS with a large panel of well characterized antibodies recognizing diverse epitopes of PrP^C (POM monoclonals (Polymenidou et al., 2008), we were astonished to notice that antibody-mediated toxicity was dependent on binding to distinct regions of PrP^C. Anti-PrP antibodies were divided into different classes of binders based on their biological effects. Among antibodies recognizing the FT, those binding to the octapeptide repeats were innocuous, whereas those binding to the charged cluster 2 (in closer proximity to the GD) induced toxicity only at high concentrations (Sonati et al., 2013). Among antibodies recognizing the GD, those specifically targeting the α1-α3 helices induced dramatic neuronal loss, whereas other GD antibodies were non-toxic. Interestingly, differential toxicity correlated strongly with specific binding sites and very poorly with binding affinity (Sonati et al., 2013).

X-ray crystallography and NMR analyses were employed to identify a potential PrP toxic conformer induced by binding of a toxic antibody to PrP^C. Surprisingly, crystallographic analyses of a toxic GD ligand bound to a recombinant prion protein did not reveal significant conformational distortions of the prion structure, whereas NMR analyses showed subtle shifts in the β1-β2 sheets of the GD (Sonati et al., 2013). The physiological implications of such changes are the subjects of current investigations.

We demonstrated that GD antibody-mediated toxicity is exerted through the engagement of the FT, as no toxicity was observed in mice expressing a shortened variant of the FT (Sonati et al., 2013). Moreover, we showed that blockade of the FT *via* FT ligands was beneficial in three models of prion toxicity, namely the antibody model, prion infection, and a toxic deletion mutant of PrP ((Baumann et al., 2007), lacking a region at the interface between the FT and the GD) (Sonati et al., 2013), designating the FT as the PrP effector module of neuronal death.

Chapter IV reports our recent findings on signalling pathways activated upon prion-infection and antibody-treatment. We identified calpains, which are calcium activated proteases, as molecular effectors of prion toxicity, suggesting that abnormal levels of calcium are upstream events of this cascade (Falsig et al., 2012; Sonati et al., 2013). Moreover, we found that radical oxygen species (ROS) are causal to prion-mediated neuronal death and that among the ROS species, superoxides are the major contributors (Sonati et al., 2013).

The establishment of the antibody model enabled important discoveries and offered great advantages by eliminating the need to work with infectious prions and by shortening the timeframes of neurotoxicity progression. This will open new avenues for the development of novel therapeutics in prion diseases.

ZUSAMMENFASSUNG

Das zelluläre Prion-Protein (PrP^C) ist ein extrazellulär vorhandenes und Glycosylphosphatidyl-inositol (GPI)-verankertes Protein, welches ubiquitär exprimiert wird und zuhauf im Zentralen Nervensystem anzutreffen ist. Es ist innerhalb verschiedener Spezies hochgradig konserviert und besteht aus zwei Domänen, einem N-terminalen flexiblen Bereich (*flexible tail*, FT) und einer C-terminalen globulären Domäne (*globular domain*, GD).

Grossflächige Ablagerungen einer aggregierten und fehlgefalteten Isoform von PrP^C, PrP^{Sc} genannt, sind das charakteristische Merkmal von fatal endenden, infektiösen Prionenerkrankungen, welche zudem von dramatischem Nervenzellverlusten begleitet werden. Obwohl es als eine etablierte Tatsache gilt, dass PrP^C für PrP^{Sc}-mediierte Toxizität in Prioneninfektionen benötigt wird (Brandner et al., 1996; Bueler et al., 1993) und demzufolge eine wichtige Interaktion zwischen PrP^{Sc} und PrP^C suggeriert, bleiben die Mechanismen, wodurch Prionenaggregate zum Nervenzelltod führen, ungeklärt. -

Fortschritte zum Verständnis der molekularer Mechanismen, die zum Nervenzelltod führen, waren lange erschwert, da geeignete *in vitro* Modelle für diese Erkrankungen fehlten. In Prion-infizierten Zellkukturmodellen, die bisher verwendet wurde, wurde zwar eine Prionenreplikation beobachtet, Zeichen von Toxizität konnten jedoch nicht beobachtet werden. Interessanterweise repräsentieren prion-infizierte organtypische kultivierte Kleinhirnscheiben (cerebellar organotypic cultured slices [COCS]), die vor Kurzem in unserem Labor etabliert wurden, das erste in vitro Modell, in welchem sich die Hauptcharakteristika von Prionenerkrankungen – Astrogliose, Nervenzellverlust, Entzündung und spongiforme Veränderungen - untersuchen lassen (Falsig and Aguzzi, 2008; Falsig et al., 2008; Falsig et al., 2012). Assays basierend auf COCS zeigen zahlreiche Vorteile durch ihre Praktikabilität, sie sind einfach mit Antikörpern oder anderen Medikamenten zu behandeln und lassen über mehrere Monate eine stabile Morphologie erkennen, wodurch sie zu einem fundamentalen Hilfsmittel zur Untersuchung von prioneninduzierter Pathogenese geworden sind.

Die Ausführungen in dieser Arbeit konzentrieren sich auf die Untersuchung der Mechanismen des durch anti-PrP-Antikörper hervorgerufenen Nervenzellverlusts und deren Ähnlichkeiten mit echten Prioneninfektionen.

Das erste Kapitel dieser Arbeit soll eine breite Einführung in Prionenerkrankungen geben.

Das zweite Kapitel beschreibt unsere Untersuchungen in COCS, die zeigen, dass ausgewählte Antikörper gegen PrP^C einen dramatischen Nervenzelltod innerhalb eines sehr kurzen Zeitrahmens verursachen, dieser Vorgang wird forthin als das „Antikörper-Modell“ bezeichnet. Der Antikörper-mediierte Nervenzelltod wurde weder durch Fc-Rezeptoren noch durch PrP-Vernetzung ausgelöst, da auch divalente $F(ab)_2$-, monovalente $F(ab)_1$-, und Einzelkettenfragmente (single chain, scFv) neurotoxisch wirkten (Sonati et al., 2013), im Gegensatz zu vorangegangenen Untersuchungen . Ebenso wie in echten Prioninfektionen haben wir gezeigt, dass anti-PrP-Antikörper-mediierter Nervenzelltod Gendosis-abhängig war und von neuronalem PrP^C abhing (Falsig et al., 2012; Fischer et al., 1996; Mallucci et al., 2003; Sonati et al., 2013).

Das dritte Kapitel berichtet basierend auf dem Antikörper-Modell über strukturelle Faktoren, die zu Prionen-mediierter Neurotoxizität führten, . Nach der Behandlung von COCS mit einem breiten Spektrum gut charakterisierter Antikörper gegen verschiedene Epitope von PrP^C – die monoklonalen Antikörper, POMs (Polymenidou et al., 2008) – waren wir überrascht zu sehen, dass die Antikörper-mediierte Toxizität von der Bindung an verschiedene PrP^C-Regionen abhängig war. Anti-PrP^C-Antikörper wurden gemäss ihrer biologischen Effekte in verschiedene Klassen eingeteilt. Unter denjenigen, die an den FT banden, waren die „Oktarepeatpeptid“-bindenden Antikörper unschädlich, wohingegen die an den „charged cluster 2“ (nahe der GD)–bindenden Antikörper nur in sehr hohen Konzentrationen toxisch wirkten (Sonati et al., 2013). Bei den GD-bindenden Antikörpern zeigten besonders die Antikörper, die spezifisch an Helices α1 und α3 binden, einen dramatischen Nervenzellverlust, während die anderen GD-bindenden Antikörper keine Toxizität zeigten (Sonati et al., 2013).

Röntgenkristallstruktur- und Kernresonanzspektroskopische (NMR) -Analysen wurden angewandt, um die Entstehung eines möglichen, toxischen PrP-Konformers durch die Bindung eines toxischen PrP^C-Antikörpers zu erkennen. Überraschenderweise zeigten die kristallographischen Analysen des toxischen GD-Liganden gebunden an rekombinantes Prion-Protein keine signifikanten Konformationsänderungen in der Struktur des Prion-Proteins, wohingegen NMR Analysen minime Verschiebungen in dem β_1-β_2-Faltblatt der GD aufwiesen. Die physiologischen Auswirkungen dieser Veränderungen sind im Moment Gegenstand weiterer Untersuchungen.

Das Kapitel IV präsentiert unsere kürzlichen Daten betreffend Prioninfektion- und Antikörper induzierte Signalkaskaden. Wir haben Calpaine, durch Calcium aktivierte Proteasen, als molekulare Auslöser der Priontoxizität identifiziert, was höher in der Signalkaskade

gelegene, abnormale Calciumspiegel suggeriert (Falsig et al., 2012; Sonati et al., 2013). Zudem konnten wir reaktive Sauerstoffspezies (reactive oxygen species, ROS) als ursächlich für Prion-mediierten Nervenzelltod nachweisen und innerhalb der ROS-Familie Superoxide als hauptsächliche Verursacher (Sonati et al., 2013).

Die Etablierung des Antikörper-Modells ermöglichte wichtige neue Entdeckungen und erschloss grosse Vorteile durch den Wegfall der Arbeit mit infektiösen Prionen sowie durch die Verkürzung der Progressionszeit des Nervenzelltodes. Dies wird neue Wege für die Entwicklung neuartiger Therapien bei Prionenkrankheiten eröffnen.

ABBREVIATIONS

AA	amino acid
Bax	Bcl-2–associated X protein
Bcl-2	B-cell lymphoma 2
BSA	bovine serum albumin
BSE	bovine spongiform encephalopathy
cAMP	cyclic adenosine monophosphate
CC1	positively charged cluster 1 of PrP^C (residues 23-27)
CC2	positively charged cluster 2 of PrP^C (residues 94-110)
CD	central domain (of PrP^C)
CDP	chronic demyelinating polyneuropathy
CDR	complementarity determining region
CGC	cerebellar granular cell
CGL	cerebellar granular layer
COCS	cerebellar organotypic cultured slices
CJD	Creutzfeldt-Jakob disease
fCJD	familial Creutzfeldt-Jakob disease
sCJD	sporadic Creutzfeldt-Jakob disease
vCJD	variant Creutzfeldt-Jakob disease
CNS	central nervous system
CWD	chronic wasting disease
DAPI	4,6-diamidino-2-phenylindole
DNA	deoxyribonucleic acid
dpe	days post-exposure
dpi	days post-inoculation
ELISA	enzyme-linked immunoassay
EM	electron microscopy
ER	endoplasmic reticulum
ERK	extracellular-signal-regulated kinase
$F(ab)_1$	monovalent fragment antigen binding
$F(ab)_2$	divalent fragment antigen binding

Fc	fragment crystallizable region
FFI	familial fatal insomnia
FRET	Förster resonance energy transfer
Fyn	proto-oncogene tyrosine-protein kinase
FT	N-proximal flexible tail of PrP^C (residues 23-124)
GAPDH	glyceralaldehyde 3-phospate deghydogenase
GD	globular domain of PrP^C (residues 124-230)
GFAP	glial acidic fibrillary protein
GPI	glycosylphosphatidyl-inositol
GSS	Gerstmann-Sträussler-Scheinker disease
HC	hydrophobic core of PrP^C (residues 112-133)
HE	hematoxylin and eosin
HRP	horseradish peroxidase
i.c.	intracerebral
i.p.	intraperitoneal
IP3	inositol 1,4,5-trisphosphate receptor
i.v.	intravenous
JNK	c-Jun N-terminal kinase
kD	kilo Dalton
LPS	lipopolysaccharide
LTP	long term potentiation
MAPK	mitogen-activated protein kinase
MBP	myelin basic protein
NBH	non-infected brain homogenate
NCAM	neuronal cell adhesion molecule
NMDA	N-methyl D-aspartate receptor
NMR	nuclear magnetic resonance
NOX2	NADPH oxidase 2
NSE	neuron specific enolase
OR	octapeptide repeats of PrP^C (residues 50-90)
PARP	poly (ADP-ribose) polymerase
PBS	phosphate-buffered saline
PI	propidium iodide
PK	protease K

PKA	protein kinase A
PKC	protein kinase C
POMs	set of 19 anti-PrP monoclonal antibodies (Polymenidou 2008)
POSCA	prion organotypic slice culture assay
PPS	pentosan polysulfate sodium
Prnp	murine PrP^{C} gene locus
PRNP	human PrP^{C} gene
***Prnp*$^{o/o}$**	*Prnp* knock-out mouse
PrP	prion protein
PrP^{C}	cellular prion protein
PrP^{Sc}	scrapie-associated prion protein
$PrP_{\Delta 32-134}$	truncated PrP version (lacking residues 32-134)
$PrP_{\Delta 105-125}$	truncated PrP version (lacking residues 105-125) also known as HC mutant
$PrP_{\Delta 94-110}$	truncated PrP version (lacking residues 94-110, CC2)
$PrP_{\Delta 94-134}$	truncated PrP version (lacking residues 94-134, CD)
$PrP_{\Delta 32-80}$	truncated PrP version (lacking residues 32-80)
PrP_{32-93}	truncated PrP version (lacking residues 32-93)
PrP_{32-106}	truncated PrP version (lacking residues 32-106)
PrP_{23-88}	truncated PrP version (lacking residues 23-88)
PrP_{32-121}	truncated PrP version (lacking residues 32-121)
rmPrP_{23-230}	full length recombinant mouse PrP (residues 23-230)
rmPrP_{90-230},	full length recombinant mouse PrP (residues 90-230)
rm$PrP_{120-230}$	full length recombinant mouse PrP (residues 120-230)
ROS	radical oxygen species
rt	room temperature
SCEPA	scrapie cell assay in end point format
ScFv	single chain variable fragment
SD	standard deviation
SDS-PAGE	sodium dodecyl sulfate polyacrylamide gel electrophoresis
SP	signal peptide
SK	small conductance calcium-activated potassium channel
SPR	surface plasmon resonance
Sti1	stress-inducible protein 1
tga20	mice overexpressing PrP^{C}

VH	variable heavy chain
VL	variable light chain
wt	wildtype mouse
TSEs	transmissible spongiform encephalopathies

CHAPTER I
INTRODUCTİON TO PRİON DİSEASES

PRION DISEASES

Prions diseases are fatal and infectious neurodegenerative disorders affecting humans and a wide variety of animal (Aguzzi and Calella, 2009). They are also called transmissible spongiform encephalopaties (TSE) because of their transmissible nature and the characteristic widespread vacuolization in the brain that is classically seen in sick individuals (Aguzzi and Calella, 2009). Prion diseases of humans include Creutzfeldt-Jakob disease (CJD), kuru, fatal familial insomnia (FFI), and Gerstmann-Sträussler-Scheinker syndrome (GSS); in animals, they include scrapie in sheep, bovine spongiform encephalopathy (BSE) in cattle, and chronic wasting disease (CWD) in cervids (Aguzzi et al., 2008).

The disease is provoked by "a **pro**teinaceous **in**fectious particle", termed prion by Prusiner, who purified and isolated it (Bolton et al., 1982; Prusiner, 1982). The discovery that the infectious agent is devoid of nucleic acids and is not a virus was first suggested by Griffith, but only accepted with the systematic work conducted by Prusiner (Griffith, 1967; Prusiner, 1982). This was mainly supported by the experimental evidence that prions are resistant to different enzymatic, chemical and physical procedures employed to destroy nucleic acids, but are sensitive to treatments that denature proteins (Alper et al., 1967; Alper et al., 1966; Griffith, 1967; Prusiner, 1982). The infectious prion was then sequenced and from this, the DNA sequence was determined to be the gene encoding for the endogenously expressed prion protein (Basler et al., 1986; Oesch et al., 1985). The most accepted hypothesis suggests that prions consist of misfolded infectious proteins which propagate, and act as a template for the conversion of the normal cellular form, PrP^{c}, into misfolded prions, PrP^{Sc} (Prusiner et al., 1998).

The histological signature of prion diseases is characterized by neuronal loss, vacuolization, astrogliosis, and PrP^{Sc} aggregate deposits, while clinical symptoms include both cognitive and motor dysfunction (Figure 1.1). PrP^{c} can be distinguished from PrP^{Sc} because of different biochemical fingerprints: whereas PrP^{c} is rich in α-helices, soluble, and sensitive to proteinase K (PK) digestion, PrP^{Sc} is enriched in β-sheet content and is therefore prone to aggregation, insoluble even in mild detergents, and partially resistant to PK (Aguzzi and Calella, 2009).

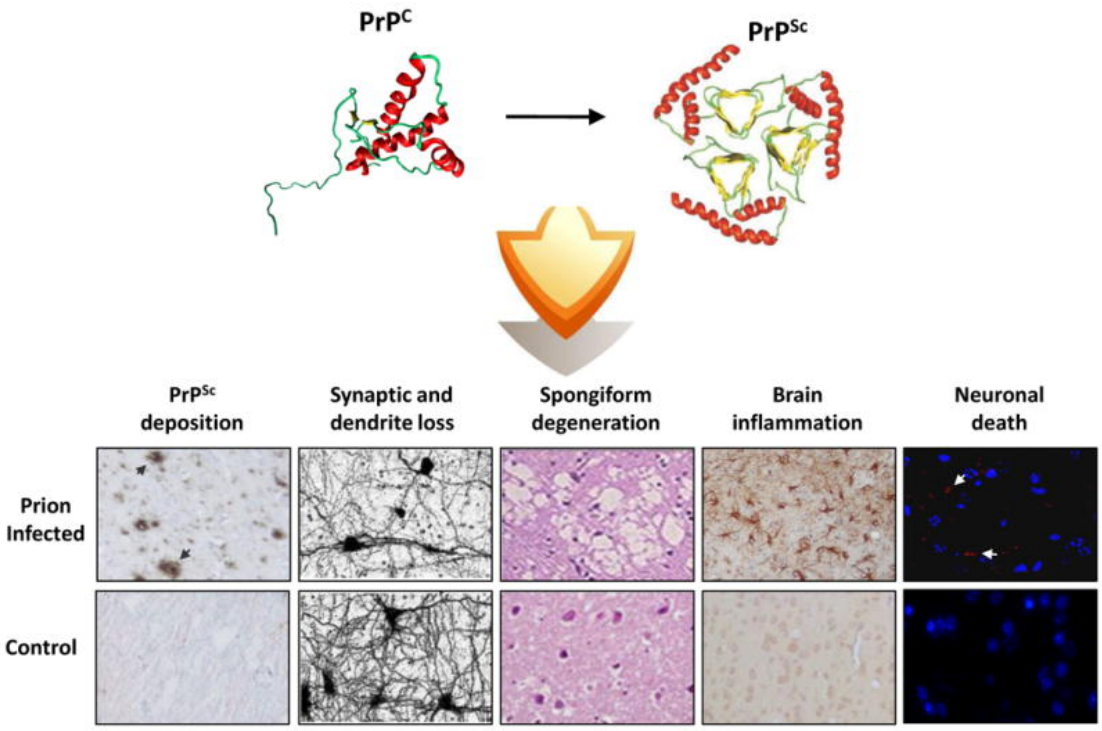

Figure 1.1. ***Illustration of main histopathological hallmarks of prion diseases.*** *PrP^{Sc} is an abnormal aggregated conformer of PrP^{C}. Prion diseases are characterized by PrP^{Sc} deposits (immunodetection by anti-PrP antibodies), synaptic and dendritic loss (visualized by silver staining), spongiform staining (H&E staining), brain inflammation (astrogliosis shown by anti-GFAP staining), neuronal death (caspase-3 staining) as respectively presented in the figure. Adapted from Soto and Satani 2010 Trends Mol Med* (Soto and Satani, 2010).

Prion diseases have been described to have many similarities with other misfolded protein disorders (such as Alzheimer's, Huntington's and Parkinson's diseases), but have the unique feature of transmissibility (Aguzzi and Haass, 2003; DeArmond, 1993); however, this concept is evolving and prion-like transmissibility has recently been introduced for other amyloidosis diseases as well (Sponarova et al., 2008; Westermark and Westermark, 2010).

PRION DISEASES IN HUMANS

Several conditions can be identified among different prion diseases in humans: Creutzfeldt-Jakob disease (CJD), kuru, Gerstmann-Sträussler-Scheinker syndrome (GSS), fatal familial insomnia (FFI), and sporadic fatal familial insomnia. The main symptoms are rapid cognitive decline, progressive dementia, and frequently, ataxia. Unfortunately, once the first clinical signs occur, death follows very rapidly (Aguzzi et al., 2008). They are all influenced by the

polymorphism at codon 129 of the *PRNP* gene (Aguzzi et al., 2008) and can be classified into inherited, sporadic and acquired forms.

Hereditary or genetic prion diseases represent 10-20% of TSEs in humans and include fCJD, GSS, and FFI (Aguzzi and Calella, 2009). fCJD is transmitted with an autosomal dominant-inheritance with diverse clinicopathological features, depending on the polymorphism at codon 129 (Aguzzi et al., 2008). The disease is caused by point mutations located in helix 2 and 3 of the GD of PrP and in some cases, also includes insertions in the octapeptide repeats (OR) of PrP (Aguzzi et al., 2008).

Another autosomal dominantly-inherited TSE is GSS, which was first described as a disease affecting an Austrian family in 1928 and 1936 (Hainfellner et al., 1995). Fifty years later, GSS was experimentally transmitted to primates, resulting in spongiform encephalopathy (Masters et al., 1981). In contrast to CJD, GSS showed an earlier age of onset, a longer duration of disease, and cerebellar ataxia. Mutations causing GSS include not only mutations in helix 2 and 3, and OR insertions, but also mutations in the central domain (CD) of PrP (Aguzzi et al., 2008; Hsiao et al., 1989; Hsiao and Prusiner, 1991; Hsiao et al., 1991). Neuropathological analyses show widespread and large multicentric amyloid plaques (Collins et al., 2001).

Fatal familial insomnia (FFI) was initially described in an Italian family in 1986, who were affected by insomnia and dysautonomia (Lugaresi et al., 1986). FFI was classified as a TSE when FFI was transmitted to mice (Tateishi et al., 1995). Since the thalamus is the main brain region affected, clinical signs typical of FFI are dysregulation of the sleep-wake cycle, sympathetic system, and endocrine system, and attention deficits (Collins et al., 2001). It is influenced by the D178N point mutation of the *PRNP* gene together with methionine at codon 129 (Gambetti et al., 1995; Medori et al., 1992).

Acquired conditions may occur after exposure to infectious material as seen in variant CJD (vCJD), kuru, and iatrogenic CJD. A risk factor for manifestation of sporadic or acquired CJD is represented by homozygosity at the polymorphic codon 129 of the *PRNP* gene encoding either methionine or valine (Collinge et al., 1991; Palmer et al., 1991). Scientists suspect that the appearance of vCJD is likely caused by eating BSE-contaminated beef from cattle, killing around 200 individuals worldwide (http://www.cjd.ed.ac.uk/). It differs from sCJD with younger patients, a longer duration of disease, as well as exhibiting a characteristic histological pattern with florid spherical plaques surrounded by a loose distribution of vacuoles (Budka et al., 1995).

Kuru is another form of prion diseases caused by dietary infections, and was first described in the mid-1950s in Papua New Guinea among the aboriginals who practiced ritualistic cannibalism (in particular eating the brain of other humans) (Gajdusek and Zigas, 1957). The disease propagated when contaminated brains were consumed, but once this cannibalism ended, kuru seemed to be eradicated in these populations.

Acquired CJD can also be caused by accidental transmission, hence termed iatrogenic CJD, due to infected surgical tools or transplantations with infected tissues (Duffy et al., 1974; Will, 2003).

The most common TSE in humans is sporadic CJD (sCJD, of unknown cause), which occurs in both men and women with an incidence of one to three cases per million people worldwide annually (Aguzzi et al., 2008). It accounts for almost 85% of human TSE cases, with a peak age of 55-60 years (Aguzzi and Calella, 2009). The term sporadic is used when no genetic or infectious cause has been identified (Aguzzi et al., 2008).

A sporadic form of FFI (sFFI) has also been documented, but not coupled to any mutation of the *PRNP* gene (Mastrianni et al., 1999; Parchi et al., 1999).

Interestingly all inherited disorders appear early in life, possibly due to the presence of an abnormal PrP throughout development and postnatal life. In contrast, sporadic prion disease may occur because of a stochastic event.

PRION DISEASES IN ANIMALS

Scrapie, which naturally occurs in sheep and goats, was initially recognized in 1737 and the name was given because those animals scraped off parts of their skin that were itchy (Lampert et al., 1972). Immunization of sheep with a vaccine derived from scrapie-affected tissue led to more than 1500 sheeps contaminated with scrapie, (Gordon, 1946) confirming its transmissibility among animals.

A recent epidemic affecting cattle, commonly known as “mad cow disease” and medically termed bovine spongiform encephalopathy (BSE), gave rise to a new variant of CJD (vCJD) in humans. The first case of BSE was reported in the early 1980s (Wells et al., 1987) and in the following years until 2007, approximately two-hundred thousand cows were affected (http://www.oie.int/). It seems that the main route of transmission was the feed with which cows were fed that contained meat and bones of infected animals, therefore causing this dramatic contamination among cattle. The animals manifested with uncoordinated movements, behavioural changes, weight loss, difficulties in walking and standing, and

decreases in milk production. From the appearance of the first clinical signs to death, a maximum of six months could be estimated.

Chronic wasting disease (CWD) in deer and elk was first reported in 1960 in Colorado and spread across the US and Canada (Sigurdson and Aguzzi, 2007). CWD is believed to be transmitted among cervids with high efficiency, but transmission to other species has not been successful (Sigurdson, 2008).

PRION CONVERSION

The prion-only hypothesis proposes that the host-encoded PrP^{C} is required for the disease (Prusiner, 1982). Prion diseases are associated with PrP^{Sc} aggregates; however, no differences in amino acid sequence were identified between PrP^{Sc} and PrP^{C}, suggesting that PrP^{Sc} is a different conformer from PrP^{C} (Stahl et al., 1993).

Two mechanisms were formulated to explain the "protein-only-hypothesis": "the template-directed refolding model" and the "seeding or nucleation model" (Weissmann, 1991b, 1999). The first model proposes that upon interaction with PrP^{Sc}, PrP^{C} undergoes a conformational change leading to new formation of PrP^{Sc} (irreversible reaction) (Weissmann, 1991b, 1999). Alternatively, according to the seeding model, PrP^{Sc} exists in equilibrium with PrP^{C} and such equilibrium is shifted towards PrP^{C}. Monomeric PrP^{Sc} would be harmless, and would acquire infectious properties when integrated into a seed or aggregate of PrP^{Sc} (Weissmann, 1991b, 1999).

The lack of high resolution structures of PrP^{Sc}, due to its high β-sheet content, insolubility and biosafety restrictions, has hampered a full understanding of the conversion event and after twenty years, the same hypotheses remain widely accepted. It is not clear which interfaces are involved in the PrP^{c}-PrP^{Sc} conformational conversion. Two domains (including residues 98-110 and 136-158) have been proposed to undergo a conformational change and are therefore part of the PrP^{Sc} core (Abalos et al., 2008).

Moreover prion aggregates manifest in different "strains" that probably reflect different conformations of PrP^{Sc} and are marked by different properties. Strains differ in incubation times, histological profiles, biochemical and immunological characteristics, organo-trophism and neuronal target cells (Aguzzi et al., 2007).

PRION PATHOGENESIS

Despite decades of intense research in prion diseases, molecular determinants leading to neuronal damage remain unclear. The lack of PrP^{C} is unlikely to be the cause because *prnp* knock-out (*prnp*$^{0/0}$) mice do no show major abnormalities or neuronal loss (Büeler et al., 1992).

Prnp$^{0/0}$ mice do not support prion replication, nor do they show clinical signs after prion inoculation (Bueler et al., 1993). Furthermore, prion infection after grafting PrP-overexpressing tissue onto *prnp*$^{0/0}$ brains resulted in PrP^{Sc} propagation, with pathological changes restricted to the grafted area (Brandner et al., 1996). Hence PrP^{Sc} might not be directly responsible for prion-dependent neuronal loss, whereas PrP^{C} seems necessary for prion replication and neurodegeneration. Transgenic mice expressing an anchorless form of PrP were still capable of PrP replication without signs of pathology (Chesebro et al., 2005), suggesting membrane-anchoring of PrP is necessary to induce pathology. Also, depletion of neuronal PrP reverses prion pathogenesis, including spongiform changes and clinical symptoms, even at 8 weeks post-inoculation despite glial accumulation of PrP^{Sc} (Mallucci et al., 2003). Moreover infectivity spreads rapidly, even in the presence of low amounts of PrP^{c}, whereas neurodegeneration is dependent on PrP^{c} expression levels and occurs at later stages of disease (Sandberg et al., 2011). These findings indicate that neurotoxicity is somehow transduced through the expression of cellular PrP^{C} on target cells and that neurotoxicity and prion propagation may be distinct and independent events.

Prion-mediated toxicity could be mediated by PrP forms other than PrP^{Sc}, such as a toxic intermediate denoted PrP*, a term introduced by Charles Weissmann (Weissmann, 1991a), offering an explanation for those cases when spongiform pathology is present with few PrP^{Sc} deposits (Aguzzi and Calella, 2009). The concept that oligomeric and even smaller units might be responsible for neurotoxicity has been recently discussed for many other neurodegenerative disorders that are accompanied by misfolded aggregates and indicates that larger aggregates might have a protective function (Ross and Poirier, 2005).

Furthermore it has been shown that the prion protein can adopt different topological forms: a translocated form (PrPsec), two transmembrane forms (PrP^{Ntm} and PrP^{Ctm}, with their N- or C-termini, respectively, on the extracellular side of the membrane) and a cytosolic form (PrP cyt). Both PrP^{ctm} and PrP^{Ntm} traverse the membrane through the hydrophobic region (112-130) and represent 10% of total amount. However in cases of mutations, such as those associated with the GSS syndrome (A117V and P105L), the percentage of PrP^{ctm} increases to 20-30% (Hegde et al., 1998) and has been associated with neurodegeneration.

Accumulation of cytosolic PrP^C caused by altered trafficking can also induce toxicity (Rane et al., 2008).

THE CELLULAR PRION PROTEIN PRP^C

THE PHYSIOLOGICAL FUNCTION OF PRP^C

PrP^c is a highly conserved, ubiquitously expressed protein that is found highly abundant in the central nervous system and, expressed by neurons and glial cells. Despite many efforts, the physiological role of PrP^c is still debated. Mice devoid of PrP do not show any severe phenotype and are viable. However, PrP-deficient mice are more susceptible to ischemic insults and (Rangel et al., 2007; Weise et al., 2006) importantly, they show a chronic demyelinating polyneuropathy (CDP) (Bremer et al., 2010). CDP manifests upon PrP ablation solely in neurons, but not if PrP is specifically ablated in Schwann cells, suggesting that neuronal PrP^c is crucially involved in peripheral nerve myelin maintenance (Bremer et al., 2010).

Many other functions have been proposed for PrP, such as modulation of cell signaling, maintenance of circadian rhythms and, neuronal development (Steele et al., 2006), however their significance has not been confirmed. Also one cannot exclude that PrP exerts diverse roles according to the cellular context, local environment and its interaction partners.

PRP^C STRUCTURE

The mature cellular prion protein is linked to the membrane via a glycosylphosphatidyl-inositol (GPI)-anchor, and includes amino acids 23-231. PrP^c consists of two moieties: the N-terminal flexible tail or FT (amino acids 23-125) and the C-terminal globular domain or GD (amino acids 126-231)(Riek et al., 1997)(Figure 1.1).

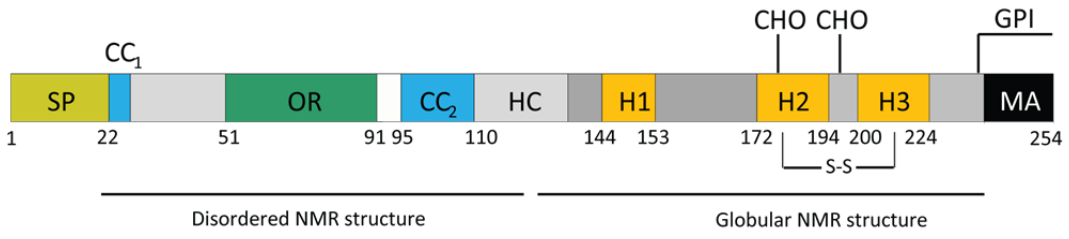

Figure 1.2. ***Illustration of main domains of the primary structure of the prion protein.*** *Signal: secretory signal at the N-terminal extremity. CC1 and CC2: charged clusters. OR four octapeptide repeats. HC: hydrophobic core. MA: membrane anchor. GPI: glycosyl phosphatidy-linositol anchor. S-S: disulphide bridge. CHO: glycosylation sites. Numbers indicate the amino acid positions. The FT has a disordered NMR structure, whereas the GD has a globular NMR structure.*

The GD consists of three alpha helices and two beta sheets (Hornemann et al., 1997; Riek et al., 1996). Specifically, the three helices encompass amino acids 144-154, 175-193, and 200-219, whereas the short antiparallel β-sheets comprise amino acids 128-131 and 161-164 (Figure 1.2) (Riek et al., 1996; Zahn et al., 2000). The region of the GD between the β-sheet and helix 2 (166-171aa) has a high degree of flexibility and its structure was only approximately determined. This flexible region of the GD has been of interest because first, it might have a functional role and second, minor structural differences between hamster, mouse, bovine and human species reside there (Lopez Garcia et al., 2000), which is in contrast to other regions of the GD that are highly conserved.

The FT includes 4 domains: five octapeptide repeats (OR) flanked by two charged clusters (CC1 and CC2), and the hydrophobic domain (HD). The OR and HD are highly conserved among species, which might reflect an important biological function (Aguzzi et al., 2008). Through biophysical analyses, Boland et al. have shown that the combination of the octapeptides and the CC1 are crucial for membrane interaction (Boland et al., 2010). The unstructured FT region of PrP has been given a broad spectrum of functions and it seems to be involved in both neurotoxicity and neuroprotection (Beland and Roucou, 2012). The OR encompasses residues 50-90 and has been shown to adopt a structure under certain conditions such as neutral pH and in the presence of copper (Hodak et al., 2009; Zahn, 2003). The presence of a disordered domain in the prion protein may be a switch for different functions by being involved in the interaction with partners or other prion proteins. Structural studies of PrP were performed by analyses of recombinant PrP that lack the GPI moiety and glycosyl groups. Therefore there are limitations to the structural information to date and one could speculate that the 3D structure of PrP^{c} *in vivo* may be different.

PrP POST-TRANSLATIONAL MODIFICATIONS AND THEIR SIGNIFICANCE

PrP is synthesized in the rough endoplasmaticum reticulum (ER), along with many membranes and secreted proteins. After translation, it consists of 253 amino acids, which undergo post-translational modifications such as removal of the signal peptide (1-22aa), addition of two glycosylation chains (highly branched glycosyl groups with sialic acid substitutions) at asparagine 181 and 197, formation of a disulphide bridge between cysteine 197 and cysteine 214, and attachment of a GPI anchor after replacement of a C-terminus peptide (Harris, 2003). PrP exists as unglycosylated, mono- and diglycosylated forms and interestingly, the ratio of these forms varies among strains (Collinge et al., 1996), suggesting a functional involvement of the glycosyl groups.

The GPI anchor is important for directing PrP^{c} to detergent-resistant microdomains (DRMs, lipid rafts), although it has been shown that the N-terminus can also perform this function (Baron and Caughey, 2003; Walmsley et al., 2003).

The role of PrP^{c} proteolysis is still debated, but it is known that PrP^{c} physiologically undergoes α-cleavage at residues 111/112, within the hydrophobic core (HC), generating the soluble N1 fragment and the membrane tethered C1 fragment, whereas analyses of brains affected by CJD show an additional cleavage at the peptide bond 90/91 with release of N2 and C2 fragments (Chen et al., 1995; Mange et al., 2004). The latter cleavage preserves the region 106-126 within the HC, a crucial domain involved in toxicity (Baumann et al., 2007; Li et al., 2007). One explanation for differential cleavage could be that the α-cleavage site is buried within PrP^{Sc} aggregates (Oliveira-Martins et al., 2010). A third type of cleavage occurs within the OR and it is induced by radical oxygen species (ROS) in the presence of copper (McMahon et al., 2001). It has been speculated that toxicity of certain PrP variants can be attributed to abnormal PrP proteolytic processing (Aguzzi et al., 2008; Shmerling et al., 1998).

The biological role of posttranslational modifications, such as glycosylation and cleavage, is still unknown; however, these modifications may lead to different isoforms whose expression and function may differ according to brain region, cell type and subcellular compartments (Schneider et al., 2011).

Aims of this thesis

Finally, prion diseases affect a large variety of animals and numerous forms have an impact on humans. It is well understood that pathogenesis requires PrP^{C}, and among the most intriguing question still poorly understood is how prions kill neurons. In an attempt to

elucidate such mechanisms and especially identify structural determinants and signalling pathways triggering neuronal death, we have employed different models. The aim of this study was to comprehend the pathology driven by anti-PrP antibodies bound to the prion protein and to correlate these findings to genuine prion infections in order to validate the relevance of the model in investigating prion pathology.

CHAPTER II

ANTİ-PRP ANTİBODY-MEDİATED NEURONAL DEATH

This chapter contains unpublished data as well as parts that are adapted or reproduced from the following manuscript accepted by Nature on the 21st of June 2013 and assigned the DOI 10.1038/nature12402:

The toxicity of antiprion antibodies is mediated by the flexible tail of the prion protein

Tiziana Sonati[1,*], Regina R. Reimann[1,*], Jeppe Falsig[1,*], Pravas Kumar Baral[2], Tracy O'Connor[1], Simone Hornemann[1], Sine Yaganoglu[1], Bei Li[1], Uli S. Herrmann[1], Barbara Wieland[2], Mridula Swayampakula[2], Muhammad Hafizur Rahman[3], Dipankar Das[3], Nat Kav[3], Roland Riek[4], Pawel P. Liberski[5], Michael N. G. James[2], and Adriano Aguzzi[1†]

[1] Institute of Neuropathology, University Hospital Zurich, Switzerland
[2] Department of Biochemistry, University of Alberta, Canada
[3] Department of Agricultural, Food and Nutritional Science, University of Alberta, Canada
[4]ETH Zurich, Physical Chemistry, ETH Honggerberg, 8093 Zurich, Switzerland
[5]Laboratory of Electron Microscopy and Neuropathology, Department of Molecular Pathology and Neuropathology, Medical University of Lodz, Lodz, Poland.
[*] These authors contributed equally to this work

[†]Corresponding author: Adriano Aguzzi; Institute of Neuropathology, University Hospital of Zurich; Schmelzbergstrasse 12, CH-8091 Zurich, Switzerland; Tel: +41-44-255-2108, Email address: adriano.aguzzi@usz.ch

INTRODUCTION

A NOVEL IN VITRO MODEL TO INVESTIGATE PRION PATHOGENESIS

Prion diseases are marked by dramatic neuronal loss; however, the molecular mechanisms leading to cell death are still unclear. One explanation could be the lack of good *in vitro* models, which have failed to reproduce prion infections since they replicate prions without toxicity (Klohn et al., 2003). A step forward was achieved in our laboratory with the work performed by Jeppe Falsig. He established the prion organotypic slice culture assay (POSCA), the first *in vitro* model recapitulating all the main characteristics of prion diseases such as prion replication, astrogliosis, neuronal cell loss, inflammation, and spongiform changes (Falsig and Aguzzi, 2008; Falsig et al., 2008). The first part of our recently published work consists of a detailed characterization of prion-infected cerebellar organotypic cultured slices (COCS). Of note, we successfully reproduced prion-dependent neuronal loss in an *in vitro* system (Falsig et al., 2012) and as previously shown by Mallucci et al. *in vivo*, ablation of PrP^{C} from neurons during prion infection reversed neuronal loss in prion-infected COCS (Falsig et al., 2012; Mallucci et al., 2002). We also confirmed that prion-mediated neurodegeneration is gene-dosage dependent, as COCS prepared from *wt* mice exposed to RML (the Rocky Mountain Laboratory, a mouse-adapted prion strain from scrapie) showed neuronal loss at 56 days post-inoculation (dpi), whereas COCS prepared from *tga20* mice (a line overexpressing PrP, (Fischer et al., 1996)) exhibited neurotoxicity at 42 dpi (Falsig et al., 2012). COCS prepared from *wt* and *tga20* mice challenged with mouse adapted-prion strains 22L, RML, and 139A exhibited strain-dependent PrP^{Sc} deposition and ultrastructurally, spongiform vacuoles (2-5µm), tubulovesicular structures, and dystrophic neurites were observed. A strong inflammatory response also occurred, as evidenced by the upregulation of cytokines such as TNFα, MCP-1, and Rantes in prion-infected *tga20* COCS (Falsig et al., 2012).

Thus, organotypic slice culture-based assays offer numerous advantages, as they are versatile and easy to manipulate with drugs and antibodies, and display an intact morphology for several months.

SAFETY OF PRP IMMUNIZATION THERAPIES

The therapeutic value of immunization therapies for prion diseases is still debated (Heppner et al., 2001; Klöhn et al., 2012; Lefebvre-Roque et al., 2007; Solforosi et al., 2004).

Encouraging results were obtained when expression of an anti-PrP antibody transgene in mice prevented prion pathogenesis (Heppner et al., 2001).

Moreover, prophylactic injections of very high concentrations of anti-PrP antibodies intraperitoneally (i.p) successfully suppressed lethality when prions where delivered i.p; however, the injections were inefficient when prions were delivered intracerebrally (i.c) (White et al., 2003). No increase in survival was observed when the treatment started at the clinical onset of disease, questioning if antibodies as a successful therapy could be pursued (White et al., 2003).

Also, only a few reports describe the toxic effects of such a therapy (Lefebvre-Roque et al., 2007; Solforosi et al., 2004). Solforosi et al. in 2005 raised the issue of the safety of two antibodies: D13, which binds to the region including residues 95-105, and D18, which binds to the region encompassing residues 133-157 (Solforosi et al., 2004). They reported widespread neuronal loss upon D13 antibody injection, but not D18. However, they did not observe any toxicity if monovalent FabD13 was injected, and toxicity was restored with an anti-Fab antibody. They concluded that antibody-induced crosslinking of PrP^C triggers cell death in a similar way to prions. Although they did not offer an explanation for this epitope-dependent toxicity, they proved that complement activation was not responsible for antibody-mediated neuronal death. Surprisingly, in a more recent report, Klöhn et al claimed that neither D13 and D18, nor their specific anti-PrP antibodies ICSM18 and ICSM35 (Klöhn et al., 2012) triggered neuronal death in the hippocampus. They followed the same protocol as Solforosi et al, but did not reproduce the antibody-mediated toxicity. Along with our own results, the reasons for such discrepancies can only be speculated upon and for convenience, will be presented in the discussion part of chapter III.

OUTLINE OF THIS WORK

The molecular mechanisms leading to neuronal death in prion diseases remain unclear. One hypothesis is that aggregation of PrP at the cell surface triggers cell death. Using a similar mechanism, Solforosi et al. speculated that antibody binding mediates PrP^C crosslinking at the surface and induces cell death (Solforosi et al., 2004). They reported that stereotactic injection of specific antibodies to the hippocampus or the cerebellum resulted in neurotoxicity in mice, whereas the injection of the corresponding Fab fragments did not; additionally, "re-dimerization" of Fab fragments using an anti-Fab antibody restored toxicity. We studied the latter using organotypic slice cultures, which I will describe in the results, and the *in vivo* data performed in collaboration with Regina Reimann will only briefly be mentioned. Our findings demonstrate that specific antibodies against PrP trigger dramatic neuronal death within 10 days and that toxicity is not Fc receptor-mediated or induced by PrP-crosslinking, as both monovalent $F(ab)_1$ and divalent $F(ab)_2$ -fragments of anti-PrP antibodies (both lacking the Fc part) are neurotoxic. Anti-PrP antibody-mediated neuronal death is restricted to the presence of neuronal PrP^C and is gene dosage-dependent, as in prion infections (Falsig et al., 2012; Fischer et al., 1996; Mallucci et al., 2003). Importantly, the degree of neurotoxicity can be modulated by the dose and duration of antibody treatment. Moreover, microglia that are neuroprotective in prion infections do not play a role in antibody-mediated toxicity. For convenience, I report in this chapter our studies conducted with POM1 (Polymenidou et al., 2008), a specific anti-PrP antibody found to mediate neuronal death upon PrP^C binding, and in chapter III, results obtained via a panel of anti-PrP antibodies targeting different epitopes of PrP will be described.

RESULTS

ANTI-PRP ANTIBODIES ARE NEUROTOXIC IN A PRP-DEPENDENT MANNER

After having successfully modelled all of the main hallmarks of prion diseases in organotypic cultured slices (Falsig et al., 2012), we decided to employ this *in vitro* system to study the neurotoxic effects of antibodies binding to PrP. COCS prepared from *tga20*, a PrP-overexpressing mouse line (Fischer et al., 1996), were cultured for 14 days prior to treatment to allow for the reduction of the glial scar observed after dissection. COCS were treated with POM1, a specific PrP antibody targeting the globular domain (Polymenidou et al., 2008), or with IgG, anti-mouse pooled immunoglobulins, as a negative control. POM1 and IgG were used at 67nM unless otherwise stated. Samples were fixed and stained with NeuN, a specific neuronal marker at 10-14 days post-exposure (dpe). Quantification of neuronal viability displayed dramatic neuronal loss in POM1-treated COCS, but not in IgG-treated controls (Fig 2.1a-b).

To ensure that POM1-mediated toxicity was mediated by PrP and not induced by any buffer contaminant or by unspecific binding, two control experiments were designed. If antibody binding to PrP was the trigger of neuronal death, POM1 treated COCS should remain healthy when co-incubated with the cognate antigen or upon PrP ablation. Therefore, in this new set of experiments, we included in the POM1-treated group 1) COCS from *tga20* mice co-incubated with full length recombinant mouse PrP ($rmPrP_{23-231}$, molar ratio 60:1) and 2) COCS prepared from $Prnp^{o/o}$ mice. Co-treatment with $rmPrP_{23-231}$ and ablation of the *Prnp* gene fully abrogated POM1-induced neurodegeneration (Fig 2.1c-d), confirming that neurotoxicity was a consequence of POM1 binding to PrP^{C}.

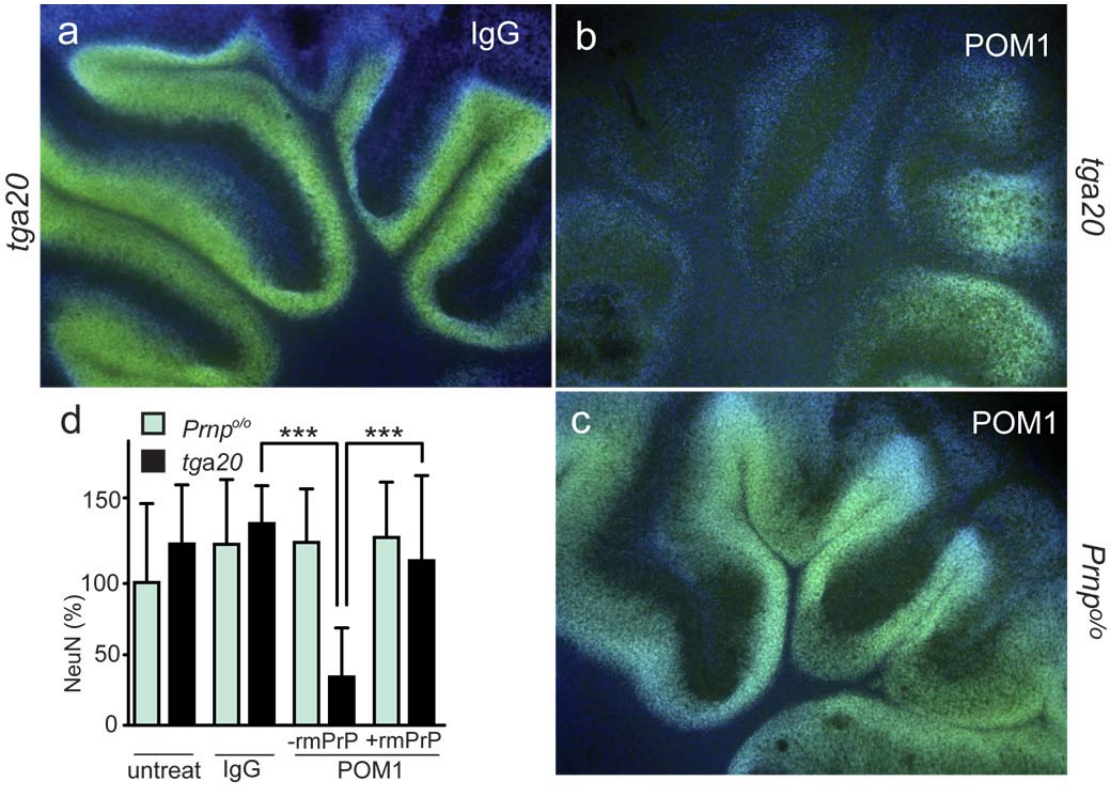

Figure 2.1. ***Dramatic neuronal loss upon POM1 treatment in tga20, but not in Prnp$^{o/o}$ COCS.*** ***a-c****) Representative pictures of tga20 and Prnp$^{o/o}$ slices exposed to IgG pooled control and POM1 for 10 days and stained with NeuN and DAPI. IgG treatment did not impact neuronal viability of tga20 and Prnp$^{o/o}$ COCS (a). POM1 was toxic in tga20 (b) and innocuous in Prnp$^{o/o}$ slices (c).* ***d****) Tga20 and Prnp$^{o/o}$ COCS were treated with IgG pooled control or POM1 in the presence or absence of rmPrP. Neuronal death was blocked by addition of rmPrP$_{23-231}$. Neuronal viability was assessed by staining with NeuN (granule neurons) and NeuN immunoreactivity was quantified by morphometric analysis (NeuN$^+$). NeuN quantification data, here and henceforth, are presented as percentage of the total tissue area and normalized to the average indicated as 100 (+/-s.d, n=9). Details about statistical analyses are reported in the Material and Methods section.*

COCS exposed to POM1 or IgG control (14 dpe) were orthogonally cut in thin sections and stained with hematoxylin and eosin (H&E), to determine the effect of POM1 treatment on tissue viability and thickness. Light microscopy revealed a dramatic thinning of the tissue and loss of a large portion of cerebellar granule cells (CGCs), whereas Purkinje cells that lack *tga20* transgene expression (Fischer et al., 1996) remained largely intact (Fig 2.2a). To obtain a qualitative picture of the effects of POM1 on other cell types, samples treated with IgG

and POM1 (14 dpe) were stained with NeuN, GFAP (marker for astrocytes), and CD68 (marker for microglia). Images taken by high resolution confocal microscopy showed only a few NeuN positive cells left upon POM1 treatment (Figure 2.2b); however, no decrease in glial cells was detected by GFAP and CD68 staining (Figure 2.2c). As expected, together with a dramatic neuronal loss, astrogliosis (proliferation of reactive astrocytes as demonstrated by an increased density of $GFAP^+$ cells) and microgliosis (increased density of $CD68^+$ cells) were observed (Figure 2.2b-c).

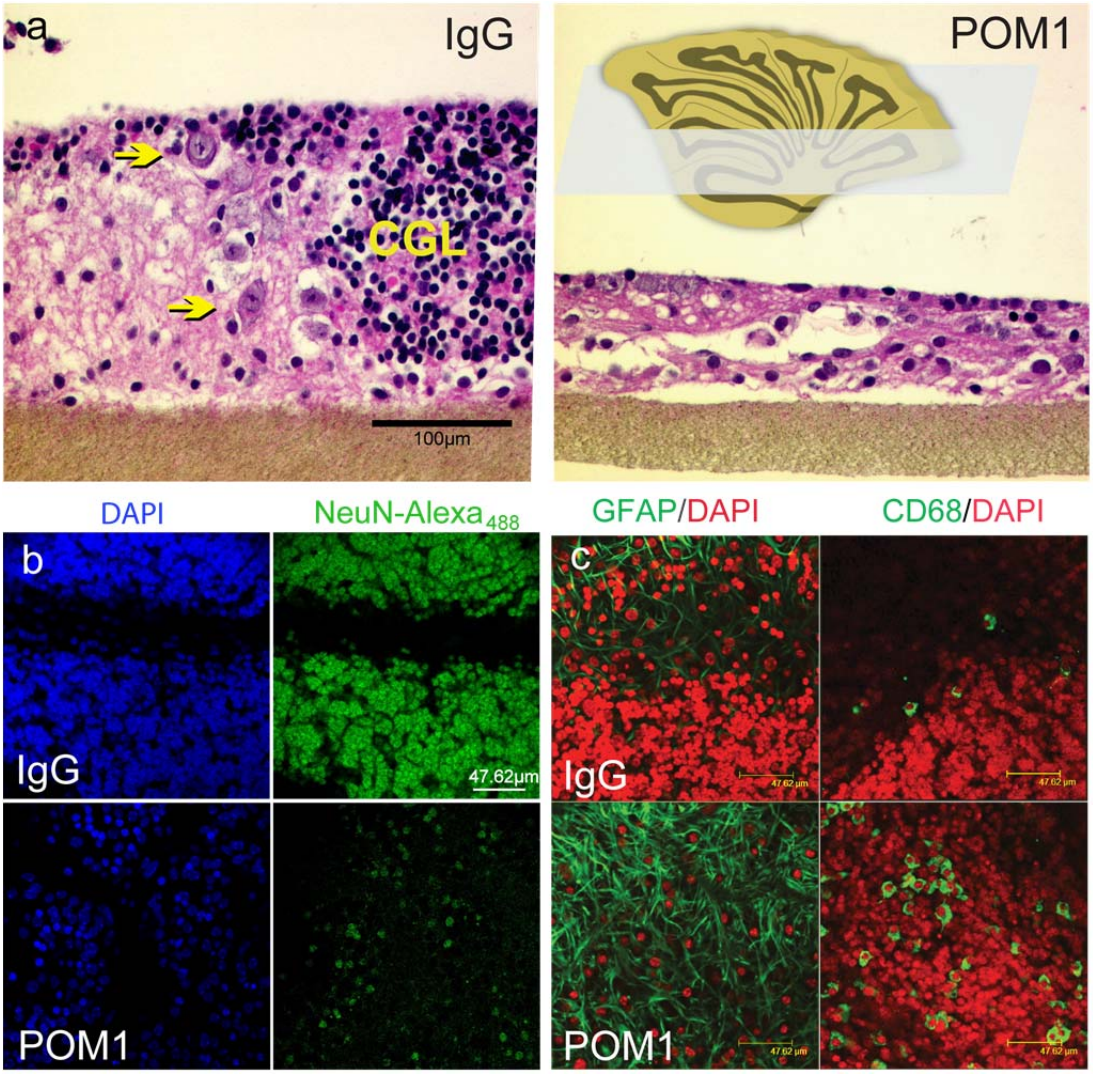

Figure 2.2. ***CGC loss, microgliosis, astrogliosis upon POM1 treatment in COCS. a****) Thin cross-sections (grey plane) of POM1 treated COCS were stained with hematoxylin/eosin, revealing conspicuous CGC loss and thinning of the tissue. CGL: cell granular layer. Yellow arrow indicates largely intact Purkinje cells, where no PrP transgene is expressed.* ***b-c****) Confocal laser scanning microscopy of COCS prepared from tga20 mice treated with IgG and POM1 for*

10 days and stained with DAPI and NeuN (b), GFAP/DAPI and CD68/DAPI(c).

ANTI-PRP ANTIBODY TOXICITY IS TIME-, DOSE-, AND GENE DOSAGE-DEPENDENT

We performed analyses with NeuN and propidium iodide (PI) at different time points, to quantify the effects of the duration of antibody treatment on neuronal cell viability. PI is a DNA-binding dye that is a marker of cell membrane integrity and is commonly used to stain damaged cells. It is membrane impermeable to viable cells, but when the cellular membrane is compromised, PI intercalates into the DNA, emitting a distinct red fluorescence. A time course of antibody-treated COCS analysed after PI incorporation was compared to quantifications of NeuN staining. PI^+ cells analyses showed that most of the damage occurred by day 3 and decreased thereafter (Figure 2.3a-b; red graph), whereas NeuN staining showed significant neuronal loss after 7 dpe (Figure 2.3a-b; blue graph). These results suggest an efficient removal of dead cells, as membrane integrity is compromised long before cell death and NeuN still stains cells undergoing cell death up until they are fully removed by microglia.

To determine whether chronic treatment is required for the dramatic neuronal loss observed, COCS were exposed to only one treatment, and the tissue was harvested at various time points (Figure 2.3c) and analysed by NeuN and PI staining. Consistently, single exposure treatment and chronic exposure highlighted that most of the damage occurred at 3 dpe, which is shown in both cases by a peak of PI-positive cells (dying cells, Figure 2.3a-d; red graphs). However, chronic treatment over 7 days with 67nM (standard concentration used for *tga20* COCS) was necessary to visualize a dramatic reduction in NeuN immunoreactive area (Figure 2.3b-c; blue graphs).

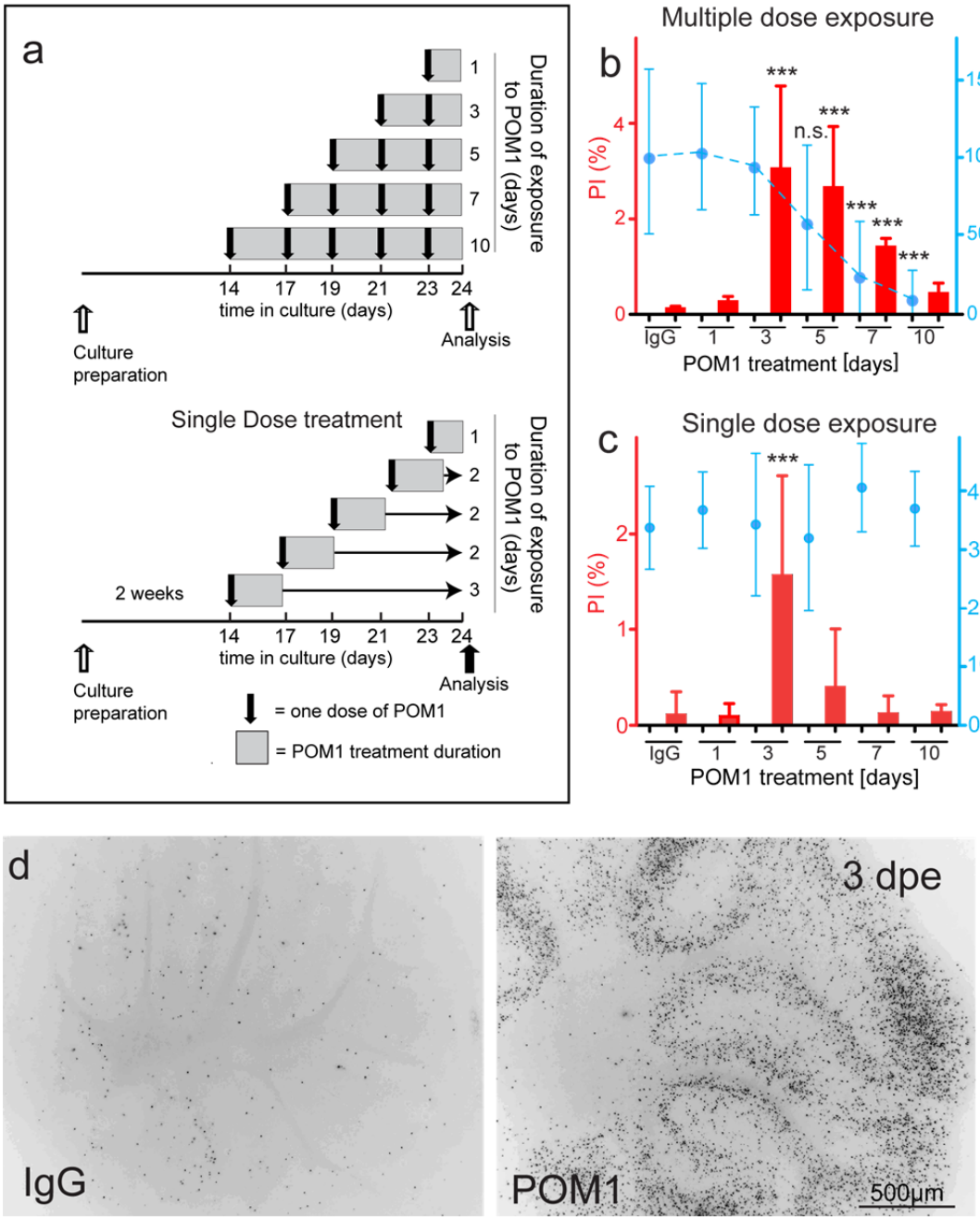

Figure 2.3. ***Time course and titration curves of antibody-treated tga20 COCS. a****) Treatment scheme for time course analysis. COCS were subjected to antibodies either continuously or only once, as illustrated.* ***b****) COCS were exposed to multiple doses of POM1 for 10 days and analysed by NeuN morphometry (blue) or PI (red). POM1 treatment showed a peak of PI^+ cells at 3 dpe, suggesting that most cell damage occurs at this time point. PI^+ cells decrease after 3 days, likely because dead cells are efficiently removed by microglia. A significant decrease in $NeuN^+$ cells was observed only at 7 dpe (blue).* ***c****) COCS were challenged with single doses of POM1 at different time intervals for 24-72h, transferred to antibody free-medium, analysed by NeuN staining (blue) and PI incorporation (red). Single treatment did*

not induce a significant CGC loss; however, a peak of PI$^+$ cells was still present at 3 days upon single exposure. ***d****) Representative images of PI$^+$ cells upon POM1 and IgG treatment. Pictures are negative representations of fluorescent images.*

We also performed TUNEL staining, which detects apoptotic fragmentation of DNA, and surprisingly, very few cells were TUNEL$^+$ upon POM1 treatment at day 3 compared to the staurosporine that was used as a positive control for cell death (Figure2.4a-b). No significant difference in TUNEL$^+$ cells was found between IgG- and POM1-treated *tga20* cultures at day 3 (Figure 2.4b), indicating that changes in membrane permeability were abundant at early stages, as shown by PI incorporation, whereas DNA fragmentation consequent to the apoptotic signaling cascade was hardly detectable at 3 dpe.

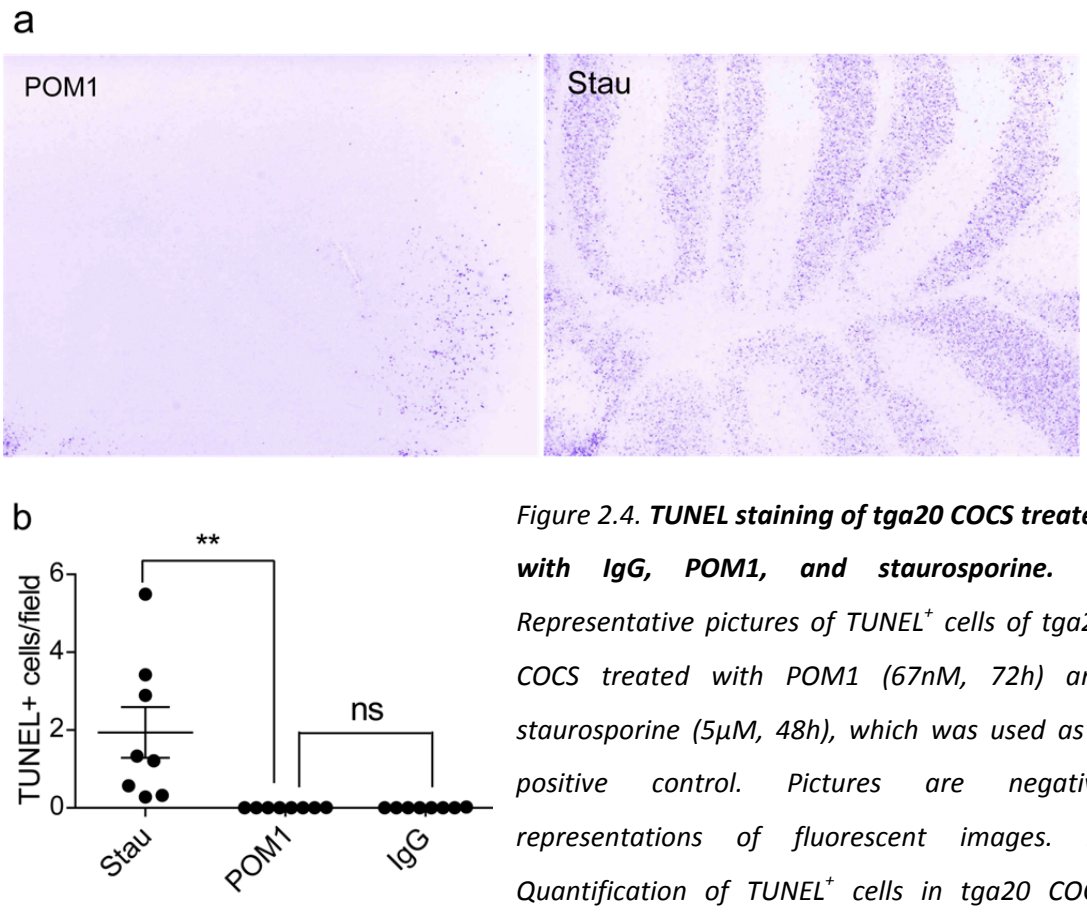

Figure 2.4. ***TUNEL staining of tga20 COCS treated with IgG, POM1, and staurosporine.*** ***a****) Representative pictures of TUNEL$^+$ cells of tga20 COCS treated with POM1 (67nM, 72h) and staurosporine (5µM, 48h), which was used as a positive control. Pictures are negative representations of fluorescent images.* ***b****) Quantification of TUNEL$^+$ cells in tga20 COCS treated with IgG, POM1, and staurosporine (conditions as in a). No significant difference between IgG and POM1.*

Antibody-mediated neurotoxicity could be clearly modulated by increasing the duration of treatment. Thus, we investigated which POM1 dose would induce significant neuronal loss at 14 dpe. Exposure to 20nM POM1, but not to lower doses, triggered significant neuronal loss in *tga20* COCS (Figure 2.5a).

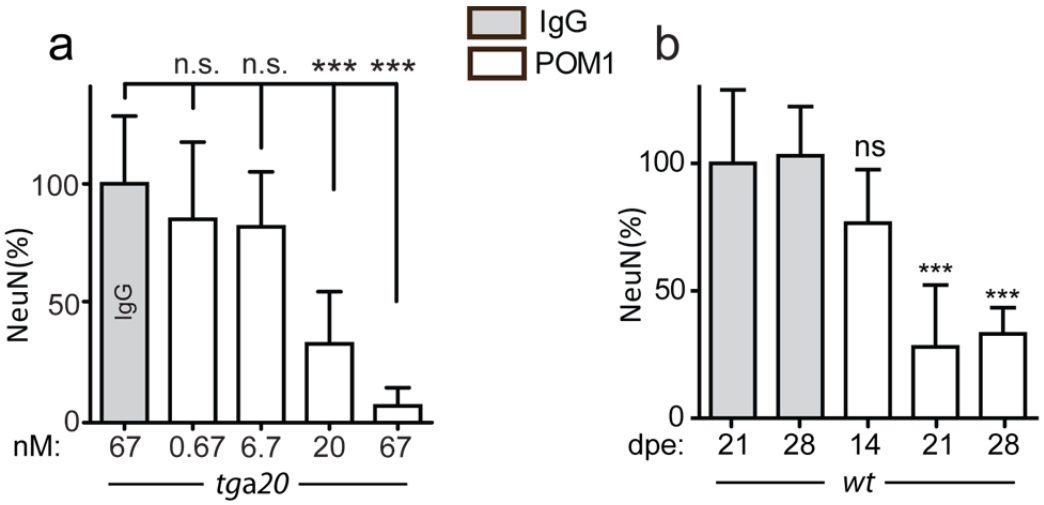

Figure 2.5. ***Antibody-mediated neuronal death is dependent on PrP expression levels. a)*** *Tga20 COCS were exposed to different concentrations of POM1 and stained at 10 dpe. POM1 treatment induced a significant decrease in NeuN-positive area at 20nM.* ***b)*** *Morphometric quantification of NeuN coverage in COCS prepared from wt mice treated with IgG and POM1 (270nM) at different time points. POM1 treatment induced significant neuronal loss at 21 dpe.*

Furthermore, we studied the course of toxicity in *wt* COCS, to confirm that toxicity was not an artefact of *tga20* transgenic mice. While *tga20* COCS showed almost 100% neuronal loss at 14 dpe (67nM, 10 µg/ml antibody, Figures 2.5a), *wt* COCS required a higher concentration of antibody (267nM, 40 µg/ml) and longer treatment times (up to 21 dpe) to display similar effects (Figure 2.5b). Hence, PrP antibody-induced toxicity is dependent on PrP gene dosage, duration, and dose of anti-PrP antibody, which is similar to genuine prion infections that are exacerbated by higher PrP expression levels and/or increased dose of inoculum (Fischer et al., 1996).

NEURONAL LOSS IS NEITHER FC RECEPTOR- NOR CROSSLINKING-MEDIATED

To investigate whether antibody-induced crosslinking of PrP^C triggers cell death in COCS as previously reported by Solforosi et al (Solforosi et al., 2004), we generated $F(ab)_1$ and $F(ab)_2$

fragments from POM1 antibody (Figure 2.6a). Divalent fragment $F(ab)_2$ should induce toxicity like the corresponding holo antibody, whereas monovalent $F(ab)_1$ fragments should be innocuous. Therefore, $F(ab)_1$ and $F(ab)_2$ were generated by enzymatic digestion of POM1, purified by size-exclusion chromatography (Figure 2.6b-c), and applied to COCS prepared from *tga20* and *Prnp*$^{o/o}$ mice. Surprisingly, both monovalent $F(ab)_1$ and divalent $F(ab')_2$ fragments (134 and 67 nM, respectively) induced toxicity in *tga20* COCS as holo antibody, and no signs of toxicity were present in the *Prnp*$^{o/o}$ COCS (Figure 2.6e). These results were in contrast with previous findings reported by Solforosi et al, calling into question the claim that toxicity is mediated by antibody-induced PrP crosslinking. In order to exclude a re-dimerization of the $F(ab)_1$ fragments in solution over time, in collaboration with Dr. Simone Hornemann, we performed size-exclusion chromatography of the $F(ab)_1$ preparation before and after carrying out toxicity studies in the COCS, confirming that no secondary aggregation occurred and that $F(ab)_1$ stayed monovalent (Figure 2.6d). As for the holo antibody, $F(ab)_1$POM1 toxicity was counteracted by addition of $rmPrP_{23\text{-}231}$ (1:2 molar ratio; Figure 2.6f).

As a further confirmation that binding the POM1 epitope is responsible for toxicity, in collaboration with Michael James' group, we engineered single-chain minibodies (scFv) containing POM1 complementarity determining regions (CDRs). Single chain minibodies are recombinant fusion proteins expressed by and purified from bacteria containing the variable regions (Fv) of the heavy and light chain of antibodies connected with a short linker (Figure 2.6a). ScFvPOM1 (264nM) was toxic in *tga20* and not in *Prnp*$^{o/o}$ COCS (Figure 3.6e), indicating that PrP-dependent neurotoxicity is a general property of ligands binding to the GD of PrP^c, and not a consequence of antibody-mediated PrP crosslinking.

Furthermore, Fab fragments and scFv minibodies lack the Fc portion, excluding engagement of effector molecules as a source of antibody-dependent cellular toxicity.

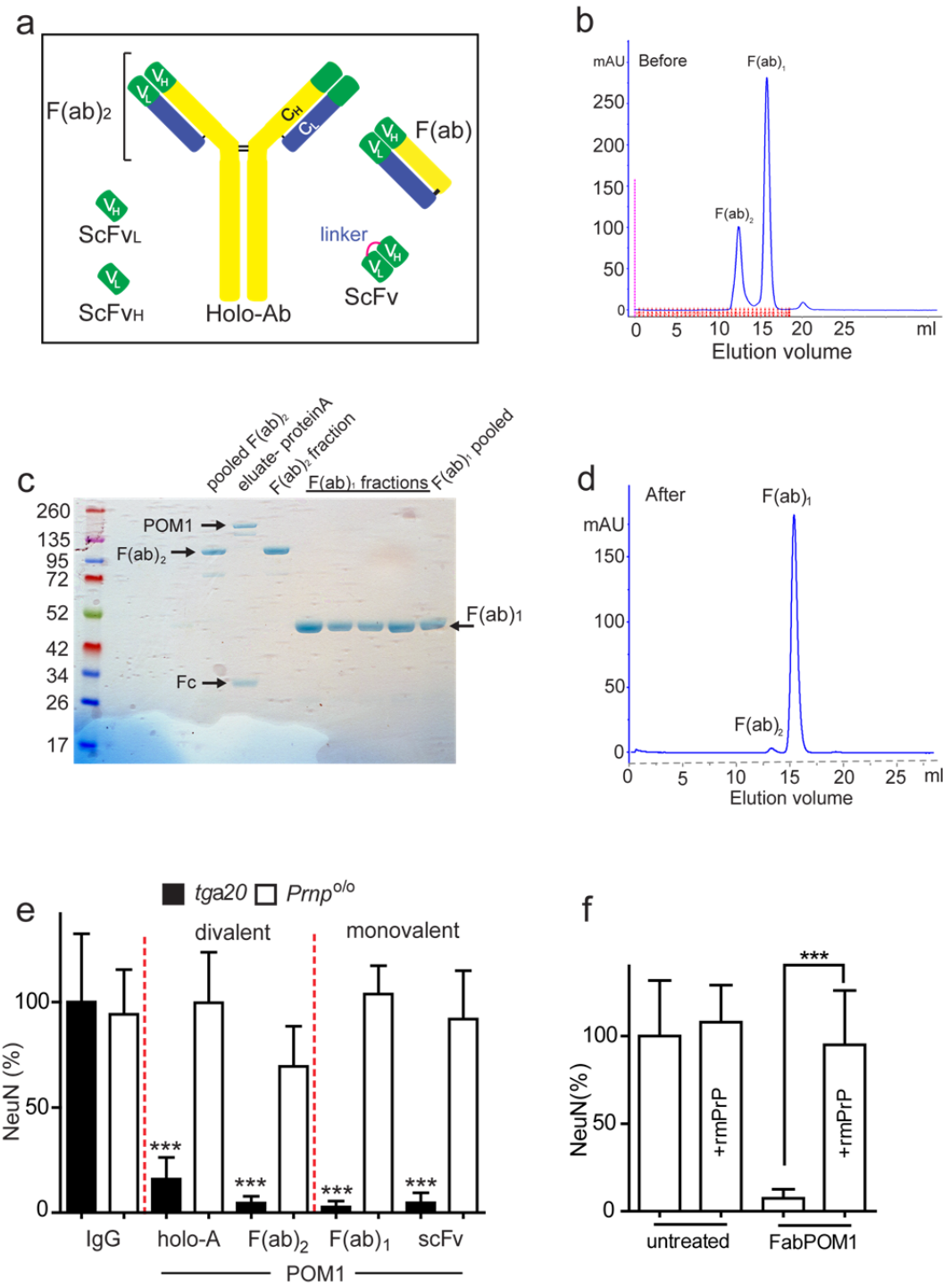

Figure 2.6. ***Preparation, toxicity, and quality controls for monovalent F(ab)$_1$ fragments****. **a)** Schematic representation of antibody derivatives, holoantibody, F(ab)$_1$, and F(ab)$_2$ fragments, and single-chain fragments (scFv, scF$_{VH}$ and scF$_{VL}$). F(ab)$_1$ and F(ab)$_2$ fragments were generated by enzymatic digestion and further purified. ScFv, scF$_{VH}$, and scF$_{VL}$ were engineered and expressed in bacteria to include the variable regions of the heavy chain and light chain. **b)** Elution profile of F(ab)$_1$ preparation after protein A column. **c)** Equal amounts*

of protein fractions from $F(ab)_1$ and $F(ab)_2$ collected after size exclusion chromatography were loaded on a Coomassie gel. Samples containing pure $F(ab)_1$ fragments were pooled and used for toxicity studies. ***d****) Size-exclusion chromatography of the pooled $F(ab)_1$ fragments of b) was performed again after finalizing toxicity studies on COCS. The elution profile of $F(ab)_1$ fragments confirms that dimerization/aggregation did not occur after time.* ***e****) Ten days of treatment with holoantibody, divalent $F(ab)_2$, monovalent $F(ab)_1$ or scFv fragments induced dramatic neuronal loss in tga20, but not in $Prnp^{o/o}$ COCS.* ***f****) Addition of $rmPrP_{23-231}$ rescued $F(ab)_1$POM1-induced toxicity, similar to holo antibody.*

Characterization of single chain minibodies-mediated toxicity

Time course and titration experiments were performed in *tga20* COCS in order to evaluate the experimental conditions for using scFvPOM1, which has a molecular weight 6 times lower than the holo antibody (25KDa and 150KDa respectively) and is expected to have a lower binding affinity. ScFvPOM1 treatment did not impact neuronal viability when used in equimolar amount to POM1 (64nM), but induced significant neurotoxicity at 264nM (Figure2.7a), showing a lower degree of toxicity compared to holo antibody. Next, *tga20* COCS were challenged with scFvPOM1 (264nM) at different time points, and NeuN analyses revealed a significant neuronal loss at 3dpe (Figure 2.7b). Since the recombinant single chains were generated in bacteria, we were concerned with the potential contamination with lipopolysaccharide (LPS), a major component of bacterial membranes. To confirm that residual LPS was not the cause of ScFvPOM1-induced neurotoxicity, scFvPOM1 was pre-incubated with $rmPrP_{23-231}$ (1: 1.4 molar ratio) (Figure 2.7c). ScFvPOM1-induced toxicity was abolished in the presence of $rmPrP_{23-231}$, confirming that the observed effect was a true consequence of antigen binding and not buffer contamination.

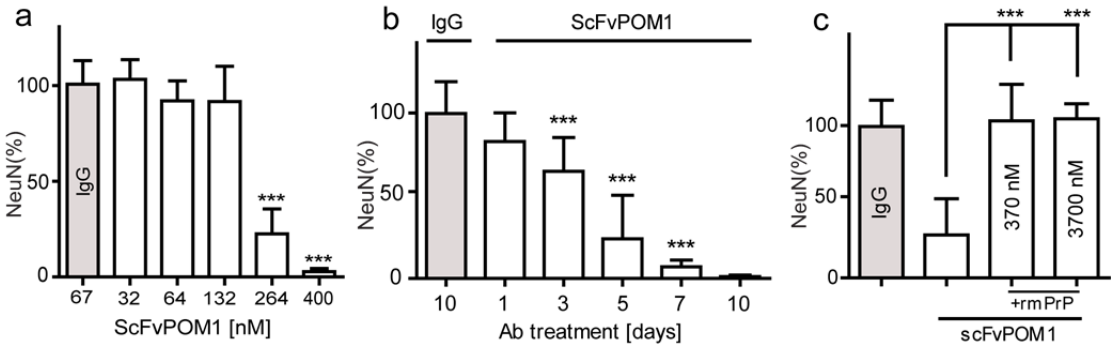

Figure 2.7. ***ScFvPOM1 induces toxicity in tga20 COCS. a****) Titration curve of ScFvPOM1*

treatment at 7 dpe. ScFvPOM1 was significantly toxic at 264nM, but not below 132nM. ***b****) Timecourse of COCS treated with 264nM scFvPOM1 revealed significant toxicity at 3 dpe. (****c****) Treatment with 400nM ScFvPOM1 for 7days in the presence or absence of rmPrP (370nM or 3700nM).*

NEURONAL EXPRESSION OF PRP^C IS NECESSARY AND SUFFICIENT FOR PRP ANTIBODY-INDUCED NEUROTOXICITY

Neuronal expression of PrP^c is required for prion pathogenesis to occur (Mallucci et al., 2003; Mallucci et al., 2002). To identify the cell types mediating POM1 toxicity, a diverse set of genetic tools was employed. First, we used two transgenic mouse lines: NSE-PrP that expresses full-length PrP^c solely in neurons under the control of the neuron-specific enolase (NSE) promoter (Radovanovic et al., 2005), and MBP-PrP that expresses PrP^c solely in oligodendrocytes under the control of the myelin basic protein (MBP) promoter (Prinz et al., 2004). Cerebella from NSE-PrP and MBP-PrP mice showed PrP^c expression levels comparable to *wt* mice (Figure 2.8a); therefore, COCS prepared from these mice were treated with 267nM POM1 (or IgG as a negative control) for 21 days. POM1 treatment elicited toxicity in NSE-PrP COCS to a similar degree as *wt* slices, but was innocuous to MBP-PrP COCS, demonstrating that neuronal PrP expression was necessary and sufficient for POM1-mediated toxicity (Figure 2.8b).

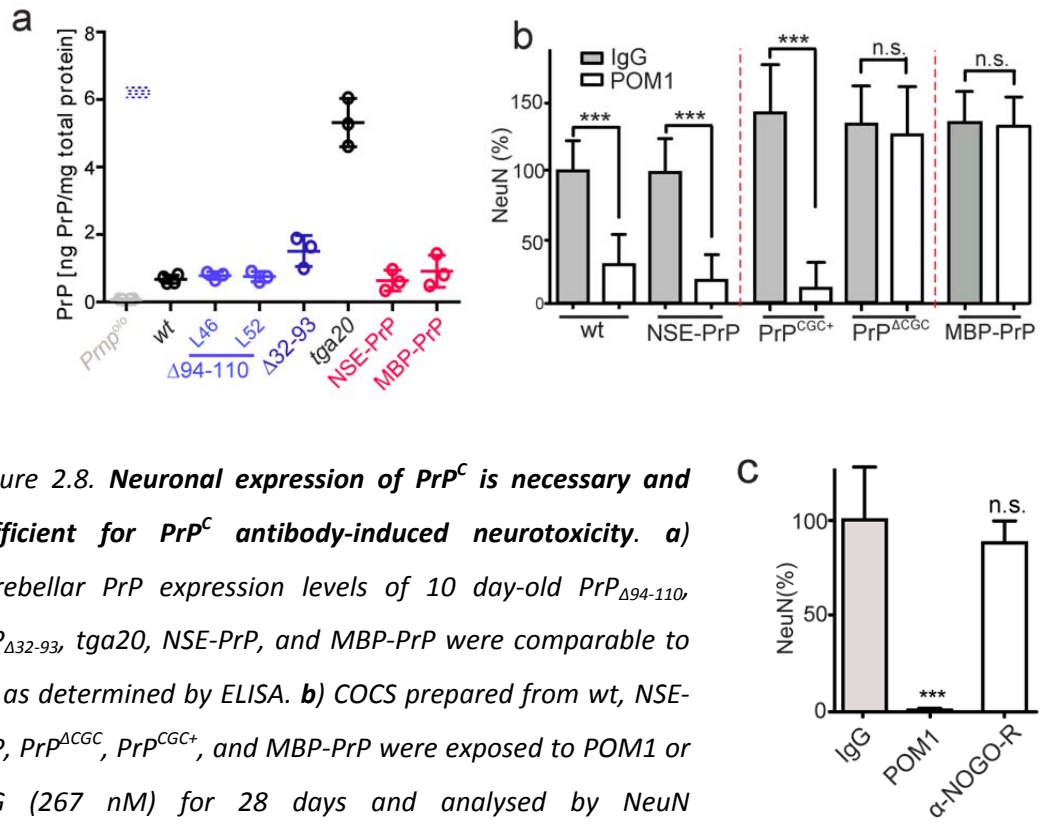

Figure 2.8. ***Neuronal expression of PrP^C is necessary and sufficient for PrP^C antibody-induced neurotoxicity***. ***a****) Cerebellar PrP expression levels of 10 day-old PrP$_{\Delta 94\text{-}110}$, PrP$_{\Delta 32\text{-}93}$, tga20, NSE-PrP, and MBP-PrP were comparable to wt as determined by ELISA.* ***b****) COCS prepared from wt, NSE-PrP, PrP$^{\Delta CGC}$, PrP^{CGC+}, and MBP-PrP were exposed to POM1 or IgG (267 nM) for 28 days and analysed by NeuN morphometry. Prnp depletion from CGCs suppressed POM1 toxicity.* ***c****) Tga20 COCS were treated with IgG, POM1, and an antibody against NOGO-R (67nM). POM1, but not anti-NOGO antibody, induced toxicity, suggesting that neuronal loss was not a general consequence of antibody binding to GPI-anchored proteins.*

To confirm the requirement of neuronal PrP^c expression for POM1-mediated neurotoxicity, we used a complementary genetic approach to see if POM1 toxicity was rescued by specific depletion of neuronal PrP^c. We availed of the Cre-loxP system to achieve neuronal-PrP^c ablation by crossing Gabaα6-Cre transgenic mice expressing Cre recombinase under the control of the Gaba$_A$ receptor α6 subunit promoter (Aller et al., 2003) on a *Prnp$^{o/o}$* background, and tg37 mice, in which a PrP^c transgene is flanked by loxP sites allowing for ablation of PrP^c upon Cre recombination (Mallucci et al., 2002). Thus, we utilized the littermates for toxicity experiments: double-transgenic Gaba$_A$α6-Cre-Tg37 mice that undergo Cre-mediated depletion of PrP^c specifically in cerebellar granular cells CGC (henceforth referred as PrP$^{\Delta CGC}$) and control littermates expressing tg37 in the absence of the Cre transgene where PrP^c expression is retained in neurons (henceforth referred to as PrP^{CGC+}). Tg37 mice express floxed PrP at slightly higher levels than *wt* mice (Mallucci et al., 2002);

therefore, we treated the COCS under the same conditions described above (267nM, 21 dpe).

As expected, COCS depleted of PrP^{c} ($PrP^{\Delta CGC}$) did not display any POM1 toxicity, whereas COCS still expressing PrP^{c} (PrP^{CGC+}) underwent cell death (Figure 2.8b), confirming that neuronal PrP^{c} is necessary and sufficient for POM1-mediated toxicity.

Next, to disprove that POM1-mediated neurodegeneration was a consequence of antibody binding to any neuronal GPI-anchored protein, *tga20* COCS were treated with an anti-NOGO receptor antibody (67nM). After 14 days of treatment (Figure 2.8c), *tga20* did not show any signs of toxicity, confirming that POM1-mediated toxicity was PrP^{C}-dependent.

MICROGLIA DEPLETION NEITHER AMELIORATES NOR WORSENS POM1 TOXICITY

Pharmacogenetic ablation of microglia has been shown to increase prion titers and PrP^{Sc} levels, and to exacerbate CGC loss in prion-infected COCS (Falsig et al., 2008; Falsig, unpublished data). Hence we investigated the contribution of microglia in the antibody model. CD11b-HSVTK (TK^{+}) mice are a very well established pharmacogenetic inducible mouse line for studying the effects of microglial ablation (Heppner et al., 2005). TK^{+} mice express the Herpes simplex virus thymidine kinase (HSVTK) under the control of CD11b, a specific microglial promoter. When COCS prepared from these mice are treated with ganciclovir (GCV), the thymidine kinase enzyme converts the prodrug GCV into a toxic metabolite, leading to selective depletion of microglia (Heppner et al., 2005) without affecting neuronal viability (Falsig et al., 2008). In order to have higher PrP^{c} expression levels and reduce the timeframe of toxicity, CD11b-HSVTK mice were crossed with *tga20* mice. COCS from HSVTK-positive or negative littermates were exposed to POM1 or IgG in the presence or absence of GCV ($5\mu ml^{-1}$). COCS were challenged with GCV for 14 days prior to antibody treatment with no impact on viability, as observed after NeuN morphometric analysis of IgG-treated COCS expressing or not expressing the transgene (TK). Crucially, no significant difference in neuronal viability was detected between microglia-depleted and microglia-retaining control COCS (TK^{+} in presence of GCV and TK^{+} in absence of GCV, respectively) upon POM1 treatment (Figure 2.9). These results indicate that microglia depletion does not worsen or diminish POM1-mediated toxicity.

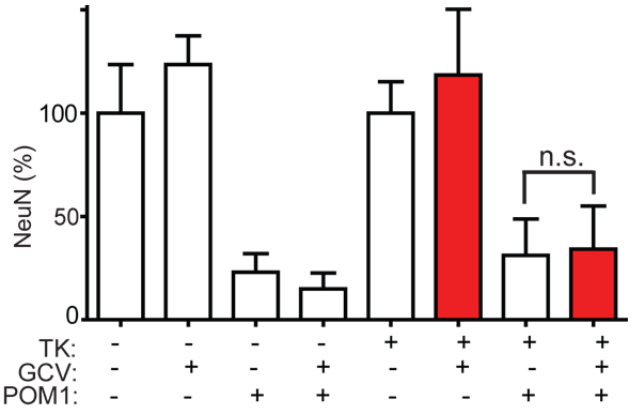

Figure 2.9. ***Pharmacogenetic-specific microglia depletion does not affect POM1-mediated neuronal death.*** *$Tga20^{TK+}$ (expressing thymidine kinase) or $tga20^{TK-}$ COCS were treated with IgG or POM1 (167nM, 21 days) and cultured in the presence (+) or absence (-) of GCV for 14 days prior to antibody treatment. Microglia depletion did not affect POM1 toxicity, as shown by NeuN quantification (red bars).*

DISCUSSION AND OUTLOOK

Neuronal loss induced by certain anti-PrP antibodies has already been documented, although the veracity of these results has recently been argued (Klöhn et al., 2012; Solforosi et al., 2004). However, this aspect has only been explored in the context of immunization therapies and safety concerns. The work presented in this thesis describes neuronal loss mediated by select antibodies specifically binding to PrP and the mechanisms by which these antibodies are toxic.

In this chapter, we saw that antibody-mediated toxicity was gene dosage-dependent, the degree of toxicity induced could be modulated by the dose and duration of antibody treatment, and that toxicity occurred *via* neuronal PrP, suggesting many similarities to genuine prion infections (Falsig et al., 2012; Fischer et al., 1996; Mallucci et al., 2003). Also, we showed that antibody derivatives (lacking the Fc portion) such as monovalent $F(ab)_1$ and divalent $F(ab)_2$ –fragments, and scFv minibodies were neurotoxic, excluding Fc-receptor mediated mechanisms responsible for cell death. Our results are in contrast with previous claims (Solforosi et al., 2004), since we demonstrate that crosslinking of PrP by antibody binding is an unlikely mode of cell death and suggest that toxicity is mediated through PrP conformational changes induced by antibody binding or through steric hindrance between PrP and an interacting receptor.

Moreover, we have shown that microglia depletion does not exacerbate or protect against POM1 toxicity, in contrast to prion infections, where microglia-ablated COCS showed a more dramatic CGC loss compared to microglia-retaining COCS (Falsig unpublished data). This suggests that microglia play a role in PrP-mediated neurodegeneration by acting on PrP^{Sc} rather than PrP^{C}.

Interestingly, whereas COCS exhibited dramatic neuronal loss upon anti-PrP antibody-treatment, mono-cultures from cortical neurons or granular cells did not show signs of toxicity. A systematic analysis conducted in our laboratory by Dr. Tracy O'Connor has identified that conditional medium from astrocytes is required to mediate POM1 toxicity in monocultures. Such experiments explain why cell cultures, in contrast to slice cultures, did not experience POM1 toxicity, and will offer a simplistic model to investigate prion-mediated toxicity.

CHAPTER III

STRUCTURAL DETERMİNANTS OF PRİON-MEDİATED NEURONAL DEATH

This chapter contains unpublished data as well as parts that are adapted or reproduced from the following manuscript accepted by Nature on the 21st of June 2013 and assigned the DOI 10.1038/nature12402:

The toxicity of antiprion antibodies is mediated by the flexible tail of the prion protein

Tiziana Sonati[1,*], Regina R. Reimann[1,*], Jeppe Falsig[1,*], Pravas Kumar Baral[2], Tracy O'Connor[1], Simone Hornemann[1], Sine Yaganoglu[1], Bei Li[1], Uli S. Herrmann[1], Barbara Wieland[2], Mridula Swayampakula[2], Muhammad Hafizur Rahman[3], Dipankar Das[3], Nat Kav[3], Roland Riek[4], Pawel P. Liberski[5], Michael N. G. James[2], and Adriano Aguzzi[1†]

[1] Institute of Neuropathology, University Hospital Zurich, Switzerland
[2] Department of Biochemistry, University of Alberta, Canada
[3] Department of Agricultural, Food and Nutritional Science, University of Alberta, Canada
[4]ETH Zurich, Physical Chemistry, ETH Honggerberg, 8093 Zurich, Switzerland
[5]Laboratory of Electron Microscopy and Neuropathology, Department of Molecular Pathology and Neuropathology, Medical University of Lodz, Lodz, Poland.
[*] These authors contributed equally to this work

[†]Corresponding author: Adriano Aguzzi; Institute of Neuropathology, University Hospital of Zurich; Schmelzbergstrasse 12, CH-8091 Zurich, Switzerland; Tel: +41-44-255-2108, Email address: adriano.aguzzi@usz.ch

INTRODUCTION

FUNCTIONAL DOMAINS OF THE PRION PROTEIN

Many deletion mutants of PrP have been generated that are aimed at elucidating PrP's function and its implication in pathology. Particularly, regions highly conserved among species, such as the OR and the HC, have been the focus of extensive research.

Truncated forms of the FT

Mice expressing PrP with truncated forms of the FT, such as $PrP_{\Delta 32-121}$ and $PrP_{\Delta 32-134}$ (Shmerling et al., 1998), exhibit severe ataxia and cerebellar granule cell (CGC) degeneration. In contrast, mice expressing shorter truncations of the FT that retain the HC, such as $PrP_{\Delta 32-80}$, $PrP_{\Delta 32-93}$, $PrP_{\Delta 32-106}$, $PrP_{\Delta 51-90}$ and and $PrP_{\Delta 23-88}$, did not display pathological signs (Fischer et al., 1996; Flechsig et al., 2000; Shmerling et al., 1998; Supattapone et al., 2001; Yamaguchi et al., 2012). These data suggest that the HC is a crucial PrP domain whose loss induces a toxic PrP conformer. Indeed, mice expressing PrP variants with HC deletions ($PrP_{\Delta 94-134}$ and $PrP_{\Delta 105-125}$) manifest a lethal phenotype one week after birth (Baumann et al., 2007; Li et al., 2007). Toxicity of $PrP_{\Delta 105-125}$ could be due to high levels of PrP^{ctm} because of failed membrane translocation (Hegde et al., 1998; Hegde et al., 1999), as increased efficiency of signal peptide sequences alleviated neurodegeneration in these mice. The toxic phenotype of $PrP_{\Delta 32-121}$, $PrP_{\Delta 32-134}$, $PrP_{\Delta 105-125}$ and $PrP_{\Delta 94-134}$, is rescued by co-expression of *wt* PrP (Baumann et al., 2007; Li et al., 2007; Shmerling et al., 1998).

Work from the Harris' group has recently uncovered a role of the CC1 (residues 23-27 of PrP^{C}) in PrP-mediated neurotoxicity. Cells expressing the construct $PrP_{\Delta 105-125}$ develop spontaneous ionic currents, show decreased viability (Solomon et al., 2010; Solomon et al., 2011), and are sensitive to select groups of cationic drugs (Massignan et al., 2011; Massignan et al., 2010). Lack of the CC1, but not of the OR, counteracted the toxicity shown by $PrP_{\Delta 105-125}$-expressing cell lines (spontaneous currents and hypersensitivity to certain antibiotics) (Solomon et al., 2011). In contrast to the Shmerling mice ($PrP_{\Delta 32-134}$), transgenic mice expressing a large deletion in the FT ($PrP_{\Delta 23-134}$) do not display any toxic phenotype, suggesting that residues 23-31 are essential for transmitting neurotoxicity (Westergard et al., 2011). Moreover, co-expression of $PrP_{\Delta 32-80}$ and $PrP_{\Delta 32-93}$ along with *wild type* PrP (Shmerling et al., 1998) prevents clinical and neuropathological signs of toxicity in $PrP_{\Delta 32-134}$ mice, whereas there is no effect with co-expression of PrP molecules lacking the CC1, such as $PrP_{\Delta 23-111}$, $PrP_{\Delta 23-134}$, and $PrP_{\Delta 23-31}$. This suggests that the CC1 is necessary for the protective activity of *wt* PrP (Turnbaugh et al., 2011). To investigate the involvement of the CC1 in prion

diseases, mice lacking this region ($PrP_{\Delta 23-31}$; KKRPKPGGW) were inoculated with prions, and they displayed lower PrP^{Sc} levels and prolonged survival times (Turnbaugh et al., 2012).

Mechanisms of toxicity induced by PrP mutants are speculative to date and could be explained by: 1) loss of homeostatic functions as a consequence of an interrupted interaction with a pro-survival or pro-apoptotic molecule using this region, 2) gain of function as consequence of the formation of a misfolded toxic protein or an artificial toxic protein due to alterations of PrP topology or 3) interruption of a functional homo-oligomeric complex of PrP molecules through the HC region (current hypothesis in our lab, Calella et al unpublished).

OR and copper binding

The OR of PrP^{C} has been an object of intense research, as it represents one of the most conserved regions among mammals (Wopfner et al., 1999); however, its role in prion pathogenesis is unclear.

PrP-deficient mouse lines expressing N-terminally truncated PrP versions with a full or partial deletion of the OR, such as $PrP_{\Delta 32-93}$ or $PrP_{\Delta 23-88}$, are less susceptible to prion infections (Flechsig et al., 2000; Supattapone et al., 2001) and displayed longer incubation times despite higher PrP expression levels. Surprisingly, these mice had almost undetectable PrP^{Sc} levels and prion titers, decreased vacuolation and little astrogliosis in their brains. In contrast, the spinal cords contained prion infectivity and pathological changes comparable to *wt* mice (Flechsig et al., 2000; Supattapone et al., 2001).

Mice devoid of the OR ($PrP_{\Delta 51-90}$) do not have increased survival times; however, prion titers and PrP^{Sc} in the brain of these mice are slightly lower than *wt* (Yamaguchi et al., 2012). Conversely, prion titers and PrP^{Sc} in spinal cords are comparable to *wt* (Yamaguchi et al., 2012). All these data from different mutants lacking regions encompassing the OR suggest that the region 32-50 confers susceptibility to prions in the brain.

Interestingly, transgenic mice expressing insertions of octapeptide repeats (PG14) show a toxic phenotype (Chiesa et al., 1998), and such insertional mutations are associated with hereditary prion diseases (Krasemann et al., 1995; Mead et al., 2006; Vital et al., 1999), indicating that the OR or possibly the length of the FT are strictly connected with pathology.

PrP has four Cu^{2+} binding sites within the octapeptide repeats at specific histidine residues 60, 68, 76, and 84 (Aronoff-Spencer et al., 2000; Burns et al., 2002; Qin et al., 2002). A fifth binding site has been shown at histidines 96 and 111 of human recombinant PrP (huPrP) in the region between the OR and the globular domain (GD) (Jackson et al., 2001). High copper concentrations stimulate PrP^{c} internalization (Lee et al., 2001; Pauly and Harris, 1998; Perera

and Hooper, 2001; Taylor et al., 2005) and it has been proposed that PrP may be involved in copper uptake into cells (Brown et al., 1999; Pauly and Harris, 1998) or have a copper-dependent superoxide dismutase activity (Brown et al., 1999). Administration of the copper chelator D-pen delayed prion disease onset, whereas a copper deficient diet had a negative effect on the survival of prion-inoculated mice (Mitteregger et al., 2009; Sigurdsson et al., 2003). Hence despite extensive efforts the role of copper in prion pathogenesis remains unclear.

Truncated forms of the GD

Mice expressing PrP lacking α2 ($PrP_{\Delta 23\text{-}88\ \Delta 177\text{-}200}$), α3 ($PrP_{\Delta 23\text{-}88\ \Delta 201\text{-}207}$), or both helices 2 and 3 ($PrP_{\Delta 23\text{-}88\ \ \Delta 141\text{-}221}$) develop ataxia and neuronal storage disease (Muramoto et al., 1997; Supattapone et al., 2001), but fail to replicate prions (Muramoto et al., 1996). Moreover, their phenotype cannot be rescued by *wt* PrP. These data suggest that helix 2 and 3 are crucial to maintain PrP structure, which seems to be essential for the transmissibility of prions.

OUTLINE OF THIS WORK

Chapter II summarized that select anti-PrP antibodies trigger dramatic neuronal death in a PrP-dependent manner, as their toxic effect is blocked by co-incubation with the antigen rmPrP and by ablation of the *Prnp* gene. Moreover, we showed that neither antibody-mediated PrP crosslinking, nor Fc effector functions are responsible for cell death. Chapter III will introduce our novel findings on the structural determinants responsible for the antibody toxicity by using a large set of antibodies targeting different epitopes of PrP (the POM monoclonals) and mice expressing truncated versions of PrP.

Treatment of COCS with the POM monoclonals antibodies (Polymenidou et al., 2008) revealed that toxicity was dependent on the region of PrP^C targeted by the antibody. Toxicity studies of the POM monoclonals revealed that antibodies recognizing selected regions of PrP induce neuronal loss; therefore, we categorized POM antibodies based on their toxic effects. Antibodies targeting the FT consist of two classes of binders: those binding the OR that were innocuous, and those recognizing the CC2 that caused toxicity only at high concentrations. Antibodies targeting the GD gave a mixed profile: those specifically binding the α1-α3 of GD induced dramatic neuronal loss, whereas others were non-toxic. Toxicity seemed to strongly correlate with specific binding sites and very poorly with binding affinity (Figure 3.1).

X-ray and NMR analyses were employed to identify a potential PrP toxic conformer induced by binding of a toxic antibody to PrP^C. Surprisingly, structural analyses of a toxic GD antibody bound to rmPrP did not reveal significant conformational distortions of the crystal structure of rmPrP, whereas NMR analyses showed subtle shifts in the β1-β2 sheets of PrP, and physiological implications of such changes require further investigation.

To evaluate the contribution of the FT in GD antibody-mediated toxicity, we employed transgenic mice expressing truncated forms of the FT. Excitingly, large deletions of the FT counteracted neurotoxicity, suggesting that select GD antibodies utilize the FT to exert their toxic effects. Supporting this hypothesis, we discovered that blocking the FT *via* FT antibodies prevented prion-dependent neurodegeneration, as antibodies binding the FT were neuroprotective in genuine prion infections. Additionally, FT antibodies prolonged the lifespan of $PrP_{\Delta 94\text{-}134}$, one of the most toxic deletion mutants of PrP (Baumann et al., 2007).

RESULTS

ANTIBODY TOXICITY IS EPITOPE-SPECIFIC

To gain insights into the structural determinants of toxicity within PrP, a large panel of anti-PrP antibodies (Polymenidou et al., 2008) recognizing specific epitopes (Figure 3.1a, Table 4.1) were screened in COCS prepared from *tga20* mice (67nM, 21 days; 67nM, 14 days indicated by symbol &; Figure 3.1b). POM2, POM11, POM12 (binding the OR), D13 (Solforosi et al., 2004) and POM3 (binding the CC2) were not neurotoxic (Figure 3.1b). Among the twelve GD antibodies, 7 antibodies were toxic (POM1, POM8, POM9, POM17, POM4, POM10, POM19), POM13 showed marginal toxicity, and the other four, POM5, POM6, POM7 and POM15, were innocuous (Figure 3.1b). The same batch of antibodies were tested in a parallel experiment in *Prnp*$^{0/0}$ COCS to exclude toxic off-target effects and none of these antibodies were found to be toxic (Figure 3.1c).

After this first screening, we concluded that anti-PrP antibodies binding the FT (OR and CC2) were innocuous and only certain antibodies against the GD were toxic. To investigate the reason for differential toxicity, *tga20* COCS were exposed to a higher dose of POM5, POM6, POM7, POM15 (333nM, 14 days, indicated by symbol $; Figure 3.1b). We detected no impact on neuronal viability, with the exception of POM13, which induced marginal toxicity at lower concentrations and showed significant neurotoxicity at higher doses (Figure 3.1b).

Following this observation with GD antibodies, we also investigated whether FT antibodies would have toxic effects at higher doses and *tga20* COCS were challenged with D13, POM3 and POM2 (200nM, 21 days indicated by symbol #; Figure 3.1b). *S*ignificant neuronal loss occurred upon treatment with higher concentrations of CC2 antibodies (D13 and POM3), whereas no signs of toxicity were observed upon treatment with POM2, which recognizes the OR (Figure 3.1b). *Prnp*$^{0/0}$ COCS treated with POM3, D13 and POM2, within the same experiment, remained healthy (200nM, 21 days indicated by symbol #; Figure 3.1b).

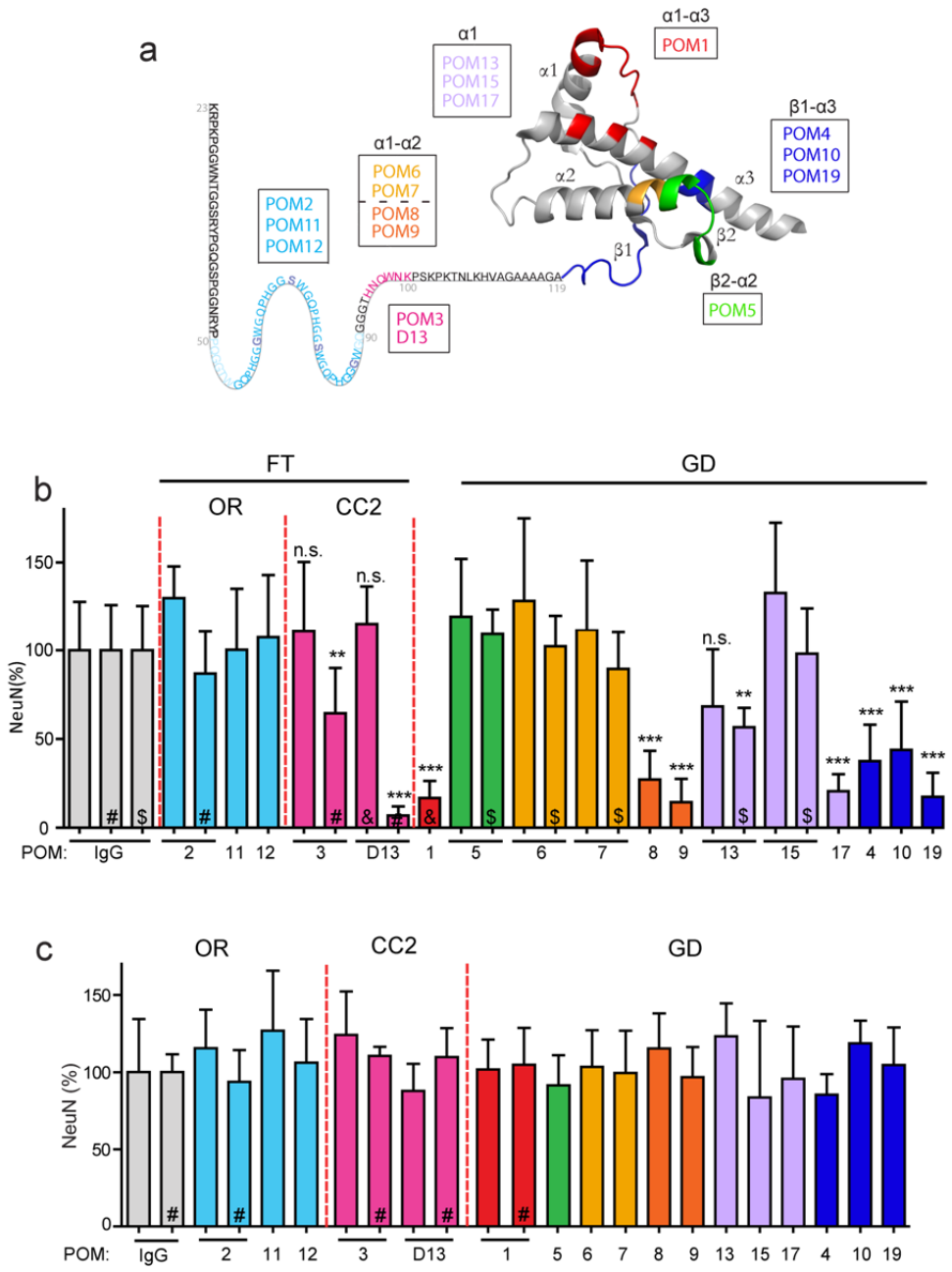

Figure 3.1. ***POM1 toxicity is epitope-specific. a****) Epitope map of the antibodies binding to PrP. POM6-9, 13, 15 and 17 bind helix 1 and compete with POM1. POM6 and 7 (light orange) show an additional binding site to helix 2 compared to POM8 and 9 (dark orange, see Table 3.1). POM5 shows a distinct binding to PrP (green). POM2, POM11, POM12 recognize the OR (turquoise). D13 (Solforosi et al., 2004) and POM3 bind to the CC2 (magenta).* ***b)*** *COCS from tga20 mice were treated with a large panel of anti-PrP antibodies that recognize the OR, CC2 and GD epitopes of PrP color-coded as in a). All antibodies were used at a concentration of 67nM for 21 days, unless indicated otherwise: & = 67nM, 10 days; # = 200nM, 21 days; $ = 333nM, 14 days.* ***c****) None of the antibodies used in a) were toxic to* $Prnp^{0/0}$ *COCS.*

The dose-dependent effect of antibodies binding to the CC2 (POM3 and D13) was crucial to explain the controversial results of D13-injected mice, where the recently published work by Klöhn et al. did not confirm the previous report published by Solforosi et al about the toxic effect of D13 (Klöhn et al., 2012; Solforosi et al., 2004). (Klöhn et al., 2012; Solforosi et al., 2004). Importantly, antibody-toxicity observed in COCS has been confirmed *in vivo* (Reimann 2013 submitted; Sonati, 2013).

Table 3.1

	Domain*	Epitope*		Toxicity#	GD protection	Affinity (nM)		
		sequence	location			Holo-Ab	$F(ab)_1$	scFv
POM2	FT (OR)	GQPHGGG/SW	57-64, 64-72, 72-80, 80-88	-	+	<0.1*	2.5	20*
POM11	FT (OR)	GQPHGGSW	64-72, 72-80	-	+		-	-
POM12	FT (OR)	GQPHGGG/SW	57-64, 64-72, 72-80,80-88	-			-	-
POM3	FT (CC2)	HNQWNK	95-100	+/-	+		-	-
POM1	GD	β1-α1 loop-α1 and α3	¥138-147; 204/208/212	+		0.58*	2.5	800
POM4	GD	β1 and α3	121-134 and 218-221	+			-	-
POM5	GD	β2-α2 loop- α2	168-174	-			16	-
POM6	GD	β1-α1 loop-α1 β2-α2 loop- α2	140/145; 158/177; 170/174	-			-	-
POM7	GD	β1-α1 loop-α1 β2-α2 loop- α2	140/145; 158/177; 170/174	-			-	-
POM8	GD	β1-α1 loop-α1 β2-α2 loop- α2	140/145; 170/174	+			-	-
POM9	GD	β1-α1 loop-α1 β2-α2 loop- α2	140/145; 170/174	+			-	-
POM10	GD	β1 and α3	121-134 and 218-221	+			-	
POM13	GD	α1		+/-			-	
POM15	GD	β1-α1 loop-α1	140/145	-			5	
POM17	GD	β1-α1 loop-α1	140/145	+			6.6	
POM19	GD	β1 and α3	121-134 and 218-221	+		0.87*	0.4	

**: data from ref (Polymenidou et al., 2008) are reproduced here for convenience. The reported epitopes are based on peptide competition and differential binding to PrP^C mutants. For POM1 epitope, crystallographic coordinates were used, revealing an additional epitope on helix3.*

[¥]: POM1 epitope has been determined by X-ray analysis (PDB 4H88 code; Figure 3.4) and NMR analyses (Figure 3.5).

[#]: +: toxic; -: nontoxic; +/-: moderately toxic

DIFFERENTIAL TOXICITY RELATES POORLY WITH AFFINITY BINDING

SPR measurements of holo-antibodies

We investigated if binding affinity was the determining factor in the differential toxicity among GD antibodies. In order to evaluate the binding constant (KD) of the antibody-rmPrP complex, we performed kinetic measurements using BIAcore T100 (Jason-Moller et al., 2006). POM antibodies showed a very slow dissociation rate, impeding the evaluation of a KD (ratio of association and dissociation constants) (Figure 3.2a). Changing the temperature from the standard 25°C to 37°C or increasing the dissociation time did not facilitate dissociation of the complex (data not shown). In order to circumvent this problem, we performed surface plasmon resonance (SPR) equilibrium analysis (Jason-Moller et al., 2006) to determine affinity constants in solution. A range of concentrations of rmPrP (ligand) was added in solution to compete for the amount of antibody (analyte, kept constant) binding to rmPrP immobilized on the surface of the chip. The amount of antibody in solution that will bind to the immobilized rmPrP (responsible for the SPR signal) was expected to decrease upon an increase in rmPrP in solution following a sigmoidal response.

Competition experiments using a constant concentration of POM antibody (0.5nM) and various concentrations of rmPrP (ranging between 0 and 5-10nM) showed an unexpected "increase" in free POM antibody at higher concentrations of rmPrP in solution (Figure 3.2b). All POM antibodies (POM1, POM19, POM5, POM13, POM15, and POM6) analysed showed similar results. We hypothesized that at higher concentrations, rmPrP might aggregate or that antibody-mediated crosslinking might occur. We then added bovine serum albumin to the HEPES buffer used for the measurements to diminish aggregation without any improvements. Therefore, we decided to carry out the binding affinity studies using Fab fragments, given that FabPOM1 was shown in a parallel experiment to have a measurable dissociation rate (shown below).

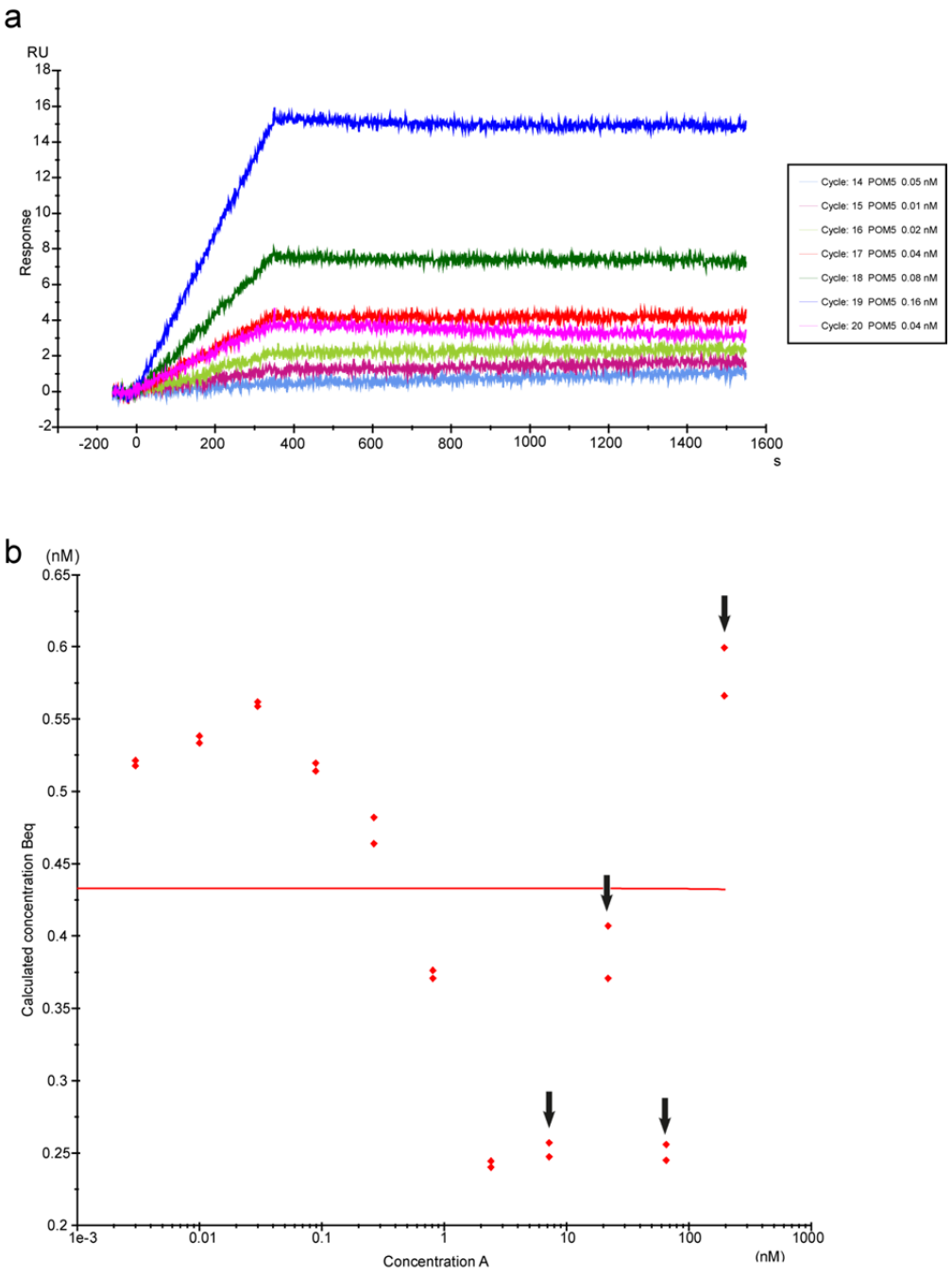

Figure 3.2. Sensograms of holoantibodies. ***a****) A representative SPR sensogram of kinetic measurements displaying POM5 binding to rmPrP$_{23-231}$. Almost no dissociation rate could be evaluated.* ***b****) A representative SPR analysis at equilibrium displaying a decrease in POM19 bound to rmPrP$_{23-231}$ on the surface as rmPrP$_{23-231}$ concentration in the solution increases. Arrows indicate unexpected increase in free POM1 binding to the surface of rmPrP$_{23-231}$ starting approximately at 2.43nM of rmPrP.*

SPR measurements and binding affinity determination of Fab fragments

We generated F(ab)$_1$ fragments from a representative set of toxic (POM1, POM17, and POM19) and nontoxic antibodies (POM2, POM5, and POM15). The binding affinity constant of the antibody-rmPrP$_{23\text{-}231}$ complex was kinetically measured using BIAcore T100. In the first set of experiments, SPR measurements were performed with a surface containing 1000 RU of rmPrP$_{23\text{-}231}$ at 25°C. Under these conditions, the results indicate a weak correlation between toxicity and affinity binding (Table 3.2); however, in the second set of experiments where measurements were performed with a less dense surface (less prone to artefacts) at 37°C, a correlation could not be confirmed (Table 3.2). The innocuous antibodies POM2 and POM15 showed higher affinity than toxic antibodies, such as POM17 (Table 3.2). We concluded that the differential toxicity correlated strongly with well-defined PrP^C epitopes but poorly with their affinity to PrP^C.

Table 3.2. Fab binding affinity constants evaluated by kinetics analyses.

	1000 RU rmPrP(23-231) T (25°)		100 RU rmPrP(23-231) T (37°)
	KD (nM)		KD (nM)
		scFv POM1	800
Fab POM2	1.4	**FabPOM5**	16
Fab POM5	0.9	**FabPOM17**	6.6
Fab POM15	0.6	**FabPOM15**	5
Fab POM17	0.5	**FabPOM1**	3.9
Fab POM1	0.2	**FabPOM2**	2.5
Fab POM19	0.03	**FabPOM19**	0.4

Binding affinity

Measurements were performed at two different temperatures and with different rmPrP density surfaces (100RU and 1000RU). By increasing temperature from +25°C to +37°C, the affinity of the Fab POMs decreases in all but one case by roughly one order of magnitude. All data fit to a first order of binding with a similar response. Only FabPOM2 affinity is the same at both temperatures. The maximal response seen in the sensogram at +25°C indicates binding of up to 4 FabPOM2 molecules per rmPrP (data not shown).

Toxicity studies of F(ab)$_1$POMs correlated with their parental holoantibodies

In order to confirm that F(ab)$_1$ fragments generated from the POM monoclonals would mediate toxicity as their corresponding parental holo-antibodies, we performed toxicity studies in *tga20* COCS. FabPOM1, FabPOM17, and FabPOM19 induced dramatic neuronal loss, whereas FabPOM5 and FabPOM15 were innocuous, reproducing the results obtained with the holo-antibodies (Figure 3.3a). None of the F(ab)$_1$ fragments were toxic to *Prnp*$^{0/0}$ COCS (Figure 3.3b).

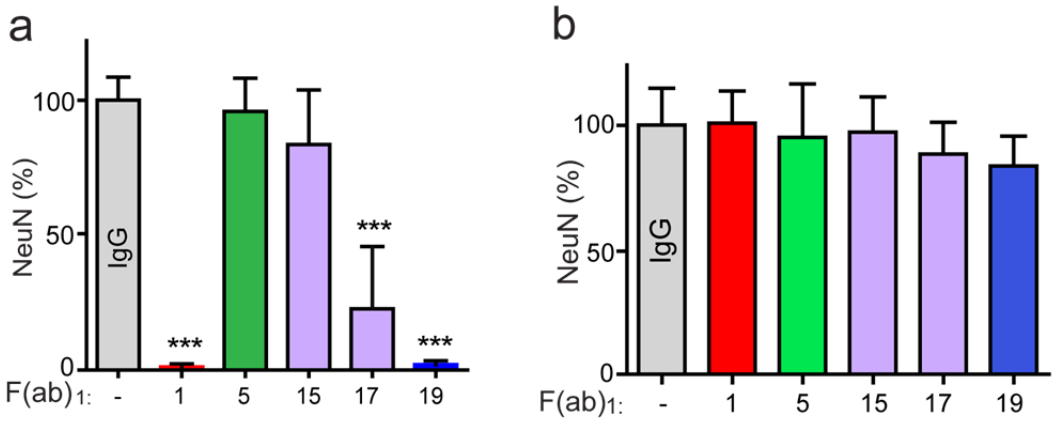

Figure 3.3. ***F(ab)$_1$ fragment-mediated toxicity reflects holo antibody results a****) Tga20 COCS were treated with various F(ab)$_1$ fragments (134nM) and stained with NeuN at 21 dpe. F(ab)$_1$ fragments of POM1, 17 and 19 were neurotoxic like the holo antibodies, whereas FabPOM5 and FabPOM15 were innocuous.* ***b****) No neuronal damage was detected in Prnp$^{0/0}$ COCS treatment with F(ab)$_1$ fragments (treatment as in a).*

ANTIBODY TOXICITY IS NOT MEDIATED BY A CONFORMATIONAL CHANGE: X-RAY AND NMR ANALYSES

Next we asked whether binding of a toxic antibody would induce a deformation of PrP structure. To answer this question and to precisely identify the residues involved in such a binding, X-ray analyses of the complex FabPOM1 bound to the N-terminally truncated rmPrP$_{120\text{-}230}$ (residues 120-230 inclusive) were performed in collaboration with Pravas Baral under the supervision of Prof. Michael James (University of Alberta, Canada). The structure of the complex was resolved at a 1.9 Å resolution (PDB code: 4H88; Figure 3.4). The POM1 epitope was found to include the distal part of α1- β1 loop and of helix 1 and the proximal part of helix 3 (Figure 3.4, Table 3.1). Hence, the FabPOM1 epitope is discontinuous with a contact interface of ca. 580 Å2, showing a larger interaction interface for heavy chain

(salmon) than for the light chain (aquamarine). It is comprised of residues 137-146 (β1-α1) and Lys203, Arg207, and Gln211 (α3) (Figure 3.4, Table 3.1). The X-ray of the complex FabPOM1-rPrP was compared to other published structures of the GD of PrP^C, and showed that no conformational change occurred upon POM1 binding. X-ray measurements provide high structural resolution, however such analyses depict a static structure and results might reflect only one conformer status.

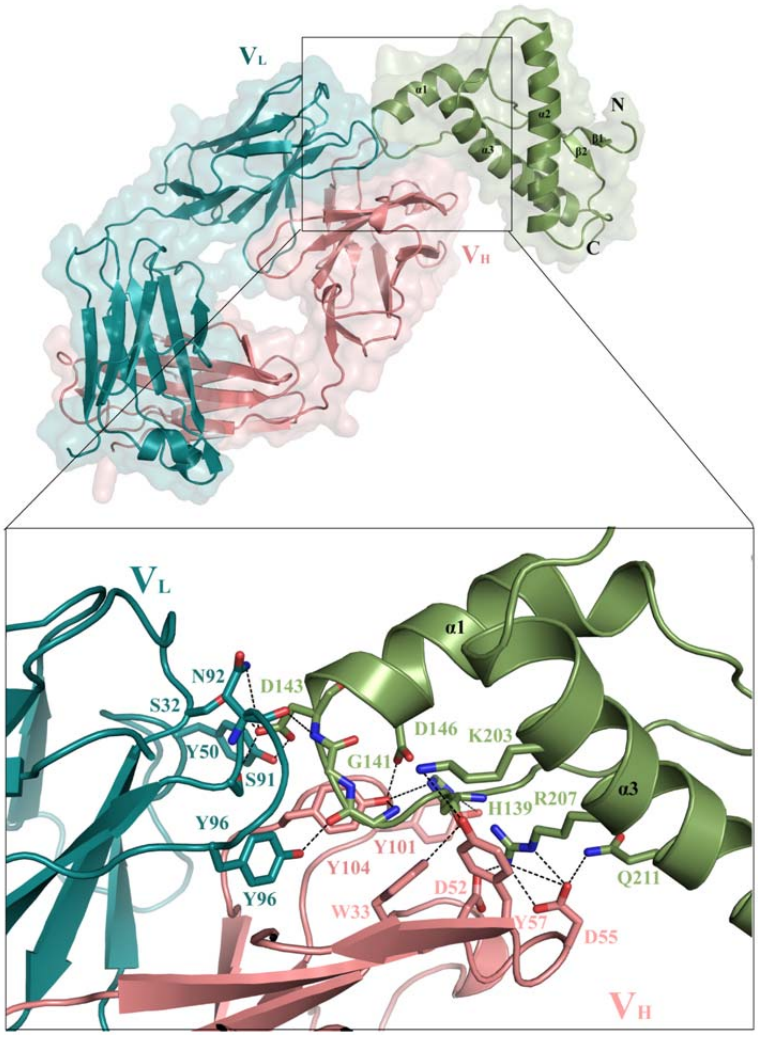

Figure 3.4. ***X-ray crystallographic structure of the complex F(ab)$_1$ and rmPrP$_{120-230}$.*** ***a)*** *The interaction interface for heavy chain (salmon) is larger than the light chain (aquamarine). This structure has been solved at a higher resolution (1.9 angstroms). V_H (salmon) and V_L (aquamarine) of F(ab)$_1$ fragment bound to rmPrP$_{120-230}$ (green). According to the X-ray analyses, the residues in contact (red) consist of amino acids 137-146 on helix1 and Lys203, Arg207 and Gln211 on helix3.*

For this reason, Dr. Simone Hornemann (Institute of Neuropathology; Zürich) performed NMR analyses of scFvPOM1 bound to rmPrP$_{23-230}$ to explore the behaviour of the complex in solution and the structural changes of the unstructured domain (FT), which was not included in the previous analyses. The overlay of the NMR spectra of rmPrP$_{23-230}$ and the complex scFvPOM-rmPrP$_{23-230}$ showed the expected chemical shifts around the contact area between

scFvPOM1 and rmPrP, but no substantial differences were observed upon POM1 binding except for subtle changes of β1/β2 sheets (Figure 3.5).

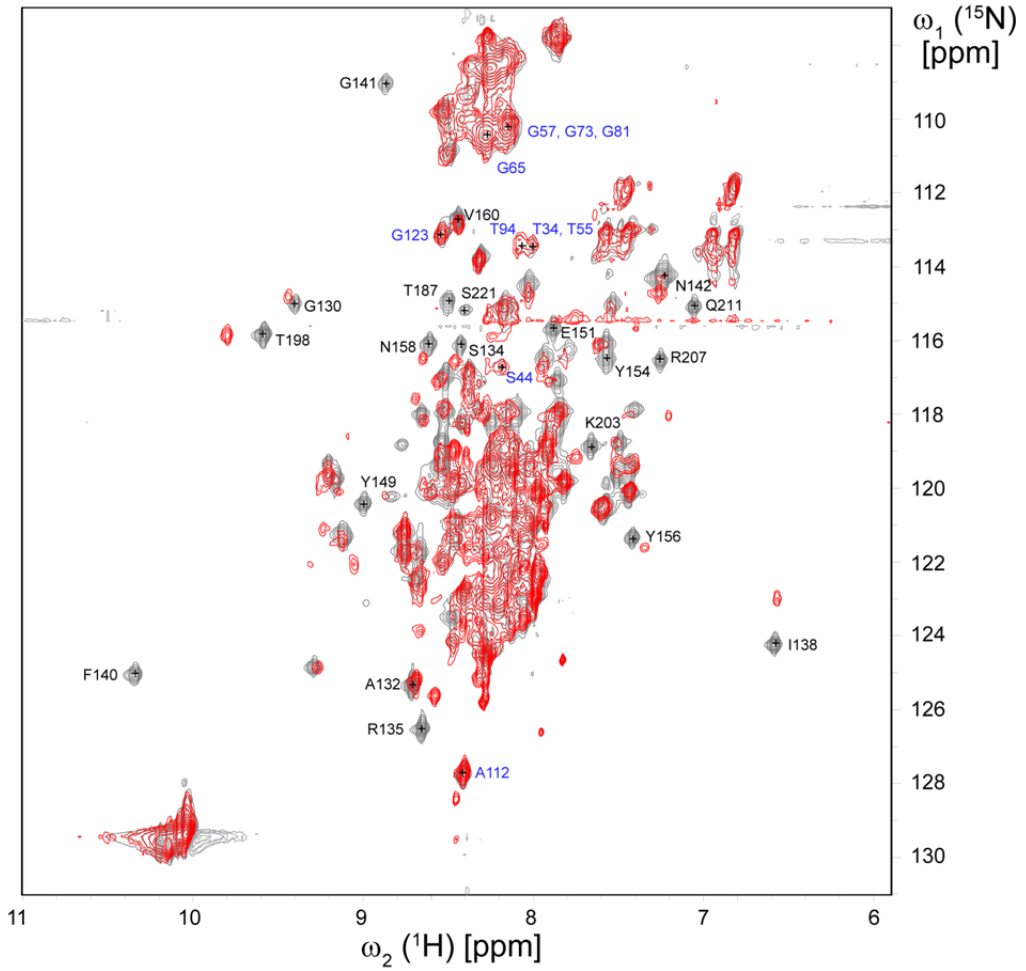

Figure 3.5. ***NMR analysis of scFv^{POM1} binding to rmPrP$_{23-230}$. a****) Superposition of 2D [^{1}H-^{15}N]-TROSY- spectra of [^{2}H,^{15}N]-labelled rmPrP$_{23-230}$ in the absence (grey spectrum) and presence (red spectrum) of stoichiometric amounts of unlabelled scFv-POM1. For simplicity, only isolated cross-peaks are marked. Residues that are in direct or close contact with scFv^{POM1} are labelled in black. Residues that belong to the FT are highlighted in blue. The overlay of the spectra show the close resemblance for the cross peaks of the residues of the FT, indicating that the scFv^{POM1} does not significantly affect the structure of the FT, whereas as expected strong chemical shift perturbations are observed for residues that interact with scFv^{POM1}. Minor chemical shifts perturbations are also visible for some β1/β2 residues (i.e. G130 and V160).*

Given these results, it is difficult to speculate whether observed changes would alter protein-protein interactions; thus, the physiological significance of such shifts remains unclear.

ENGINEERING NEW MOLECULES: LIGHT CHAIN AND HEAVY CHAIN, CYCLIC PEPTIDES

X-ray analyses identified a larger surface of interaction for the heavy chain of the antibody than for the light chain (Figure 3.6a). Therefore single chain variable fragments of light chain and heavy chain were engineered (Pravas Baral and Barbara Wieland), respectively referred to as, V_H and V_L (Figure 2.6a). Neither V_H nor V_L triggered toxicity in *tga20* and *Prnp*$^{0/0}$ COCS (838nM, Figure 3.6b), suggesting that both regions are required for toxicity. We also investigated whether V_H and V_L would block POM1 toxicity when administered in high concentrations (838nM, 10µM). We found that POM1-induced neurotoxicity was not affected by pre-incubation with V_H or V_L (Figure 3.6c).

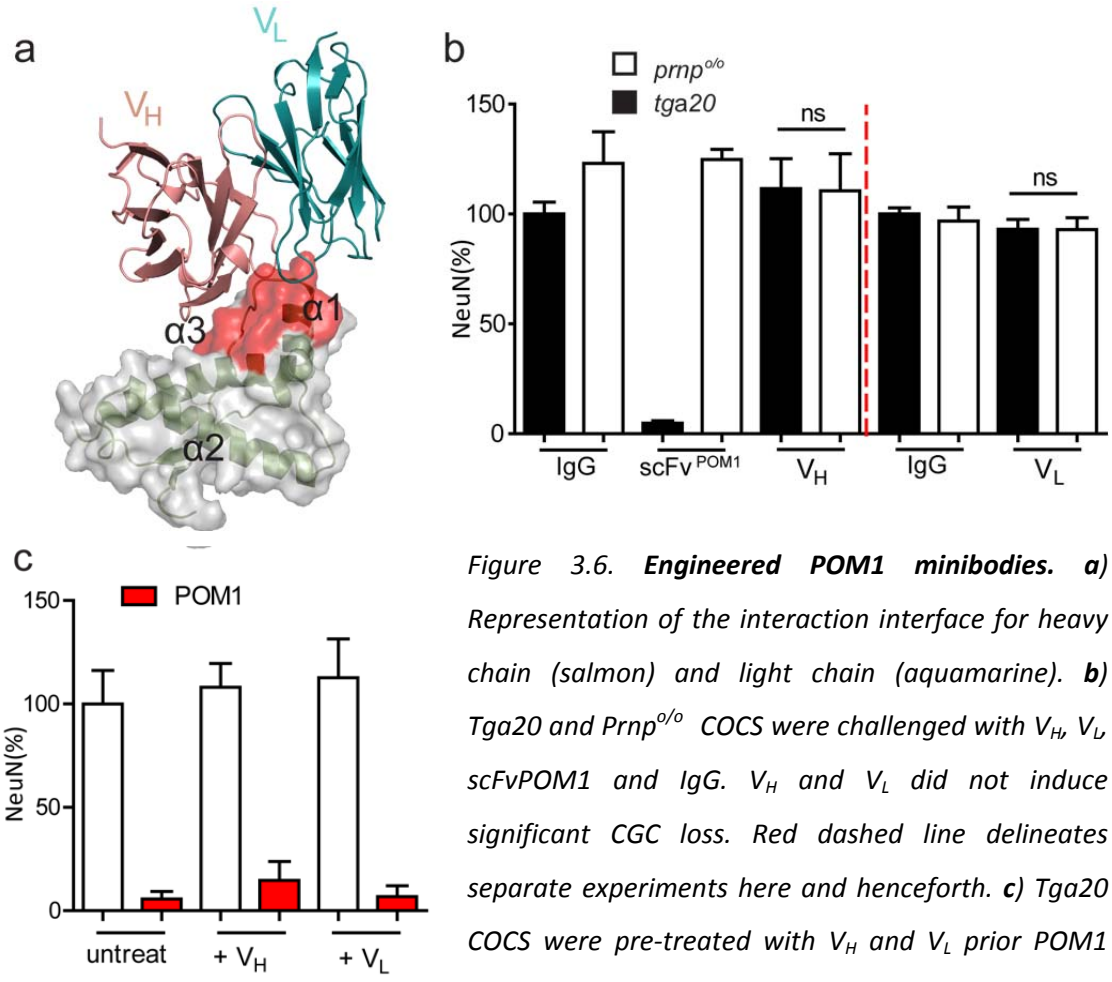

Figure 3.6. ***Engineered POM1 minibodies.*** ***a)*** *Representation of the interaction interface for heavy chain (salmon) and light chain (aquamarine).* ***b)*** *Tga20 and Prnp$^{o/o}$ COCS were challenged with V_H, V_L, scFvPOM1 and IgG. V_H and V_L did not induce significant CGC loss. Red dashed line delineates separate experiments here and henceforth.* ***c)*** *Tga20 COCS were pre-treated with V_H and V_L prior POM1 treatment. No neuroprotective effect was quantified.*

In order to understand whether the lack of toxicity by VH and VL was due to poor binding affinity, we performed SPR measurements for these antibodies. SPR measurements showed almost no binding of V_H and V_L to $rmPrP_{23-230}$ (data not shown). Quality control of batches of V_H and V_L are needed to see if degradation has occurred before making any conclusions.

In a parallel set of experiments, we used cyclic peptides of 8-10 amino acids designed by Pravas Baral and Michael James to mimic POM1 binding in order to identify the smallest region that would trigger toxicity. Those peptides were referred to as PEP1 (targeting the loop between β1 and α1), PEP2 (targeting α3), and PEP3 (targeting α1) (Figure 3.7a). They were tested at a higher concentration (200 µg/ml, 200µM) than scFvPOM1; however, no signs of toxicity were observed in *tga20* and *Prnp*$^{0/0}$ COCS (Figure 3.7b). Afterwards, SPR measurements showed lack of binding between any of the peptides and $rmPrP_{23-230}$ (SPR signal was almost equal to noise). This clearly indicated that no toxicity studies should be performed before optimal design of such peptides is achieved and binding to PrP confirmed.

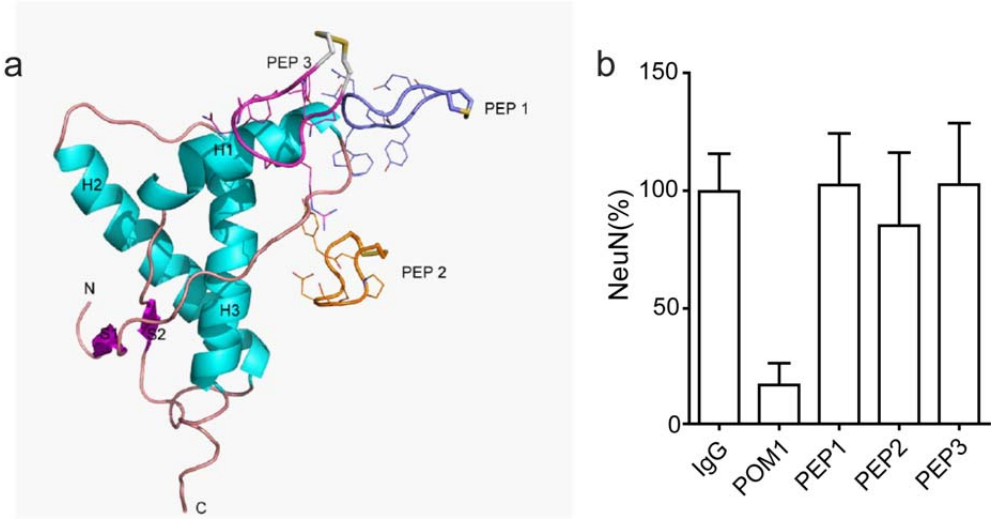

Figure 3.7. ***Smaller molecules designed to mimic POM1 binding sites failed to induce toxicity. a****) Representation of peptides designed to bind the POM1 epitope. PEP1, targeting the loop between β1 sheet and helix α1, PEP2 targeting helix α3, and PEP3, targeting helix α1. Illustration is a courtesy of Dr. Pravas Baral (University of Alberta, Canada).* ***b****) Tga20 COCS were challenged with PEP1, PEP2, and PEP3 (200µM). POM1 was used as positive control and IgG as negative control. None of the peptides triggered significant neuronal loss.*

PEPTIDE 106-126 DOES NOT EXACERBATE POM1 TOXICITY

Residues 106-126 of PrP^C are highly conserved (Rivera-Milla et al., 2006) and the lack of this region leads to a toxic phenotype in mice (Baumann et al., 2007; Li et al., 2007). The PrP106-126 peptide shares many similarities with PrP^{Sc} including a resistance to proteolysis, high β-

sheet content, and a propensity to aggregate into fibrils (De Gioia et al., 1994; Salmona et al., 1999; Selvaggini et al., 1993; Tagliavini et al., 1993). PrP 106-126 was extensively used to investigate PrP-mediated cell death, as it induces toxicity in PrP^C expressing cell lines from various brain regions without impairing the viability of PrP-deficient cortical cell lines (Brown et al., 1994; Brown et al., 1996; Forloni et al., 1993; Jobling et al., 1999); however, such toxicity has been debated (Kunz et al., 1999). Therefore, PrP106-126 was added in combination with IgG and POM1 in *wt* COCS to investigate its potential to interfere with POM1 effects. At the concentrations used, toxicity in IgG-treated COCS and/or exacerbation of POM1 toxicity were not observed (Figure 3.8). A follow-up experiment will be carried out with larger amounts of peptides or using *tga20* COCS to confirm these results.

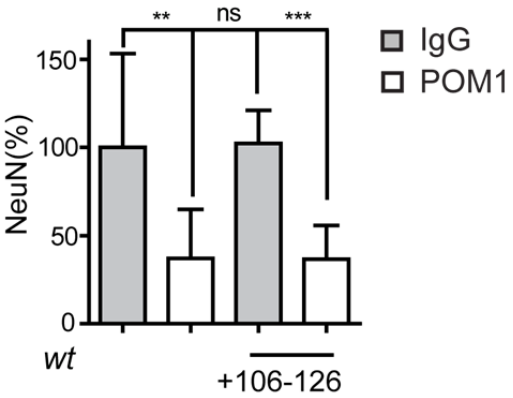

Figure 3.8. ***PrP106-126 does not induce toxicity or exacerbate POM1 effects.*** *Treatment with the peptide 106-126 (20 µM) did not impact neuronal viability of IgG or POM1 (167nM, 28 dpe) treated wt COCS.*

THE N-TERMINUS IS THE EFFECTOR DOMAIN OF TOXICITY

$PrP_{\Delta 32\text{-}134}$ COCS develop spontaneous neuronal loss *in vivo*

Transgene expression of a truncated version of PrP lacking residues 32-134 ($PrP_{\Delta 32\text{-}134}$) under the control of the *Prnp* promoter causes early onset of ataxia associated with cerebellar granule cell (CGC) degeneration and death at 2-3 months of age in PrP^c-deficient mice (Shmerling et al., 1998). This phenotype is fully reversed by co-expression of full length PrP^C, suggesting that neurodegeneration is caused by disruption of a cellular signalling pathway in which PrP is critically involved. However, PrP-deficient cells expressing $PrP_{\Delta 32\text{-}134}$ do not experience toxicity. Therefore, we investigated whether CGC loss was reproducible in COCS prepared from $PrP_{\Delta 32\text{-}134}$ mice (Figure 3.9a). We observed a progressive loss of granule cells, which was significant (30% loss of neurons compared to control) at 49 days and dramatic (75% loss of neurons compared to control) at 66 days (9 weeks) (Figures 3.9b-d) in a time

scale similar to the *in vivo* mouse model (Shmerling et al., 1998). COCS prepared from mice negative for the $PrP_{\Delta 32-134}$ transgene (littermate controls) did not show any signs of toxicity after 66 days in culture (Figures 3.9b-d).

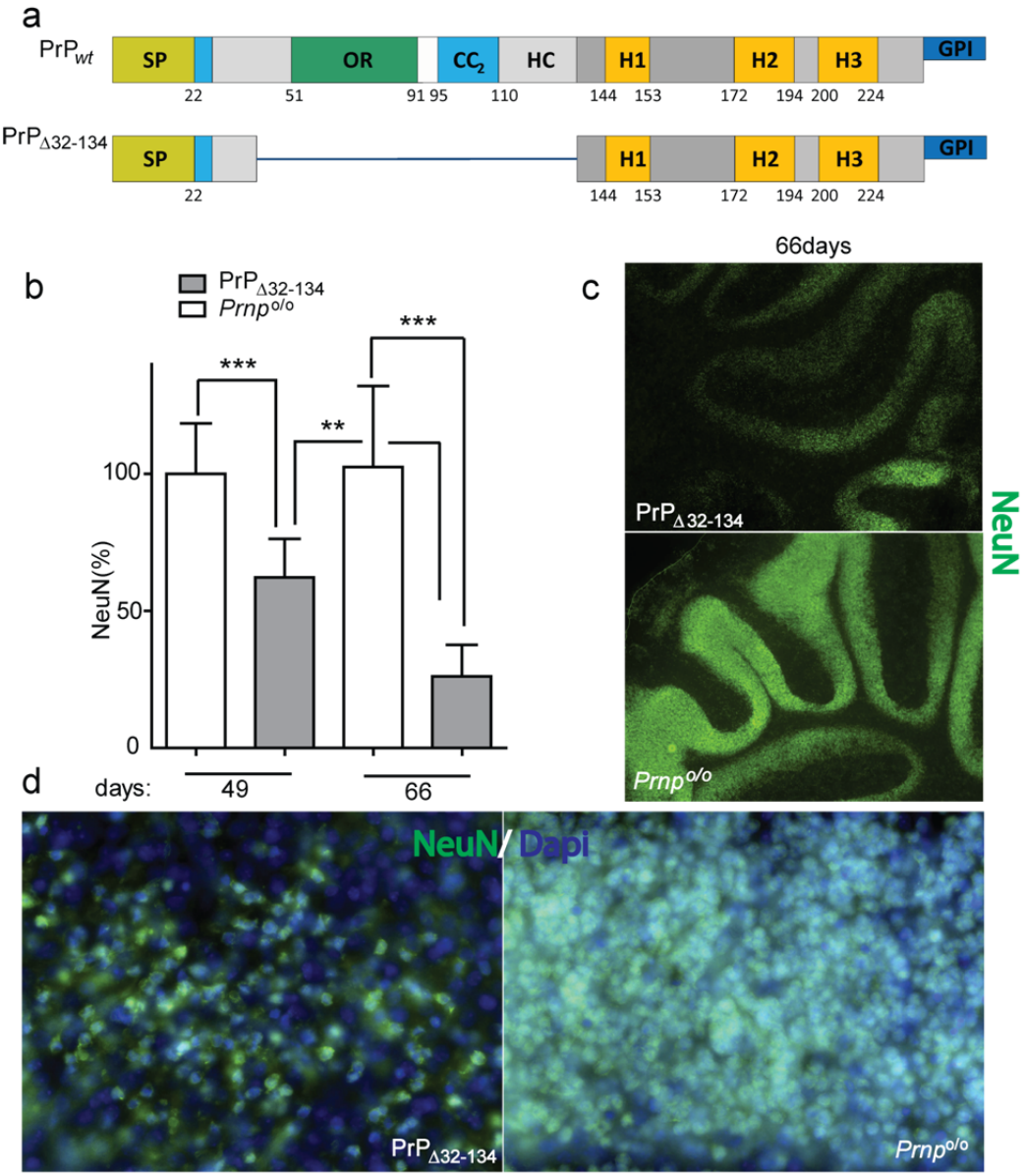

Figure 3.9. ***$PrP_{\Delta 32-134}$ slices develop neurodegeneration****. **a**) Schematic representation of wt PrP and $PrP_{\Delta 32-134}$ domains. **b**) COCS prepared from transgene positive $PrP_{\Delta 32-134}$ mice in a $Prnp^{o/o}$ background (referred as $PrP_{\Delta 32-134}$) and transgene negative (referred as $Prnp^{o/o}$) were cultured for 49 and 66 days. $Prnp^{o/o}$ COCS were unaffected in culture, whereas $PrP_{\Delta 32-134}$ showed significant neuronal loss already at 49 days and an almost complete loss of the granular cell layer at 66 days. **c-d**) Representative images taken by epifluorescence microscope of NeuN staining at 5x (c) and, NeuN-DAPI overlay at 40x magnification (d). $PrP_{\Delta 32-134}$ COCS exhibited a dramatic neuronal loss compared to $Prnp^{o/o}$ COCS at 66 days.*

SP, signal peptide; OR, octapeptide repeat; CC1-CC2, charged cluster 1 and 2; HC, hydrophobic core; α1-3, helices α1-3; GPI, glycosylphosphatidyl-inositol anchor.

Lack of residues 32-93 of PrP blocks GD antibody neurotoxicity

To identify the PrP domains required for GD antibody-mediated neurotoxicity, COCS prepared from mice expressing non-toxic truncated forms of the FT, such as $PrP_{\Delta 32\text{-}93}$ (Flechsig et al., 2000) and $PrP_{\Delta 94\text{-}110}$ (Bremer et al., 2010), were exposed to POM1 and IgG (Figure 3.10a-c). $PrP_{\Delta 32\text{-}134}$ (Shmerling et al., 1998) COCS were also treated and harvested at a time point where neurodegeneration is not significant in order to investigate if a lack of a larger portion of the FT would impair POM1 effects. Surprisingly, $PrP_{\Delta 32\text{-}93}$ and $PrP_{\Delta 32\text{-}134}$ COCS, both devoid of the octarepeats, were resistant to POM1 toxicity (Figure 3.10a-b) despite a higher expression of the PrP mutant in the cerebella of 10 day-old mice compared to *wt* (Figure 3.10c). Lack of the CC2 did not block toxicity ($PrP_{\Delta 94\text{-}110}$), but neuronal loss was enhanced in comparison to *wt* (occurred within 2 weeks) despite comparable expression levels of $PrP_{\Delta 94\text{-}110}$ (Figures 2.8a and 3.10c-d).

To investigate whether POM1 binding would be affected by a large deletion of the FT, we performed SPR experiments for the complex $F(ab)_1$POM1 bound to $rmPrP_{23\text{-}230}$ and to its N-terminally truncated form $PrP_{90\text{-}231}$. Kinetic measurements indicated similar binding affinity for the complexes $F(ab)_1$POM1-$rmPrP_{23\text{-}230}$ and $F(ab)_1$POM1-$rmPrP_{90\text{-}230}$ (2.5 and 2.9 nM, respectively; Table 3.1), indicating that removal of most of the FT did not compromise the POM1 binding site and did not affect its affinity.

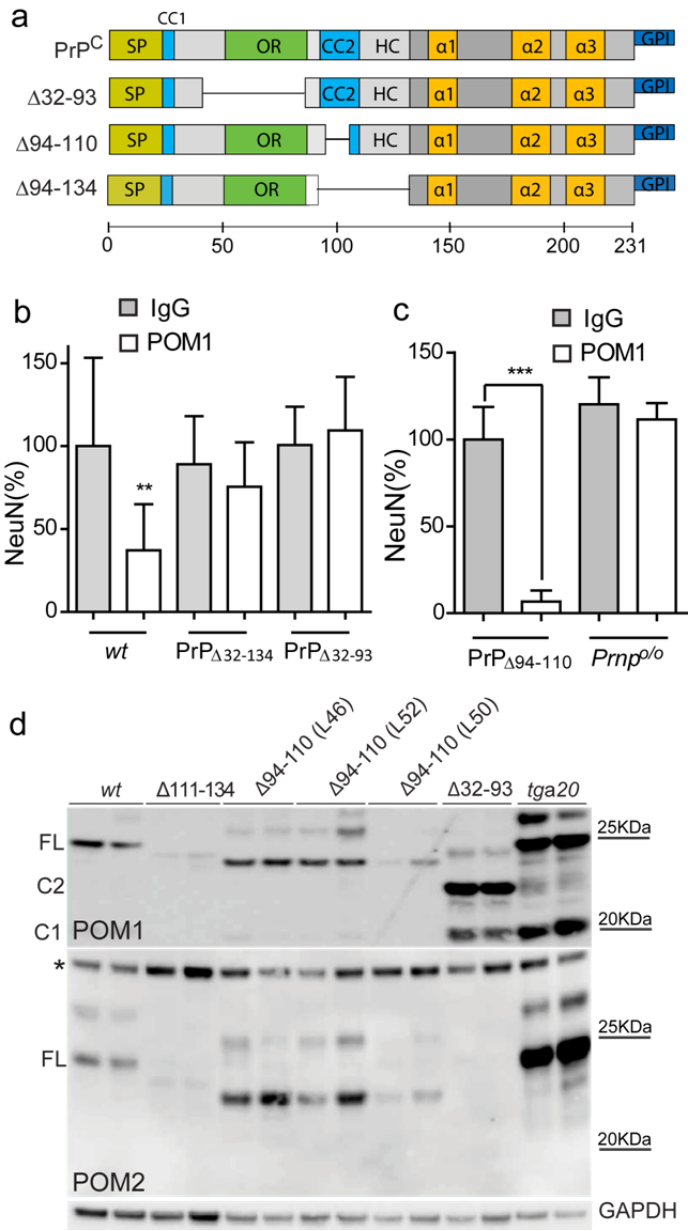

Figure 3.10. ***PrP versions lacking residues 32-93 are resistant to POM1 toxicity.*** ***a****) Schematic representation of wt* PrP^{c} *and truncated versions of PrP.* ***b-c****) Morphometric quantification of NeuN coverage in COCS prepared from wt,* $PrP_{\Delta 32-134}$, $PrP_{\Delta 32-93}$, $PrP_{\Delta 94-110}$, *and* $Prnp^{0/0}$. $PrP_{\Delta 32-134}$ *and* $PrP_{\Delta 32-93}$ *COCS were resistant to POM1 (167nM, 21 dpe) neurotoxicity (a), whereas* $PrP_{\Delta 94-110}$ *treated with POM1 (267nM, 14 dpe) underwent dramatic neuronal loss (b).* ***d****) Homogenates of cerebella from 10 day old pups were PNGaseF treated to remove glycosyl groups and western blots were probed with POM1 (anti-GD) and POM2 (anti-FT) anti-PrP antibodies.* $PrP_{\Delta 32-134}$, $PrP_{\Delta 94-110}$ *(L46) and* $PrP_{\Delta 94-110}$ *(L52) expression levels were higher than or equal to wt mice.* $PrP_{\Delta 94-110}$*(L50) and* $PrP_{\Delta 111-134}$ *expression was lower than wt and not used for POM1 toxicity experiments. GAPDH was used as a loading control. FL: full-length PrP; C1 and C2: carboxy proximal PrP cleavage fragment (110/111-230 and 89/90-230, respectively). As expected, POM2 did not recognize* $PrP_{\Delta 32-93}$ *as well as the C1 and C2 cleavage fragments, since it is directed to the OR.*

To confirm that the lack of the region encompassing residues 32-93 would prevent the neurotoxic effects of other GD antibodies, and not only POM1 effects, $PrP_{\Delta 32-93}$ COCS were additionally exposed to POM4, POM8 and POM19. Similar to POM1, these GD antibodies did not provoke a significant loss of neurons in $PrP_{\Delta 32-93}$ COCS (Figure 3.11). These results were unexpected because if the GD was the only PrP region responsible for transducing toxicity,

truncated forms of the FT, like $PrP_{\Delta 32\text{-}93,}$ should also have experienced toxicity. Therefore we speculated that GD antibodies, targeting β1-α3 (i.e POM4, POM19) or α1-α3 (i.e POM1) might all require the FT as the common effector of toxicity.

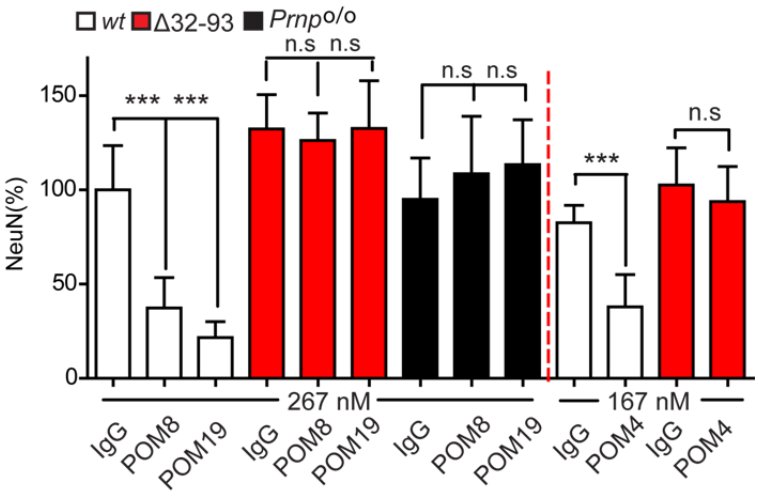

Figure 3.11. ***$PrP_{\Delta 32\text{-}93}$ counteracts GD antibody-mediated neurotoxicity. a)*** *Wt COCS treated with GD antibodies, POM4, POM19 and, POM8 (167-267nM, 28 dpe) experienced toxicity consistent with results obtained from tga20 COCS. $PrP_{\Delta 32\text{-}93}$ COCS did not show any signs of toxicity, confirming that the lack of residues 32-93 confers resistance against GD toxicity.*

FT antibodies are neuroprotective against GD antibody-mediated neuronal loss

If the FT mediates the toxicity of GD ligation, non-toxic FT antibodies might counteract the toxicity of GD antibodies. Indeed, we found that pre-incubation of *tga20* COCS with POM2 and POM11 blocked POM1-toxicity (Figure 3.12a). Pre-incubation of the COCS with FT antibodies was required to achieve a protective effect (Figure 3.12a-b) because co-incubation of POM1 with POM2 was not effective (data not shown). Interestingly, POM1-induced toxicity was also counteracted by pre-incubation with a sub-toxic concentration of POM3 and D13 (against CC2 region), suggesting that blockade of the FT (OR or HR) was protective against POM1-induced toxicity (Figure 3.12b).

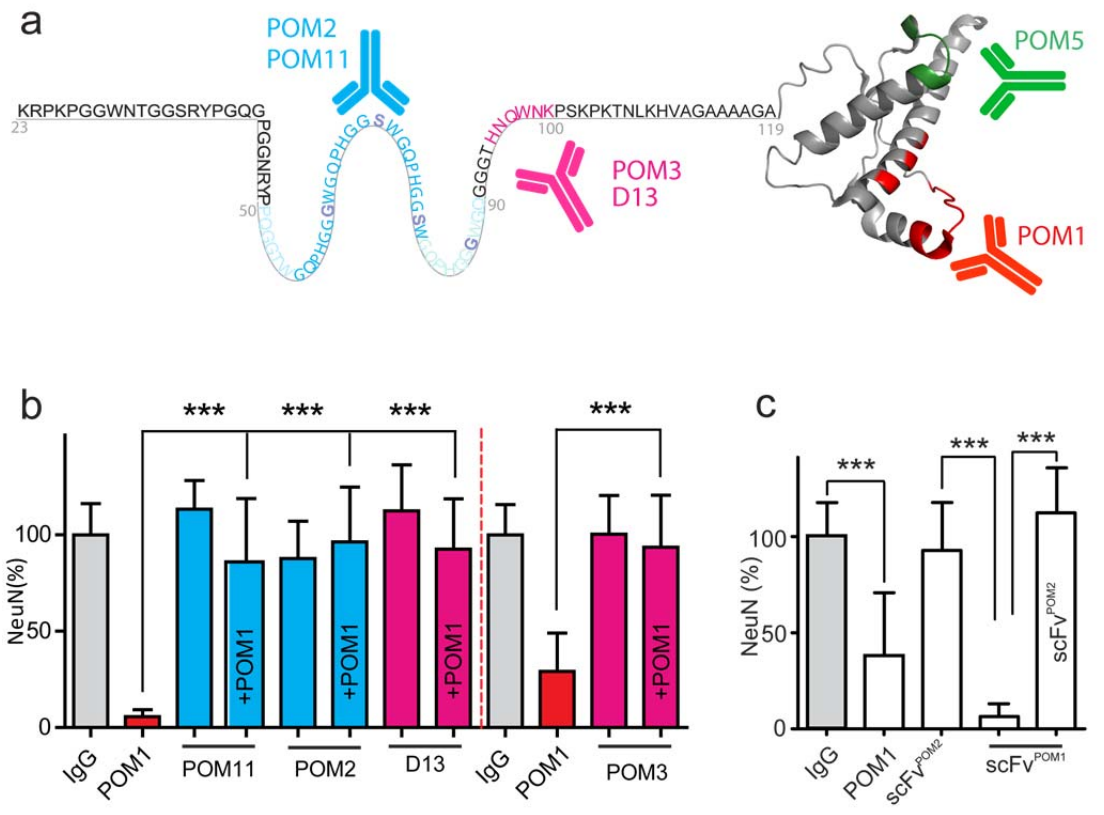

Figure 3.12. ***Antibodies targeting the FT protect against POM1-mediated toxicity. a****) Schematic illustration of the PrP binding sites of antibodies used for pre-treatment experiments.* ***b****) Tga20 COCS were exposed to POM1 after pre-treatment with POM11, POM2, POM3, or D13. NeuN morphometry was performed at 14 dpe. All antibodies targeting the FT of PrP (OR and CC2) prevented POM1 toxicity.* ***c****) Pre-treatment with scFv^{POM2} protected tga20 COCS from scFv^{POM1} toxicity.* ***d****) Pre-treatment with POM5 did not protect tga20 COCS from POM1 toxicity.*

These results reveal a complex scenario for antibodies against the CC2, as they can lead to two opposite outcomes depending on the concentration of the antibody used: neuroprotective against GD antibodies at lower concentrations and neurotoxic when used at higher doses (Figures 3.1b and 3.12b).

Since PrP is around 37KDa in size and the antibodies are around 150KDa, to exclude that steric hindrance was the reason for such a protective effect, we designed the following two experiments. In the first approach, we made use of single chain antibodies (6 times smaller

in size than the holo antibody). Pre-incubation with POM2 single chain fragment (ScFvPOM2, generated by Mridula Swayampakula) conferred neuroprotection against toxicity caused by ScFvPOM1 (Figure 3.12c). In a second approach, *tga20* COCS were pre-incubated with a non-toxic GD antibody, POM5, which binds a distinct epitope on β2-α2 and does not compete with POM1 binding as shown by SPR experiments (Polymenidou et al., 2008). Pre-incubation with POM5 did not rescue POM1 toxicity, indicating that blocking the OR or CC2 region of the FT is crucial for the neuroprotection, and is not dependent on steric hindrance (Figure 3.12d). Sandwich enzyme-linked immunoassays and fluorescence resonance energy transfer assays showed that POM2 or POM3 did not sterically hinder POM1 binding (Falsig et al., 2012; Polymenidou et al., 2008), supporting these findings.

Antibodies targeting the FT are neuroprotective against prion infections and neurotoxic PrP deletion mutants devoid of the central domain

To investigate whether the FT also mediates neurodegeneration in prion infections, *tga20* COCS were infected with prions (RML strain) and treated with POM2. While the IgG treated COCS showed neuronal loss by 44 dpi, no toxicity was observed in POM2-treated COCS (n=18, $p<0.001$, Figure 3.13a).

We then studied the effects of POM2 on PrP^{Sc} aggregation by western blotting after PK digestion. RML-infected COCS were exposed to IgG or POM2, harvested at 35 dpi, PK-treated, and analysed by western blots. POM2 slightly reduced PrP^{Sc} deposition (Figure 3.13b), indicating that protection was not due to a dramatic decrease of PrP^{Sc} accumulation.

Therefore, we asked whether POM2 exerted its neuroprotective effect by decreasing infectivity. In collaboration with Li Bei, we performed SCEPA on RML-infected COCS in the experimental conditions outlined above to measure prion infectivity levels and found that POM2 did not significantly affect prion titers (Figure 3.13c). These findings suggest that FT blockade is crucial to rescue not only GD antibody- but also prion-induced neurotoxicity; however, it does not impact prion replication and PrP^{Sc} deposition.

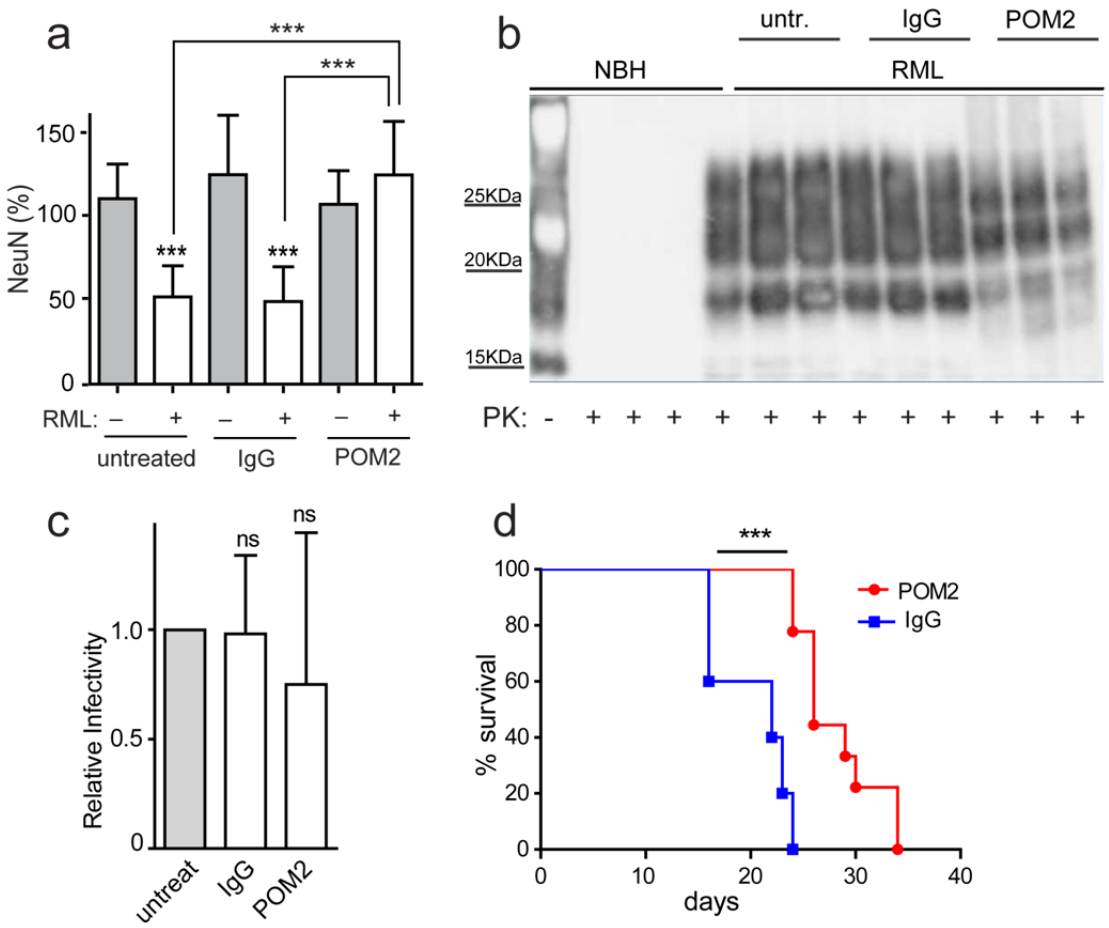

Figure 3.13. ***Antibodies targeting the OR protect against RML- and PrP$_{\Delta 94\text{-}134}$-mediated toxicity. a)*** *Tga20 COCS were exposed to NBH or RML and treated either with IgG or POM2 (335nM; 44 dpi) and stained with NeuN antibody for measurement of viability. POM2 treatment conferred significant neuroprotection against RML infection.* ***b)*** *Samples from a) were loaded after PK digestion. Immunoblots showed that POM2 treatment slightly decreased and changed the pattern of PK-resistant material.* ***c)*** *SCEPA of slice homogenates treated as in a. Data are indicated as infectious units ± SD.* ***d)*** *Survival of mice expressing the PrP$_{\Delta 94\text{-}134}$ transgene was prolonged by intraventricular POM2 treatment (4 μg).*

To investigate the neuroprotective effect of POM2 in a third model of PrP-dependent toxicity, we asked whether POM2 would ameliorate the phenotype of the toxic PrP mutant, PrP$_{\Delta 94\text{-}134}$, still retaining the POM2-binding site (Baumann et al., 2007). A single intraventricular injection to newborn mice (P0) resulted in a significant increase in the median survival after POM2 treatment (26 days, *n*=9) compared to the IgG control injection (22 days, *n*=5) (Figure 3.13d), suggesting that the FT is also mechanistically involved in the neurotoxicity of PrP deletion mutants (in collaboration with Tracy O'Connor).

COPPER INVOLVEMENT IN ANTIBODY-MEDIATED TOXICITY REMAINS UNCLEAR

We have shown that the lack of the region 32-93 (including the OR) blocks GD antibody toxicity. The OR of PrP contains four binding sites for copper; however, the biological relevance of it is still unclear (Mitteregger et al., 2009; Sigurdsson et al., 2003). Also, free copper is toxic to cells because it catalyses the production of ROS (Fenton reaction) (Jomova et al., 2010) and we have shown that extracellular ROS are involved in POM1 induced toxicity (chapter IV). One possibility is that POM1 binding interferes with copper binding and copper then catalyses ROS production. Therefore, we asked whether POM1-induced neurodegeneration or POM2-mediated neuroprotection was influenced by copper binding to the OR. To investigate this possibility we checked whether 1) copper addition would interfere with POM1-mediated neuronal loss or POM2 neuroprotective effect, 2) copper chelation would prevent or enhance POM1 toxicity.

We first co-incubated COCS with copper salts, $CuSO_4$ and $CuCl_2$, in the presence or absence of POM1 and POM2. $CuSO_4$ significantly protected against POM1, however $CuCl_2$ did not (Figure 3.14a). Also, $CuSO_4$ impeded POM2 protection but $CuCl_2$ did not (Figure 3.14b). We determined that these results concerning copper addition were contradictory and inconclusive. Follow-up experiments are required to convincingly answer this question.

Second, we tested whether blocking copper ions in the media might influence GD antibody toxicity and we co-treated the COCS with different concentrations of the copper chelator D-Penicillamine (D-pen). The horse serum is the only component of the slice culture medium that contains copper at the concentration of 190-247 µg/dl (Bell et al., 1987) corresponding to 30-40µM. Several concentrations of the chelator were used ranging from 10µM to 100-fold higher. However, D-pen did not confer significant neuroprotection at any of the concentrations employed in the experiment (Figure 3.14c). Despite the fact that the OR has a striking affinity for copper ions, since the copper chelator D-penicillamine failed to prevent POM1 toxicity, the interactions of copper with the octarepeats may be irrelevant to POM1-mediated toxicity.

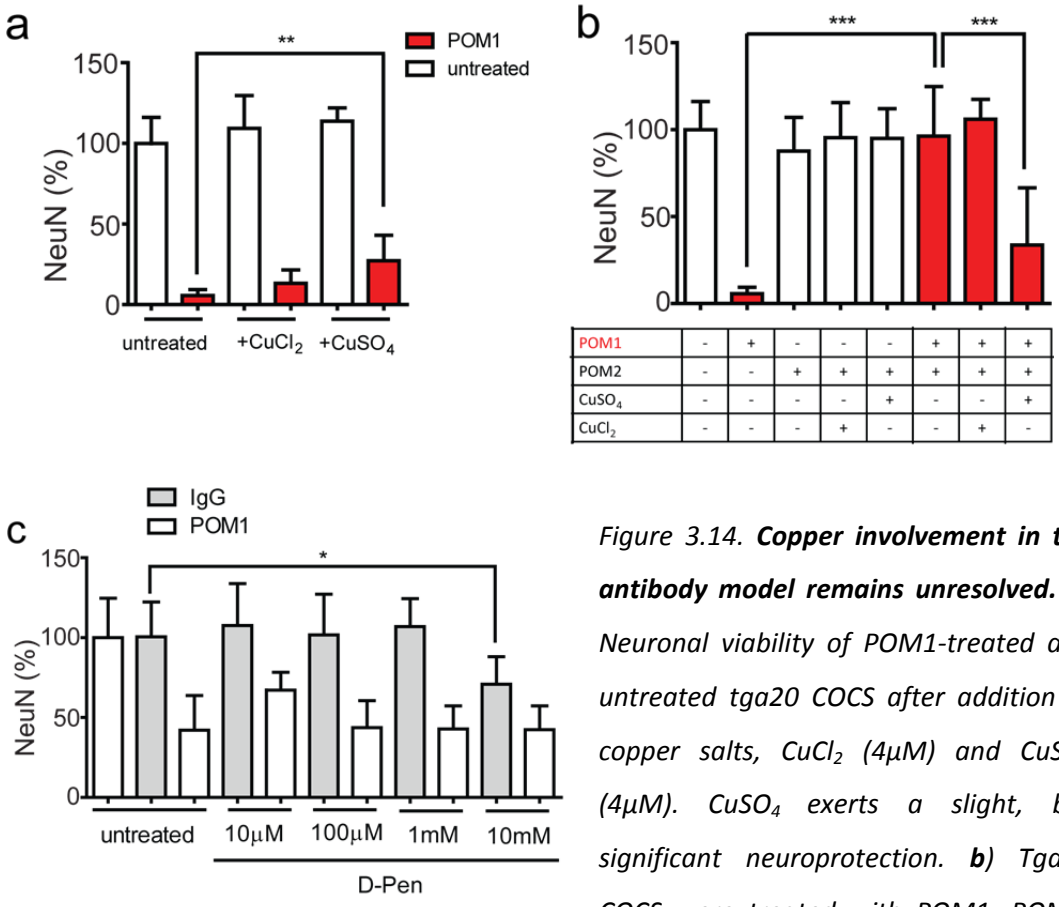

Figure 3.14. ***Copper involvement in the antibody model remains unresolved.*** ***a****) Neuronal viability of POM1-treated and untreated tga20 COCS after addition of copper salts, $CuCl_2$ (4µM) and $CuSO_4$ (4µM). $CuSO_4$ exerts a slight, but significant neuroprotection.* ***b****) Tga20 COCS were treated with POM1, POM2, $CuCl_2$ and $CuSO_4$ according to the table below the graph; (+) presence and (-) absence of those components. POM1 treatment is indicated in red. Co-treatment with $CuCl_2$ prevents the POM2 neuroprotective effect, whereas $CuSO_4$ does not.* ***c****) Various concentrations of D-pen did not diminish POM1 neurotoxicity in tga20 COCS.*

The potent anti-prion compound -PPS- does not block POM1-mediated toxicity

PPS was shown to largely delay prion disease onset in mice (Doh-ura et al., 2004), and *in vitro* studies indicated that PPS exerts this activity by binding to the OR (Taubner et al., 2010). Co-treatment of COCS with PPS did not protect against POM1-mediated neuronal loss (Figure 3.15), in contrast to prion infections (Falsig et al., 2012). Follow-up experiments using different conditions i.e. higher concentrations or pre-treatment will confirm these findings. Remarkably, we have shown that PPS strongly decreased neuronal loss, infectivity, PrP aggregation, and PK resistance in prion-infected COCS, suggesting that its neuroprotective effect is exerted by acting on prion replication (Falsig et al., 2012). This would explain why PPS does not protect against GD antibody-mediated toxicity, as it is possible that the toxicity mediated by GD binding acts downstream of prion replication.

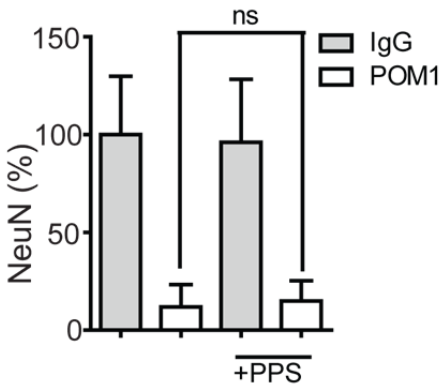

Figure 3.15: ***PPS did not block POM1-mediated toxicity.*** *IgG- and POM1-treated tga20 COCS were co-incubated with PPS (5µg/ml) for 14 days. No neuroprotection was observed in the presence of PPS.*

DISCUSSION AND OUTLOOK

THE FT AS A NEUROTOXIC TRANSDUCER MOIETY?

PrP-deficient mice expressing $PrP_{\Delta 32\text{-}93}$, which lack a large portion of the FT including the OR, have a longer survival curve, lower prion titers, and no histopathological changes when prion infected (Flechsig et al., 2000). Interestingly, these deletion mutants are resistant to GD antibody toxicity (Figures 310b and 3.11). In addition to the rescue effect against POM1 toxicity, these mice still replicate prions but do not show signs of pathology. These data suggest that the PrP region 32-93 uncouples prion toxicity from prion replication and plays an important role in prion-mediated neurodegeneration.

Since a large deletion of the FT and pre-treatment with FT antibodies prevented PrP-dependent neurodegeneration, we concluded that toxic GD antibodies and smaller derivatives utilize the FT to mediate toxicity.

Moreover, we have shown that the FT is also the effector domain of toxicity in two other models, as blockade of the FT *via* FT antibodies suppressed neurodegeneration in prion-infected COCS and prolonged the life of mice expressing a toxic truncated variant of PrP ($PrP_{\Delta 94\text{-}134}$).

Furthermore, many PrP mutants with a large deletion of the FT, including the HC, develop a neurotoxic phenotype (Shmerling et al., 1998) and mice with smaller deletions encompassing the HC manifest a more severe phenotype (Baumann et al., 2007; Li et al., 2007). Why should a smaller deletion trigger more toxicity? Given our data about the FT as the effector domain of toxicity, one could speculate that a larger deletion of the FT leads to a less toxic phenotype because the effector domain of toxicity (OR and CC2) is missing.

However, as already mentioned in the introductory section, the FT region of PrP has been given a thorough range of functions, including neuroprotection (Beland and Roucou, 2012). Supporting this view, PrP undergoes proteolysis physiologically, with release of N1 (residues 23-90) that exhibited protective effects *in vivo* and *in vitro* (Guillot-Sestier et al., 2009). Furthermore, unpaired cleavage of certain deletion mutants strongly correlates with chronic peripheral demyelination (Bremer et al., 2010), and fusion of the FT with the toxic doppel, the C-terminal paralog of PrP, was beneficial in mice (Baumann et al., 2009; Yoshikawa et al., 2008).

These data suggest an important role of the FT in neuroprotection; however, one could speculate that the FT exerts its neurotoxic effects when it is in a constrained conformation

and/or in closer vicinity to the membrane. In support of this hypothesis, mice expressing the FT fused to the GPI anchor (NGPI mice, $PrP_{\Delta 141-231}$), manifest dramatic neuronal loss (Paolo Dametto unpublished).

Interestingly, neurodegeneration observed in mice and humans with OR insertional mutations (Chiesa et al., 1998; Krasemann et al., 1995; Mead et al., 2006; Vital et al., 1999) may be triggered by similar mechanisms since we found that removal of a region encompassing the OR counteracts GD antibody toxicity. It is plausible that elongation of the FT may lead to derangements at the cell membrane and intracellular signals of cell death. In such a case, blockade of the FT *via* specific ligands may be a potential therapy for these people.

Biophysical mechanisms leading to cell death remain uncovered and there are several explanations for the role of the FT as transducer of toxicity. First is the possibility that prions/GD ligands or a toxic conformer of PrP may displace survival partners or enhance interaction with toxic signalling proteins. This is supported by the long list of interaction partners connected with PrP and the various biological functions associated with them (Aguzzi et al., 2008). Second is that pathology is triggered by loss of function as toxic phenotypes of PrP mutants may be explained by adopting an altered conformation (Baumann et al., 2007; Li et al., 2007; Shmerling et al., 1998). The third possibility is that altered PrP topology causes toxicity and this is supported by the toxic topological variants, PrP^{ctm} and PrP^{Ntm}, associated with neurodegeneration (Hegde et al., 1998). Fourth is that the formation of a pore in the membrane through contact of the FT with the membrane leads to sustained altered membrane potential and cell death, as suggested by altered and unspecific currents displayed by PrP mutant cells (lacking the HC) (Solomon et al., 2010; Solomon et al., 2011). Fifth is altered cellular trafficking supported by evidence that accumulation of PrP in the cytosol causes toxicity (Rane et al., 2008). Sixth is disruption of the physiological complex of homo-prion protein complex, which is supported by biochemical evidence that PrP exists physiologically as a homo-complex (Calella et al. drafted manuscript). This emerging view that PrP may exist as a multimeric functional complex (perhaps acting as a channel) and that anti-PrP antibodies may disrupt such complex and therefore trigger death (Calella et al. drafted) is very appealing and is supported by some biochemical results. Perhaps studies utilizing high resolution microscopy, such as TIRF microscopy that has the advantage to have the highest resolution at the cell surface (Suzuki et al., 2012), may confirm such an incredible discovery.

DIFFERENTIAL TOXICITY OF ANTIBODIES

The literature reports controversial findings about the safety of immunization therapies (Klöhn et al., 2012; Solforosi et al., 2004), however our data obtained in COCS and in mice confirm that certain anti-PrP antibodies are toxic. Furthermore, our results clarify that D13, whose toxicity is debated, (Klöhn et al., 2012; Solforosi et al., 2004) is neurotoxic and reasons for such discrepancies in toxicity may be due to the doses used, as they were close to the minimal toxic concentration. Such findings raise many questions about the safety of anti-PrP antibodies and indicate that dose-escalation studies will be required when considering prion immunotherapies. While we confirm D13 toxicity (Solforosi et al., 2004), our findings on monovalent antibodies also leading to neuronal death suggest that antibody-induced crosslinking of PrP at the cell surface is unlikely to be the mode of cell death and that different mechanisms may play a role (as speculated in the previous paragraph).

Importantly, we have identified the residues mediating the binding between PrP and POM1, encompassing helices α1, α3 and β1-sheet, suggesting that at least one of these residues and possibly its neighbouring interactions are involved in prion-dependent neurotoxicity. Subtle β1-β2 shifts of PrP upon POM1 binding displayed by NMR analyses remain of unclear significance and only carrying out in-depth studies of the binding interface between various antibody-complementarity-determining regions (CDRs) and rmPrP will clarify structural determinants triggering prion pathogenesis. In particular, detailed epitope mapping of the antibodies binding to helix1 (POM13, 15, 17) and helix1-2 (POM6, 7, 8, 9) will clarify differential toxicity of these antibodies.

Existing data on NMR and X-ray analyses of the POM-rmPrP complex will also give information about conformational changes and overlapping and non-overlapping binding interfaces and this information will be a fundamental guide for targeted therapeutic drug design. These studies are ongoing in our laboratory (Dr. Simone Hornemann) and in collaboration with Dr. Michael James and his group at the University of Alberta, Edmonton, Canada. Based on the already available NMR and X-ray data, small cyclic peptides mimicking the interaction region between PrP and POM1 will be designed and tested in our system in order to obtain further insights into the structural properties of this interaction, narrowing down regions mediating toxicity. Furthermore, a randomized library (provided by Lilly Company) will be screened using POM pairs conjugated to APC and Europium in our robotic FRET-platform in order to identify compounds competing with the POM1 binding site and to explore their potential use as therapeutics.

CHAPTER IV

SIGNALLING PATHWAYS INVOLVED IN PRION-MEDIATED NEURONAL DEATH

This chapter contains unpublished data as well as parts that are adapted or reproduced from the following manuscript accepted by Nature on the 21st of June 2013 and assigned the DOI 10.1038/nature12402:

The toxicity of antiprion antibodies is mediated by the flexible tail of the prion protein

Tiziana Sonati[1,*], Regina R. Reimann[1,*], Jeppe Falsig[1,*], Pravas Kumar Baral[2], Tracy O'Connor[1], Simone Hornemann[1], Sine Yaganoglu[1], Bei Li[1], Uli S. Herrmann[1], Barbara Wieland[2], Mridula Swayampakula[2], Muhammad Hafizur Rahman[3], Dipankar Das[3], Nat Kav[3], Roland Riek[4], Pawel P. Liberski[5], Michael N. G. James[2], and Adriano Aguzzi[1†]

[1] Institute of Neuropathology, University Hospital Zurich, Switzerland
[2] Department of Biochemistry, University of Alberta, Canada
[3] Department of Agricultural, Food and Nutritional Science, University of Alberta, Canada
[4] ETH Zurich, Physical Chemistry, ETH Honggerberg, 8093 Zurich, Switzerland
[5] Laboratory of Electron Microscopy and Neuropathology, Department of Molecular Pathology and Neuropathology, Medical University of Lodz, Lodz, Poland.
[*] These authors contributed equally to this work

[†] Corresponding author: Adriano Aguzzi; Institute of Neuropathology, University Hospital of Zurich; Schmelzbergstrasse 12, CH-8091 Zurich, Switzerland; Tel: +41-44-255-2108, Email address: adriano.aguzzi@usz.ch

INTRODUCTION

PRP IN CELLULAR SIGNALING

Due to PrP^c's extracellular localization, many efforts have been invested to identify potential interacting partners involved in cellular signalling. The interaction of PrP^c-NCAM has been determined to activate Fyn-dependent neurite outgrowth (Santuccione et al., 2005), while the extracellular matrix protein laminin has been shown to stimulate neurite outgrowth upon interaction with PrP^c (Graner et al., 2000) and promote memory consolidation through PKA and ERK-dependent pathways (Coitinho et al., 2006). Sti1, a soluble factor released by astrocytes, has also been proposed to interact with PrP^c and induce neuroprotection and neuritogenesis through PKA and ERK signalling (Lopes et al., 2005; Martins et al., 2010).

Recently, PrP has been identified as a receptor for amyloids; however, whether PrP mediates impairment of synaptic plasticity in Alzheimer's disease models is still debated (Balducci et al., 2010; Calella et al., 2010; Gimbel et al., 2010; Kessels et al., 2010; Lauren et al., 2009; You et al., 2012).

Investigations in various prion models confirmed the role of PrP in the regulation of the MAPK pathway (Chiarini et al., 2002; Krebs et al., 2006; Lee et al., 2005; Monnet et al., 2004; Mouillet-Richard et al., 2000; Nixon, 2005; Uppington and Brown, 2008). Congruently, bioinformatic studies, which made use of approximately 50 interacting partners identified for PrP by protein microarray analyses, indicated that PrP is part of the AKT, JNK, and MAPK signalling network (Satoh et al., 2009). Additionally, biochemical studies displayed reduced AKT activation, and enhanced ERK1/ERK2, STAT1, and caspase 3 activity in $Prnp^{0/0}$ brains when exposed to ischemic insults in comparison to *wt* and *tga20* mice (Spudich et al., 2005; Weise et al., 2006). Stimulation of PrP with anti-PrP antibodies in various cell lines led to Fyn-dependent hyperactivation of ERK, which correlated with NADPH-mediated ROS generation (Pietri et al., 2006).

Other pathways that may involve PrP include the activation of PKC and cAMP/PKA, which were suggested by studies of the effects of recombinant PrP on embryonic rat hippocampal neurons and of PrP^C-binding peptides, respectively (Chiarini et al., 2002; Kanaani et al., 2005). Furthermore, a role of PrP in calcium-dependent cellular signalling has been proposed since abnormal calcium responses were found in neuroblastoma cell lines (Kristensson et al., 1993) and neurophysiological studies on $Prnp^{0/0}$ mice revealed alterations in calcium homeostasis (Fuhrmann et al., 2006; Herms et al., 2000).

All of these findings suggest a role of PrP in different signalling pathways; however, prion infected cell lines or cell lines treated with anti-PrP antibodies do not show signs of toxicity, presenting a major limitation in identifying effector molecules activated in prion-mediated neuronal death in primary cultures.

CASPASE INVOLVEMENT IN PRION PATHOLOGY

It is still debated if apoptosis, necrosis, autophagy or a combination of them is leading to cell death in neurodegenerative disorders. Apoptosis is a programmed mode of cell death that is accompanied by DNA fragmentation, cell shrinkage, and formation of apoptotic bodies. It is biochemically characterized by activation of the caspase cascade, which includes caspase-3, 7, and 6 as the main effector caspases (Yuan et al., 2003). In this process, activation of the pro-apoptotic molecule Bax leads to increased mitochondrial permeability and release of cytochrome c to the cytoplasm. Subsequently, caspases are activated by an increase of cytosolic calcium levels (Yuan et al., 2003). Binding of anti-apoptotic Bcl-2 to Bax prevents these events and subsequent release of pro-apoptotic molecules.

An apoptotic mode of cell death mediated by caspase activation has been described in humans and in animal models of prion diseases (Kovacs and Budka, 2010; Liberski et al., 2004). Bax and Bcl-2 involvement has been shown in mice expressing modified forms of PrP (Chiesa et al., 2005; Li et al., 2007; Nicolas et al., 2007). Specifically, PrP mutants with a nine-octapeptide repeat insertion (PG14) (Chiesa et al., 1998), similar to the human genetic variant of prion disease (Krasemann et al., 1995; Mead et al., 2006; Vital et al., 1999), show Bax-dependent CGC loss with no pathology in the white matter (Chiesa et al., 2005). Deletion of Bax also blocked CGC loss in $PrP_{\Delta 32\text{-}134}$ mice, but not in the toxic mutant $PrP_{\Delta 105\text{-}125}$ (Li et al., 2007). Similarly, Bcl-2 overexpression reduced and delayed caspase-3 activation, CGC loss, and p53 activation in $PrP_{\Delta 32\text{-}134}$ mice (Nicolas et al., 2007). Hence, whereas PG14 and $PrP_{\Delta 32\text{-}134}$ showed a Bax-dependent CGC loss, $PrP_{\Delta 105\text{-}125}$ exhibited a caspase-independent, non-apoptotic CGC death (Christensen et al., 2010a), suggesting that Bax-dependent neuronal death is not always used in PrP mutant-mediated neurodegeneration. Furthermore, Bax ablation and Bcl-2 overexpression are not neuroprotective against prion toxicity *in vivo* (Steele et al., 2007), excluding a crucial involvement of Bax- and Bcl2-mediated apoptosis in prion pathogenesis.

However, Caspase 12 cleavage is connected with ER stress and has a role in prion diseases (Hetz et al., 2003; Moreno et al., 2012); nevertheless, caspase-12 deficiency does not delay

prion disease onset (Steele et al., 2007). Thus, the role of caspases in prion diseases remains ambiguous and requires further examination.

EMERGING ROLE OF CALPAINS IN NEURODEGENERATIVE DISORDERS

Calpains are cytoplasmic cysteine proteases that are activated by calcium, active at neutral pH, and belong to a superfamily ubiquitously expressed in a wide variety of organisms (Suzuki et al., 2004). The best characterized calpain family members are calpain 1 and calpain 2, which are heterodimers that include an identical 28kDa subunit and a large 80kDa subunit with approximately 50% sequence homology. Calpain 1 (or μ-calpain) and calpain 2 (or m-calpain) differ in the calcium concentration required for their activation (micro and millimolar, respectively), and in their cellular localization; calpain 1 is cytosolic or located near to the membrane, whereas calpain 2 is expressed at the plasma membrane. Their activity is regulated by the endogenous specific inhibitor calpastatin. Under physiological conditions in the CNS, calpains may be involved in cytoskeleton remodelling, LTP, and memory (Liu et al., 2008). However, their hyperactivation, and consequently the loss of calcium homeostasis, accompanies several neurodegenerative diseases such as Alzheimer's disease, Parkinson's disease, and Huntington's disease. A dysregulation of calpain activity leads to increased cleavage of many cellular proteins and ultimately results in neuronal death (Liu et al., 2008). Calpain-mediated proteolysis has been shown in necrotic and apoptotic conditions, while caspase 3 is only implicated in neuronal apoptosis (Wang, 2000). Specific to prion diseases, calpains were reported to affect PrP proteolysis since calpain inhibition decreased the levels of C2, a predominant cleavage product in prion-infected cell cultures (Yadavalli et al., 2004). Furthermore, activation of m-calpain was found in the hippocampus of prion-infected mice (Gray, 2006). Only recently, our work has uncovered a causal role of calpains in prion-mediated neuronal death (Falsig et al., 2012).

OUTLINE OF THIS WORK

Neuronal loss is one of the hallmarks of prion diseases; however, molecular determinants of the signalling cascade leading to neuronal death are still unknown. Progress has been hampered by the lack of good *in vitro* models because prion-infected cell lines replicate prions, but do not show signs of toxicity. Here, I report our findings using two models for studying prion-mediated cell death. The majority of the results will be about signalling pathways activated upon anti-PrP antibody-binding to PrP. Each of the results will then be compared to those in genuine prion infections obtained in collaboration with Dr. Jeppe Falsig. Remarkably, many similarities have been found when comparing the two models, suggesting that anti-PrP antibody-driven cell death is a powerful model to investigate prion pathophysiology.

Our recent findings in prion-infected and antibody-treated COCS identified calpains and not caspases, as effectors of prion toxicity, which supports macroscopic morphological analyses that describe an atypical apoptotic mode of cell death in these models (Falsig et al., 2012; Sonati et al., 2013). In particular, we found that the CGC loss occurring in the two models is accompanied by calpain activation and rescued by calpain inhibition, suggesting that abnormal levels of calcium are upstream events of this cascade (Falsig et al., 2012; Sonati et al., 2013).

We uncovered a causal role of radical oxygen species (ROS) to prion pathogenesis and among the ROS species, we specifically identified an involvement of superoxide species (Sonati et al., 2013). Interestingly, ablation of the cellular ROS-generator NADPH NOX2 enzyme alleviated neuronal damage, identifying one of the cellular sources of ROS contributing to prion-mediated cell death (Sonati et al., 2013).

Pharmacological screenings failed to identify any involvement of excitotoxic pathways in both models and these results, on one hand support similarities of these models and on the other hand will need further evaluations.

RESULTS

ULTRASTRUCTURAL ANALYSES OF ANTIBODY-TREATED COCS

To gain insights into the macroscopic morphological changes occurring upon antibody treatment, IgG- and POM1-treated *tga20* COCS were analysed by electron microscopy. Ultrastructural analyses revealed an atypical apoptotic cell death (non-necrotic) in POM1-treated samples, which was similarly described for mice expressing a truncated version of PrP lacking the HC (Christensen et al., 2010b). Upon POM1 treatment, the granular cell layer (GCL) exhibited an increase of pyknotic cells over time with shrunken cell bodies; however, an intact membrane was present without blebs or rupture of the cell bodies (Figure 4.1b-c). Degenerating CGCs containing small, irregular, and disperse condensed chromatin appeared at 3 dpe and peaked at 7 dpe of POM1 treatment in comparison to IgG treated COCS that showed healthy morphology of CGCs (Figure 4.1a-d).

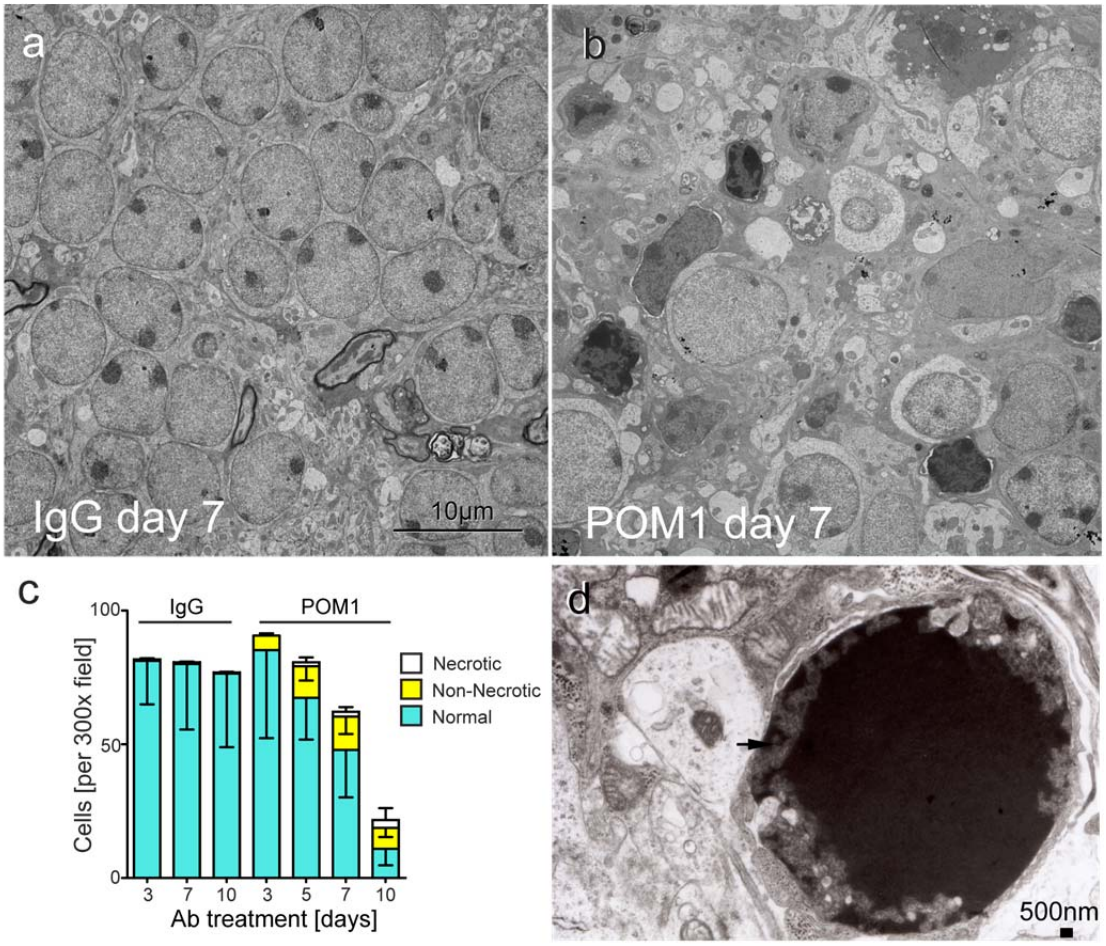

Figure 4.1. ***EM of antibody treated COCS reveals features of prion diseases. a-d****) COCS were treated with POM1 or IgG for 7 days at 67 nM and analysed by electron microscopy.* ***a****) IgG-treated cultures exhibited healthy cell morphology at 7 dpe.* ***b****) After POM1 treatment, many*

CGCs displayed irregular and condensed nuclear chromatin. ***c****) Number of cells exhibiting normal, non-necrotic, or necrotic morphology upon IgG and POM1 treatment at different time points (3, 5, 7, 10 dpe).* ***d****) High magnification of nuclear chromatin condensation in POM1-treated COCS.*

Moreover, in POM1-treated COCS Prof. Liberski identified myelinated vacuoles reminiscent of prion-induced spongiosis (Figure 4.2a), nerve terminals with branching cisterns (Figure 4.2b), and dystrophic neurites containing autophagic vacuoles (Figure 4.2c) similar to those found in infected-neuronal cells, prion-infected COCS, as well as human brain biopsies (Heiseke et al., 2010; Liberski et al., 2008; Schatzl et al., 1997).

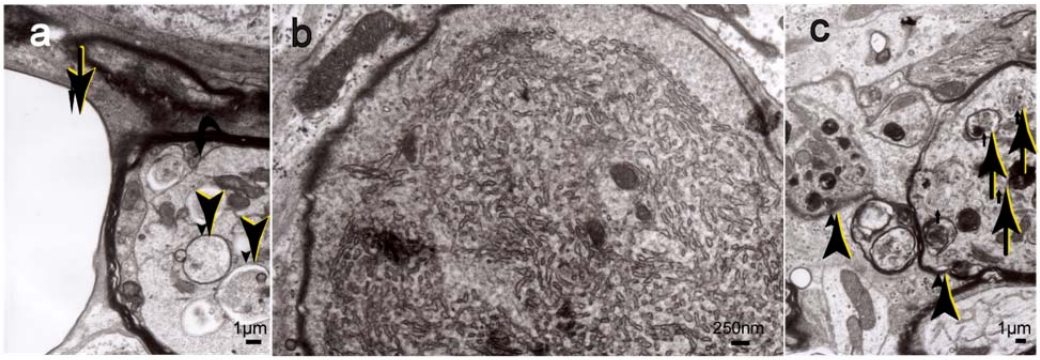

Figure 4.2. ***EM analysis depicts morphological features typical of prion diseases****.* ***a-c)*** *COCS treated with POM1 or IgG for 7 days and analysed by electron microscopy exhibited vacuolation (a), intraneuritic branching cisterns (b) and dystrophic neurites (arrowheads) containing autophagic vacuoles at various stages (arrows) (c). Magnification x8'300.*

CALPAINS AND NOT CASPASES ARE THE MAIN EFFECTORS OF GD LIGAND-MEDIATED CELL DEATH AS IN PRION INFECTIONS

We have recently identified that prion-infected COCS undergo neuronal death in a calpain-dependent manner, as calpain inhibitors and protease inhibitors prevented prion-dependent neurotoxicity (Falsig et al., 2012). In contrast, a wide range of different caspase inhibitors (z-DEVD-fmk and z-VAD-fmk) were not neuroprotective (Falsig et al., 2012). Persistent activation of calpains, triggered by elevated calcium levels, leads to calpain activation and degradation of many intracellular substrates crucial for cellular function and survival. Hence, enhanced calpain proteolysis was confirmed by biochemical assays (Falsig et al., 2012).

To investigate whether similar mechanisms were activated upon POM1-treatment, we targeted caspases and calpains pharmacologically. *Tga20* COCS were exposed to POM1 antibody or IgG as control and co-treated with caspase or calpain inhibitors for the entire duration of antibody treatment. Similar to prion-infected COCS, targeting calpains with calpeptin resulted in complete neuroprotection, whereas caspase inhibition (by z-VAD-fmk) did not suffice to rescue POM1- mediated neuronal death (Figure 4.3a, POM1 treatment upper panel, RML-infection lower panel). Accordingly, inhibition of the mitochondrial membrane permeability transition pore (using Methazolamide and Ciclosporine A), which regulates cytochrome c release and caspase activation, did not protect against POM1-induced neurodegeneration, as was also observed in prion-infected COCS (Figure 4.3a). None of the compounds affected the viability of IgG-treated COCS (Figure 4.3b IgG upper panel) or in longer treatments of control COCS with non-infected brain homogenate (NBH) (Figure 4.3b NBH lower panel).

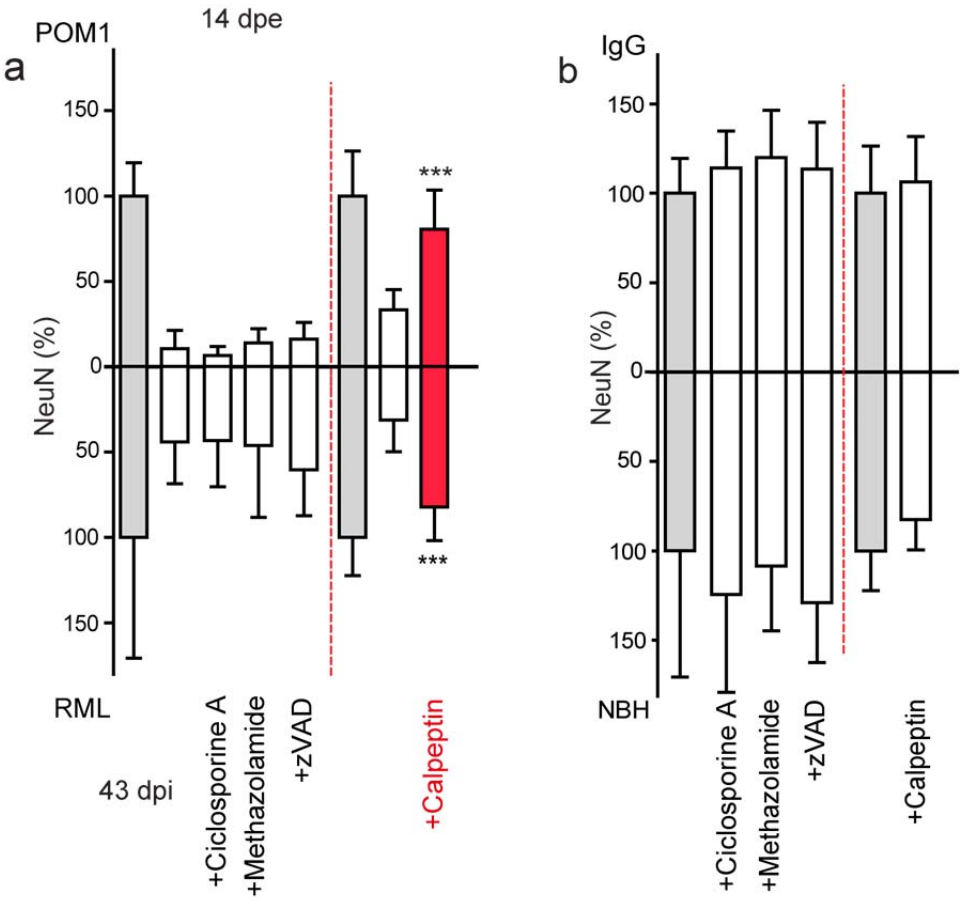

Figure 4.3. ***Pharmacological inhibition of calpains, but not of caspases confers neuroprotection against RML- and POM1-mediated neurotoxicity. a****) Tga20 COCS were*

treated after 14 days with POM1 and co-incubated with tool compounds for 14 days (upper panel. RML infected tga20 COCS were incubated after prion inoculation (21 dpi) and then exposed to certain tool compounds for 14 days before harvest (lower panel). Concentrations of tool compounds used here and henceforth are summarized in Table 4.1. Indicated in red are compounds which conferred protection in both models. ***b****) Experimental conditions as in a. None of the compounds reduced viability of control IgG or NBH-treated COCS as assessed by NeuN morphometry. Grey bars: IgG- or NBH-exposed COCS. White bars: POM1 or RML exposure treated with tool compounds as indicated below the graph.*

We then examined calpain activity by looking at αfodrin-proteolysis, which results in distinct breakdown products 150, 145KDa and 150, 120KDa bands, specific of calpain- and caspase-cleavage, respectively (Miura et al., 2006; Wang, 2000).

Tga20 slices were treated with IgG and scFvPOM1 for 3 days and tissue lysate was analysed by western blot and probed with an antibody against αfodrin. Similar to prion-infected COCS (Falsig et al., 2012), scFvPOM1 treatment induced elevated levels of calpain-induced 150-145kDa fragments, compared to IgG control-treated COCS (Figure 4.4a). To introduce a more stringent negative control than FabIgG, *tga20* COCS were treated with FabPOM1 pre-incubated with $rmPrP_{23-230}$. If the fodrin cleavage observed was strictly PrP-dependent, then pre-incubation of FabPOM1 with the cognate antigen should have blocked it. Indeed, elevated levels of 150-145KDa cleavage products were abolished in COCS treated with FabPOM1 pre-incubated ith rmPrP (Figure 4.4b) and such levels were comparable to FabIgG treatment. Fodrin cleavage was investigated using COCS treated with monovalent antibodies (scFvPOM1 and FabPOM1) for their smaller sizes (25KDa and 50KDa), in contrast to holoantibodies (150KDa) that overlapped with fodrin cleaved fragments (data not shown).

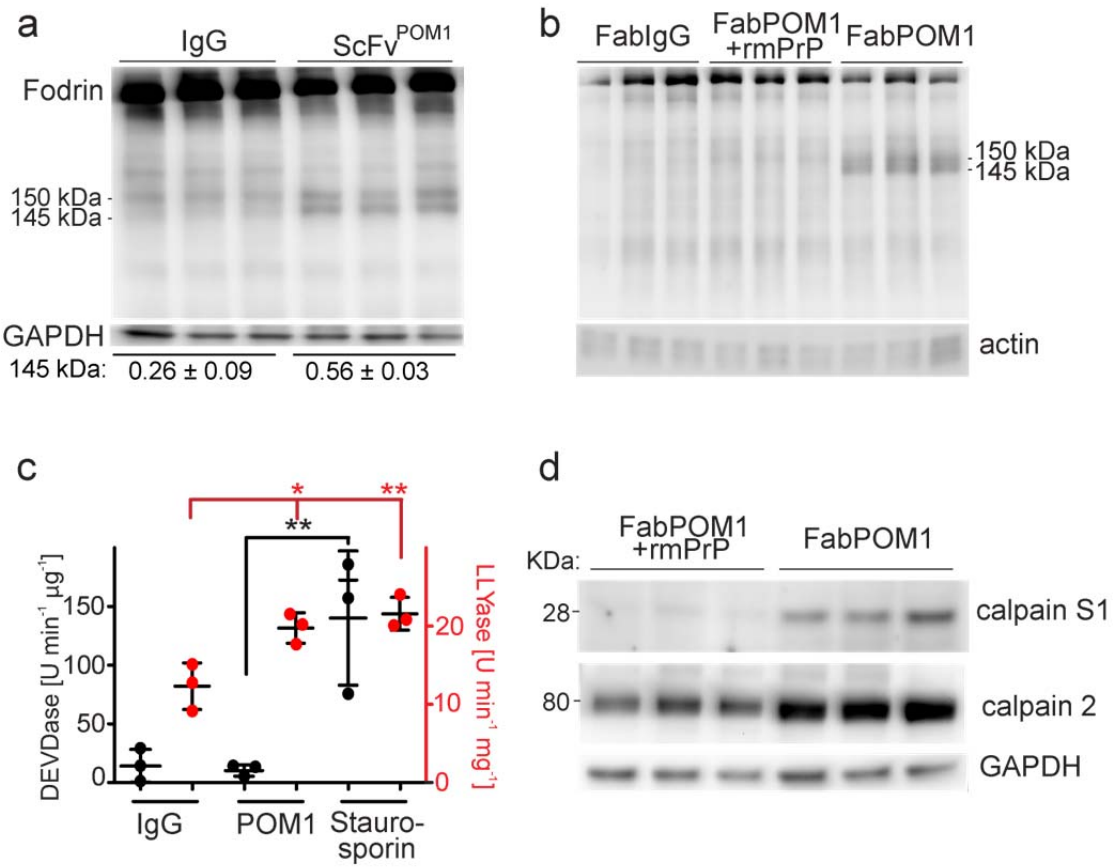

Figure 4.4. ***Calpain activation is confirmed by biochemical read-outs. a****) Western blot of scFvPOM1- or IgG-treated tga20 COCS at 3 dpe probed with anti-fodrin antibody. αfodrin is cleaved by calpains and caspases, generating a common 150KDa fragment, a calpain specific 145KDa and a caspase specific 120KDa cleavage product. ScFvPOM1 treatment induced an increase of the 145KDa fragment, confirming calpain activation. GAPDH was used as a loading control.* ***b****) Western blot of FabPOM1-(67nM) in the presence or absence of* $rmPrP_{23-230}$ *(molar ratio 1:3) and FabIgG- (67nM) treated samples probed with anti-fodrin antibody. GAPDH was used as a loading control.* ***c****) Tga20 COCS were treated for 3 days with IgG and POM1. Staurosporine was used as positive control (24h, 5µM). Fluorescence emitted by cleavage of a specific caspase substrate Ac-DEVD-AMC and a distinct calpain substrate Ac-LLVY-AFC was monitored. POM1 treatment induced significant increase of LLYase activity but not in DEVDase activity.* ***d****) Western blot of FabPOM1- (67nM) treated samples in presence or absence of* $rmPrP_{23-230}$ *(molar ratio 1:3) probed with antibodies against calpain 2 or calpain subunit 1 (S1).*

In order to quantitatively evaluate caspase and calpain activity levels, we used an additional read-out and measured their respective fluorescent cleavable products, Ac-DEVD-AMC and Ac-LLVY-AFC. Hence, we performed these assays in COCS treated with IgG (negative control) and POM1 after 3 days of treatment. Staurosporine was included as positive control because it is known to induce caspase- and calpain-dependent cell death (Miura et al., 2006). DEVDase activity spiked in staurosporine treated COCS, but was not significant between IgG and POM1 treated cultures (Figure 4.4c, black graph). In contrast, POM1 treated COCS exhibited significantly higher levels of LLVYase activity than IgG treated COCS and comparable levels to staurosporine-treated samples (Figure 4.4c, red graph), confirming that calpains are involved.

Calpain 1 and 2 (activated by micromolar or millimolar concentrations of calcium, respectively) are both heterodimers including an identical 28KDa regulatory subunit (calpain small subunit 1) and a large 80-KDa subunit. To look at calpain levels, *tga20* COCS were treated with FabPOM1 (33.5nM) or FabPOM1 pre-incubated with $rmPrP_{23\text{-}230}$ (molar ratio 1:3) for 3 days, and tissue lysate was analysed by western blot probed with antibodies against calpain subunit 1 (small subunit common to calpain 1 and 2) and calpain 2. FabPOM1 treatment showed higher levels of calpain small subunit 1 and calpain 2 when compared to the control FabPOM1 incubated with its cognate antigen (Figure 4.4d), suggesting that calcium overload is in the millimolar concentration range, leading to activation of m-calpains (or calpains 2).

PHARMACOLOGICAL SCREENING DID NOT IDENTIFY THE SOURCE OF PRION-INDUCED CA^{+2} INFLUX

We have shown that POM1 and prion-mediated neurotoxicity occur in a calpain-dependent manner (Falsig et al., 2012; Sonati et al., 2013) and it is well established that a persistent elevation of calpains by calcium leads to calpain activation and degradation of many intracellular substrates crucial for cellular function and survival (Vosler et al., 2008). Therefore, to investigate calcium influx and its cellular source as a proximal cause of calpain activation, we tested many inhibitors of intracellular calcium sources for their ability to interfere with prion-mediated neurotoxicity. First, we blocked receptor-mediated calcium entry by targeting NMDA receptors with MK-801 and AMPA/kainate receptors with CNQX. None of these treatments prevented POM1- mediated cell death (Figure 4.5a).

Next, we targeted the ER stores, which are the main calcium storage centres of the cell. Calcium release from the ER occurs through two major routes: the IP3 receptor and the

ryanodine receptor (Macmillan and McCarron, 2010). We used U73122, an inhibitor of phospholipase C that would block G-protein coupled receptor-induced IP3 generation and release of calcium from IP3Rs in the ER, and Ryanodine and dantrolene to block ryanodine receptors. None of the inhibitors had an effect even when calcium levels where decreased using medium with lower amounts of calcium (LCM) (Figure 4.5b).

A larger screen of potential calcium channels was performed in prion-infected COCS. L-type (nicardipine), P-type (W-agatoxin), and R-type (SNX-482) voltage gated calcium channel inhibitors failed to confer protection in prion infected COCS (Falsig unpublished). T-type channels were not tested because their inhibitors (mibefradil and pimozide) were toxic to COCS (Falsig unpublished). Also, blockade of TRP channels, acid-gated channels, and ER calcium stores did not afford any neuroprotection in prion-infected COCS (Falsig unpublished).

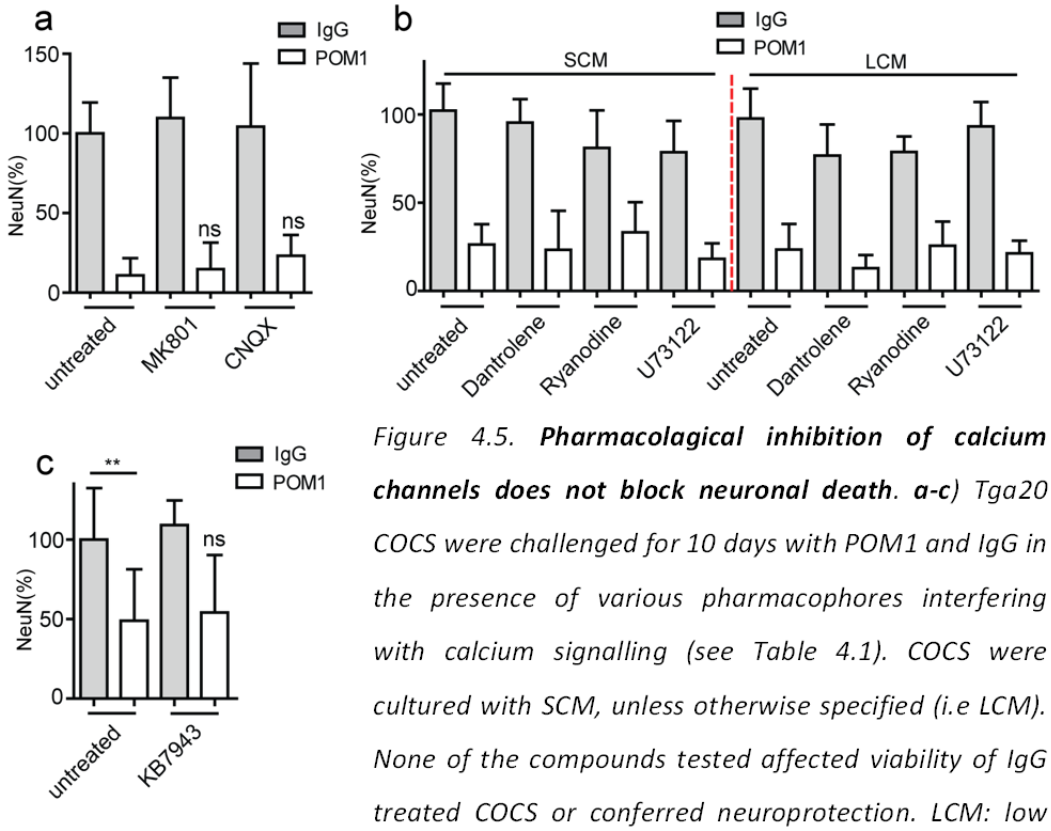

Figure 4.5. ***Pharmacolagical inhibition of calcium channels does not block neuronal death****. **a-c**) Tga20 COCS were challenged for 10 days with POM1 and IgG in the presence of various pharmacophores interfering with calcium signalling (see Table 4.1). COCS were cultured with SCM, unless otherwise specified (i.e LCM). None of the compounds tested affected viability of IgG treated COCS or conferred neuroprotection. LCM: low calcium medium; SCM: slice culture medium.*

Surprisingly, preliminary results showed that inhibition of the sodium/calcium exchanger (NCX3) blocked prion-mediated neuronal loss (Falsig unpublished data). We therefore tested if NCX3 was also involved in POM1-mediated neuronal death. *Tga20* COCS challenged

with POM1 or IgG were co-treated with KB7943 (NCX3 inhibitor), but no beneficial effect was observed at the concentration used (Figure 4.5c).

SUPEROXIDE SPECIES PLAY A MAJOR ROLE IN PRION-MEDIATED NEURODEGENERATION

To investigate if ROS were contributing to neuronal death, we treated *tga20* COCS with POM1 or IgG and co-incubated them with various antioxidants. Interestingly N-acetyl cysteine (a glutathione precursor) and ascorbate, two of the main antioxidants used in cellular defenses (Fatokun et al., 2008), blocked POM1 toxicity (Figure 4.6a). Furthermore, the iNOS inhibitor 1400W (Mander and Brown, 2005) did not exert any protective effect, whereas the superoxide dismutase mimetic MnTBAP (Aarts et al., 2003) prevented POM1-mediated cell death, identifying a role of superoxide production in POM1-mediated toxicity (Figure 4.6a). Resveratrol, a molecule contained in red wine known for its antioxidant properties, did not inhibit antibody mediated toxicity (Figure 4.6c). In contrast, isoascorbate, a membrane-impermeable isomer of ascorbate, was protective, indicating an involvement of extracellular ROS (Figure 4.6d). None of the antioxidants were toxic to IgG-treated COCS (Figure 4.6b-d).

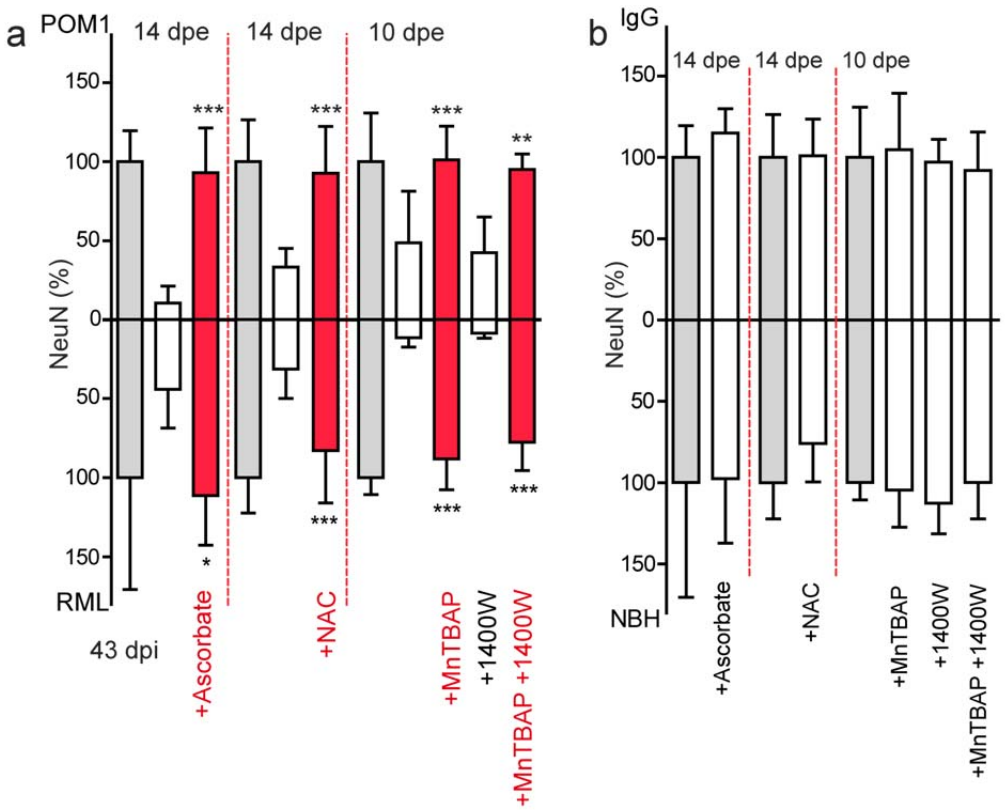

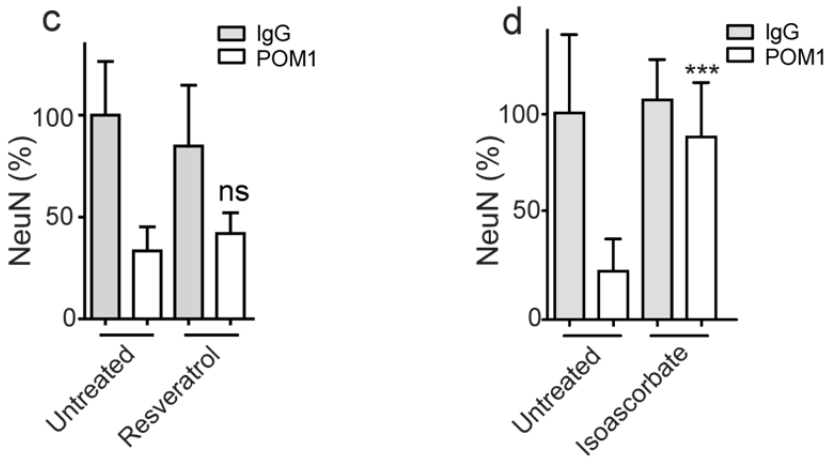

Figure 4.6. ***ROS involvement in prion-mediated neurodegeneration. a****) COCS prepared from tga20 mice were exposed to POM1 (or IgG as control) for 10 days and co-treated with antioxidants. Red bars indicate coumpounds that conferred neuroprotection against POM1 toxicity.* ***b****) Same conditions as in a. None of the compounds were toxic to IgG-treated COCS. Grey: no tool compound added to IgG-treated COCS. White: tool compounds indicated in the figure added to IgG-treatment.* ***c****) Same conditions as in a. Resveratrol was not neuroprotective.* ***d****) Same conditions as in a. Isoascorbate, a cell impermeable analogue of ascorbate, was protective.*

Next we asked if the neuroprotective effect of ascorbate was dose-dependent, so we incubated *tga20* COCS with different concentrations of ascorbate in the range of 20-2500μM. Ascorbate was not significantly protective at 20 μM, but was at 100 μM and higher concentrations (Figure 4.7a).

To exclude the possibility that ascorbate would block antibody-mediated toxicity by affecting antibody stability and its consequent binding to PrP^c, we incubated different concentrations of POM1 (10-1000pg/ml) with high concentrations of ascorbate (50-5000μM) for 2 days at 37°C and performed an ELISA binding assay (Polymenidou et al., 2008). No differences were observed in the binding of POM1 to $rmPrP_{23-230}$ in the presence or absence of ascorbate, excluding any effects of antioxidants on antibody stability (Figure 4.7b).

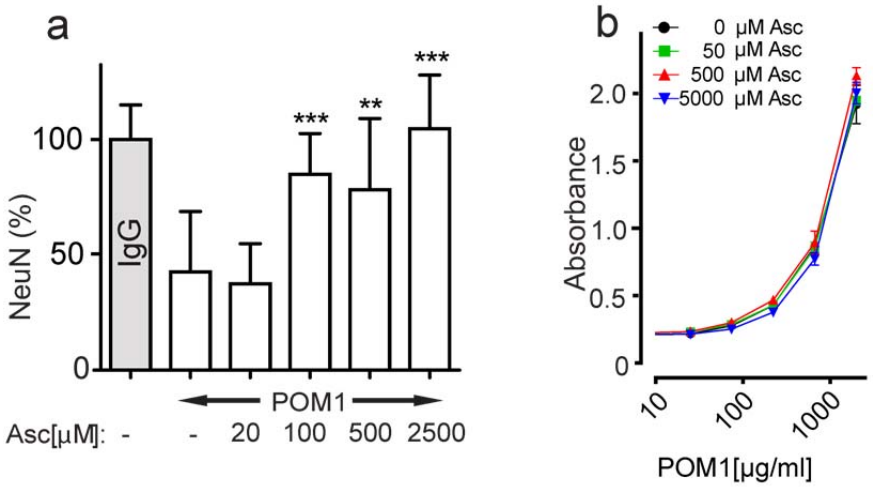

Figure 4.7. ***Ascorbate is neuroprotective in a dose-dependent manner and it does not affect antibody stability.*** ***a****) COCS prepared from tga20 mice were treated with various concentrations of ascorbate and exposed to POM1 for 10 days. Ascorbate was protective at concentrations of 100-2500 µM but not at a concentration of 20 µM.* ***b****) POM1 was incubated with various concentrations of ascorbate for 48h at 37°C. A dilution curve of POM1 binding to rmPrP$_{23-230}$ coated plates was detected with anti-mouse IgG HRP-conjugated secondary antibody by chemiluminescence. The presence of ascorbate did not exert any influence on the binding capacity of POM1.*

Pharmacological approaches identified superoxide as the ROS species involved, and to visualize that superoxide species are indeed generated upon POM1 treatment, extensive efforts were invested in establishing functional assays. Elevated levels of ROS, and in particular superoxide, were measured in POM1-treated COCS compared to IgG-treated controls by diverse assays, such as dihydroethidine (DHE) or tetrazolium salt (Choi et al., 2006; Peshavariya et al., 2007) (Hermann and Falsig unpublished). Additionally, we employed a chemiluminescence assay based on lucigenin conversion in the presence of superoxide. COCS were treated with scFvPOM1 or IgG for 3 days, tissue was homogenized, and lucigenin conversion was measured by chemiluminescence. A significant increase in lucigenin conversion was exhibited by ScFvPOM1 treatment in comparison to IgG COCS and was reversed by short exposure to DPI, a specific NOX2 inhibitor (Figure 4.8a).

NADPH oxidase NOX2 enzymes are one of the main cellular superoxide sources (Sorce and Krause, 2009) and crucially, genetic ablation of NOX2 (Pollock et al., 1995) blocked POM1

toxicity *in vivo* (Sonati et al., 2013). NADPH-dependent ROS production was previously shown (Pietri et al., 2006) and our work demonstrates, for the first time, a role of ROS as promoters of neurotoxicity and especially underlines NADPH oxidase NOX2 enzymes as one of the ROS sources causally involved in prion-mediated neurotoxicity. To investigate this finding *ex vivo*, we treated NOX2 depleted COCS overexpressing PrP with POM1 and unexpectedly found that POM1-induced neurotoxicity was not blocked (Figure 4.8b). These data remain inconclusive until new experiments are performed using the same mice; however, it potentially suggests that the neuroprotective effect exerted by NOX2 ablation may be dependent on PrP expression levels and degree of toxicity.

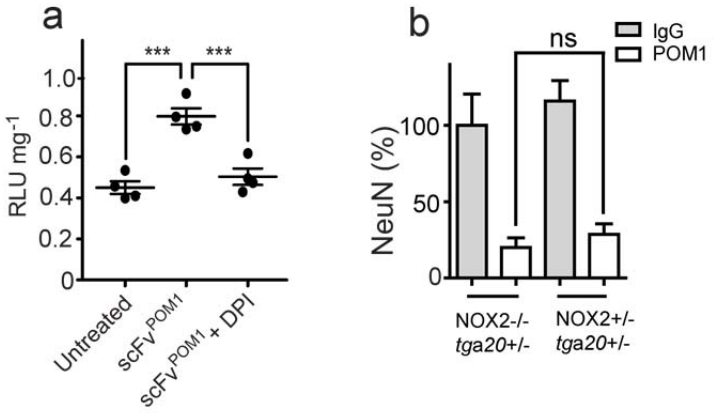

Figure 4.8. ***Identification of the cellular source of superoxide remains unclear in COCS. a)*** *Lucigenin conversion assay of COCS exposed to scFvPOM1 (400nM, 24h) with the optional addition of DPI (n=4 pools of 9 slices; p<0.001).* ***b)*** *NOX2-deficient mice and heterozygous littermate controls were exposed to POM1 and IgG (167nM, 14days). Deficiency of the NOX subunit of the NADPH enzyme, a cellular generator of superoxide, did not afford neuroprotection in COCS.*

Strikingly, antioxidants were also neuroprotective in prion-infected COCS (Figure 4.6a lower panel) and administration of the potent antioxidant acetylated hydroxyl tyrosol significantly prolonged the lifespan of prion-infected mice (Falsig et al. unpublished). Moreover, superoxide generation was confirmed both by pharmacological approach and biochemical read-outs in prion-infected COCS, as shown in antibody-treated COCS (Falsig et al. unpublished).

ERK IS ACTIVATED UPON POM1 TREATMENT

The mitogen-activated protein kinases of the MAPK family are serine/threonine kinases that modulate events involved in cell differentiation, proliferation, apoptosis, gene expression, and inflammation (Whitmarsh and Davis, 1999). Members of the MAPK cascade can be

divided into 3 groups that sequentially activate each other: MAPKK kinases, MAPK kinases, and MAP kinases. MAPK kinases include four groups: ERK (extracellular signal-related kinases), c Jun-amino terminal kinases, p38 proteins, and ERK5. Membrane receptors such as tyrosine kinases and G protein-coupled receptors activate Raf (a MAPKKK) that trigger phosphorylation of MEK1/2 (MAPKKs) and consequently ERK1-2, which in turn phosphorylates different substrates such as membrane proteins, nuclear proteins, and transcription factors (Cheung and Slack, 2004).

We started to dissect the MAPK kinase cascade by analysing the levels of phosphorylated signalling molecules such as MEK1/2, p38, c-Jun, and ERK1/2. Therefore, *tga20* COCS were challenged with POM1 and IgG for different time points, tissue was harvested, and proteins were blotted and probed for phosphorylated kinases. We found hyperactivation of ERK and AKT, but not c-Jun and p38, confirming a role of of PrP in the MAPK cascade, as previously reported (Figure 4.9a-b) (LaCasse et al., 2008; Lee et al., 2005; Nixon, 2005; Schneider et al., 2003).

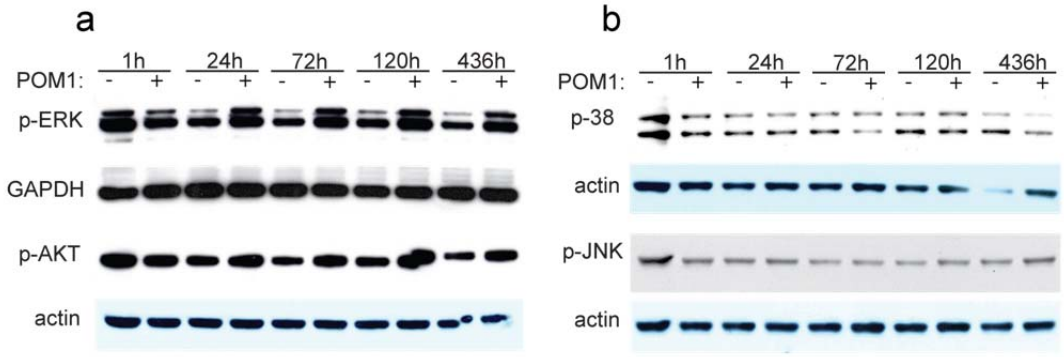

Figure 4.9. ***Increased levels of p-Erk upon POM1 treatment****.* ***a-b****) Tga20 COCS were exposed to POM1 and IgG for different periods of time (1h-436h). POM1 treatment resulted in higher p-ERK and p-AKT levels compared to IgG control treated COCS (a), whereas p-38 and p-JNK were unchanged (b). Actin and GAPDH were used as loading controls.*

To examine a potential role of the members of the ERK/MEK cascade in PrP-induced neurotoxicity, we used U0126, a specific inhibitor of MEK1/2 and also inhibited upstream activators such as src (using PP2) and tyr kinases (using genistein); however, none of them conferred protection against POM1 toxicity (Figure 4.10a). Furthermore, inhibition of other MAPK kinases, such as JNK (using SP600125) and p38 (using SB203580), did not confer neuroprotection (Figure 4.10a).

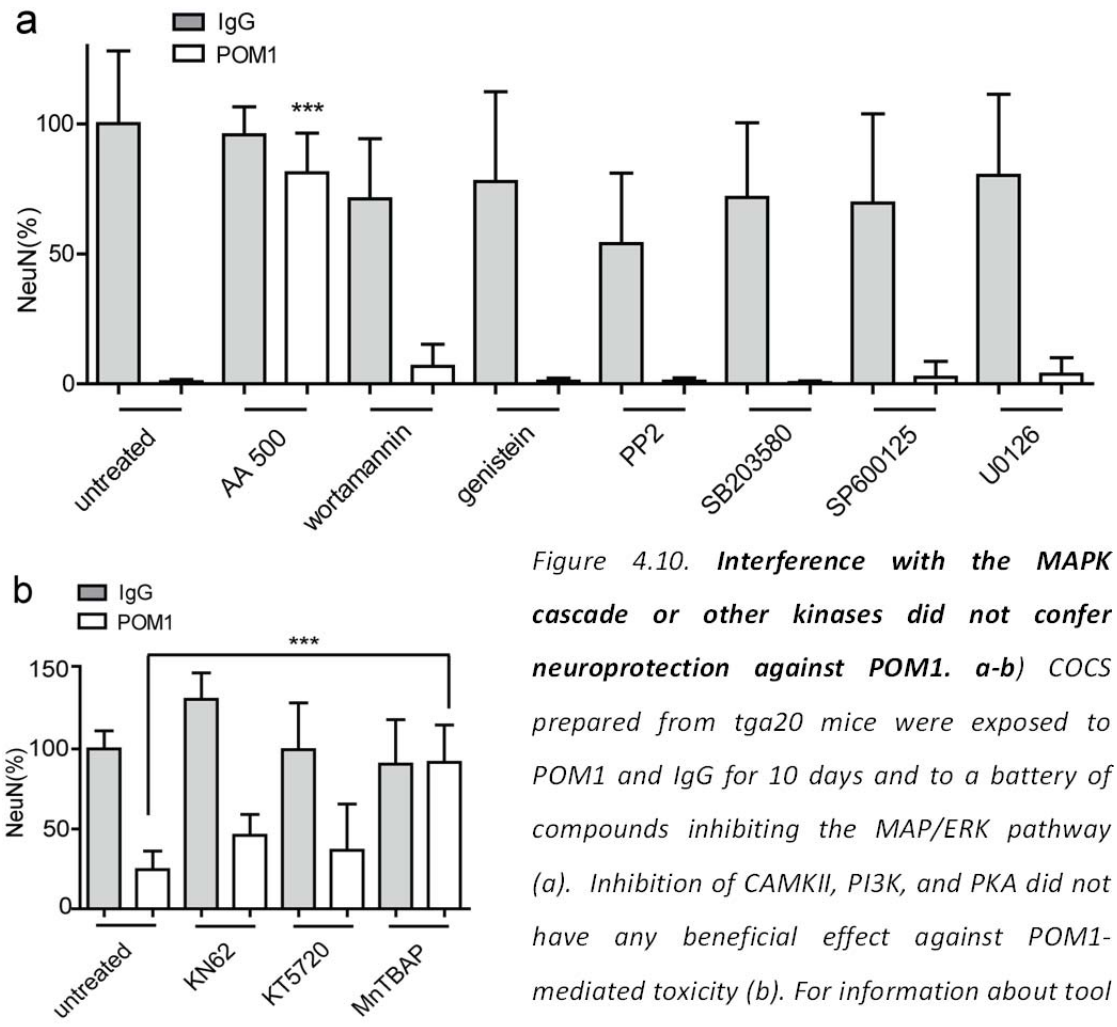

Figure 4.10. ***Interference with the MAPK cascade or other kinases did not confer neuroprotection against POM1.*** ***a-b****) COCS prepared from tga20 mice were exposed to POM1 and IgG for 10 days and to a battery of compounds inhibiting the MAP/ERK pathway (a). Inhibition of CAMKII, PI3K, and PKA did not have any beneficial effect against POM1-mediated toxicity (b). For information about tool compounds used refer to Table 4.1. No compounds conferred neurotoxicity to IgG treated COCS; however, no compounds gave significant neuroprotection at the concentrations tested, except for ascorbate (500µM) used as neuroprotective control compound.*

In addition to inhibiting kinases of the MAPK cascade, we targeted other kinases such as PI3K, CamKII, and PKA dependent on cyclic AMP that have been reported to be involved in PrP-dependent signal transduction pathways (Chen et al., 2003; Chiarini et al., 2002; Takenouchi et al., 2012) or more generally implicated in neuronal death (Berdichevsky et al., 2013; Vest et al., 2010). Inhibition of CamKII (using KN62), PI3 kinase (using wortamannin), or PKA (using KT5720) did not significantly diminish POM1-mediated toxicity (Figure 4.10a-b).

OTHER CELLULAR TARGETS INVESTIGATED

Mass-spectrometry analyses of PrP isolated from cow brain identified many proteins as potential interacting partner and among those, attractive candidates that could be involved in neuronal death were the small conductance calcium-activated potassium (SK) channels and NMDAR (Calella et al. unpublished).

Apamin is a specific inhibitor of SK channels, and we asked whether POM1 induced neuronal death was prevented by apamin using our standard experimental conditions (antibody treatment for 10 days at 67nM in *tga20* COCS). However, no significant improvement of neuronal viability was measured (Figure 4.11a). We did not continue with this experiment because the interaction of SK channels with PrP could not be confirmed by immunoblots. The other interesting candidate identified by mass spectrometry was NMDR since PrP^C is highly expressed in the hippocampus (DeArmond et al., 1987) and both pre- and postsynaptic localization has been reported (Fournier, 2000; Sales et al., 1998) . Pharmacological interference with NMDAR did not diminish POM1-mediated neuronal death (Figure 4.5a) in the cerebellum; however, one cannot exclude that there might be different mechanisms leading to cell death depending on the brain region investigated.

We also checked for levels of pre- and post-synaptic markers in *tga20* COCS exposed to FabPOM1 or FabPOM1 pre-incubated with rmPrP, as PrP^C has been suggested to be involved in synaptic activity (Aguzzi et al., 2008). Interestingly, a decrease of the presynaptic phosphoprotein synapsin-1 has been observed in COCS at 3dpe of POM1 treatment, whereas synaptophysin levels remained the same (Figure 4.11b). It is unanswered whether the decrease in synapsin I is a consequence of neuronal loss or is a primary event.

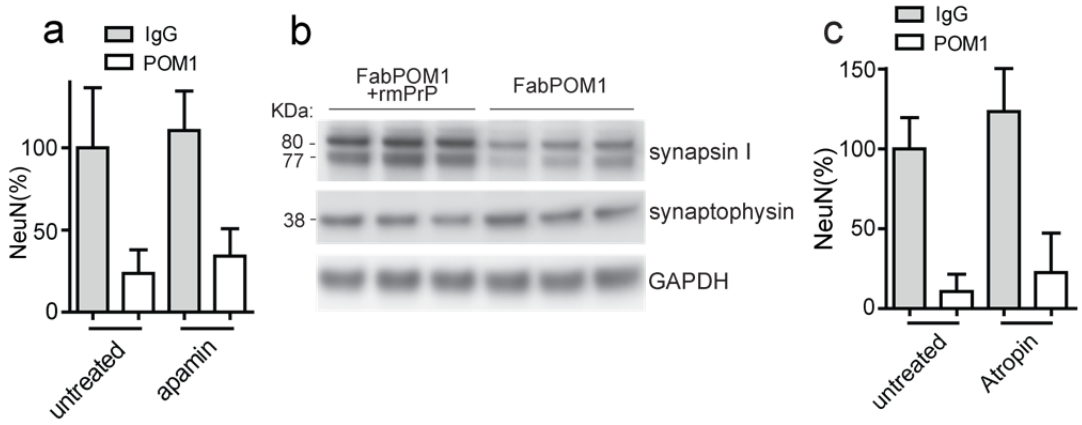

Figure 4.11. **Levels of Synapsin I were decreased upon FabPOM1 treatment. a**) COCS from *tga20* mice were challenged with POM1 and IgG for 10 days and co-incubated with a tool compound. SK calcium blockade (apamin) did not prevent POM1 toxicity. **b**) *Tga20* COCS

were treated with FabPOM1 in the presence or absence of rmPrP. Western blots probed with synapsin I or synaptophysin showed decreased levels of synapsin I, but no changes in synaptophysin in FabPOM1-treated COCS. **c**) Same conditions as in a. Antagonist of muscarinic receptor did not block POM1-mediated neuronal loss.

Moreover, activation of muscarinic receptors increases PrP proteolysis (Alfa Cisse et al., 2007) and it is not clear whether it contributes to pathological changes; however, inhibition of muscarinic receptors using atropine did not alleviate the toxic effects induced by POM1 (Figure 4.11c).

Table 3.1: Description of tool compounds used in the study

Compound	**Primary target (according to published data)**	**Neuroprotection**	
		POM1	**prion**
1400W	Nitric oxide synthase 1 and 2 (Mander and Brown, 2005)	no	no
Ascorbate	ROS scavenging (Avshalumov and Rice, 2002)	yes	yes
Calpeptin	Cysteine-proteases: Calpains and cathepsins (Bano et al., 2005; Fox et al., 1991)	yes	yes
CNQX	Ionotropic AMPA and kainite receptors (Aarts et al., 2003; Brennan, 2009)	no	no
Cyclosporine A	Mitochondrial membrane permeability transition pore (Malouitre et al., 2009)	no	no
DPI	NOX inhibitor (Abramov et al., 2007)	n/a	n/a
Isoascorbate	ROS scavenging (Avshalumov et al., 2000)	yes	yes
Methazolamide	Mitochondrial membrane permeability transition pore (Wang et al., 2008)	no	no
MK801	NMDA receptor (Aarts et al., 2003; Abramov et al., 2007; Brennan, 2009; Windelborn, 2008)	no	no
MnTBAP	Superoxide and H_2O_2 scavenging (Aarts et al., 2003)	yes	yes
N-acetyl-cysteine	ROS scavenging (Hsiao et al., 2008)	yes	yes

zVAD-fmk	Broad-spectrum caspase inhibitor (Bano et al., 2005)	no	no
Ryanodine	Ryanodine receptor (agonist) (Leski et al., 1999; Torres et al., 2010)	no	no
KT5720	Protein kinase A inhibitor (antagonist) (Li et al., 2011)	no	no
Dantrolene	Ryanodine receptor (agonist) (Torres et al., 2010)	no	no
U73122	Phospho Lipase C (antagonist) (Macmillan and McCarron, 2010)	no	no
KB7943	Na+/Ca+2 exchanger blocker (Gerencser et al., 2009)	no	yes
Apamin	SK channel blocker (Shakkottai et al., 2004)	no	no
Wortamannin	PI3K inhibitor (irreversible) (Shehata et al., 2012)	no	no
Genistein	Tyrosin kinases inhibitor (Wu et al., 2013)	no	yes
PP2	Src family of tyrosin kinases (Wu et al., 2013)	no	no
SB203580	P38 MAPK inhibitor (Zhao et al., 1999)	no	no
SP600125	JNK II inhibitor (Bennett et al., 2001)	no	no
U0126	MEK I/ MEK II inhibitor (Favata et al., 1998)	no	yes
Atropine	Muscarinic antagonist (Gulledge and Stuart, 2005)	no	no
Resveratrol	Antioxidant (Fukui et al., 2010)	no	no

n/a: not amenable to assessment due to toxic effects

data reported for the prion-infected COCS have been generated in collaboration with Dr. Jeppe Falsig

DISCUSSION AND OUTLOOK

MOLECULAR PLAYERS OF PRP-MEDIATED NEURONAL DEATH:

ROS PLAY A PIVOTAL ROLE IN PRP-DEPENDENT NEURONAL LOSS

PrP-deficient neurons are susceptible to oxidative stress and this effect is restored by antioxidants (Brown et al., 1997a). Furthermore, a potential link between PrP and ROS generation has been reported in a neuronal model upon PrP stimulation with anti-PrP antibodies. Antibody-mediated PrP ligation triggers increased NADPH-induced ROS levels, accompanied by elevated phosphorylation of Erk (p44 and p42) (Schneider et al., 2003). Inhibition of NADPH with diphenyleiodonium (DPI) reduces antibody-induced ROS levels, suggesting that ROS was NADPH dependent (Schneider et al., 2003). Inhibition of Fyn kinase prevents antibody induced ROS production and activation of the MAPK/ERK kinase (MEK) pathway, suggesting Fyn as a regulator of PrP signalling cascade. Even though a link between ROS and homeostatic prion protein signalling has already been described (Brown et al., 1997a; Brown et al., 1997b; Mouillet-Richard et al., 2000; Schneider et al., 2003), our work shows for the first time a causal role of ROS in prion-mediated neurotoxicity both *in vitro* and *in vivo*.

Our studies on the antibody model have suggested a role for the NOX2 enzyme in prion-mediated neurotoxicity (Sonati et al., 2013) and current work in our lab proves that ablation of this enzyme is also beneficial in genuine prion infections (Dr. Silvia Sorce unpublished data).

However, NADPH oxidase is not the only cellular ROS generator and we cannot exclude that other cellular compartments (i.e. ER and mitochondria) are contributing to ROS generation (Fatokun et al., 2008) or that other ROS species are causative to cell death. In this direction, establishment of newly developed mass spectrometry-based assays (Zielonka et al., 2009; Zielonka et al., 2008a; Zielonka et al., 2008b) will help identify the ROS species produced and visualize ROS sources at the sub-cellular level, i.e mitochondria, ER (Dr. Silvia Sorce & Dr. Sergey Yakushev).

CALPAIN AS EFFECTORS OF PRION-MEDIATED NEURONAL DEATH

An apoptotic mode of cell death mediated by caspase activation was described for prion diseases (Chiesa et al., 2005; Kovacs and Budka, 2010; Li et al., 2007; Nicolas et al., 2007); however, more recent work does not support this hypothesis (Steele et al., 2007).

Importantly, our recent findings in prion-infected and antibody-treated COCS identified calpains as effectors of prion toxicity, suggesting that abnormal levels of calcium are upstream events of this cascade (Falsig et al., 2012; Sonati et al., 2013). Data from *in vitro* models speculate that prion-mediated toxicity is mediated by ion influx (Solomon et al., 2010; Solomon et al., 2011) or abnormal calcium homeostasis (Torres et al., 2010); however, the intracellular source of calcium remains unknown.

We failed to identify intracellular sources of calcium using a palette of pharmacological inhibitors. However, a major methodological advance to understand calcium's contribution to prion-induced neuronal death has been achieved in the lab with the generation of genetically encoded calcium indicators (Despina Goniotaki and Dr. Silvia Sorce in collaboration with Prof. Fritjof Helmchen' group, University of Zürich), in addition to chemical calcium dyes. These recently developed tools have enabled visualization of increased calcium levels upon POM1 treatment in COCS and *in vivo*. Thus, it remains crucial to discover which subcellular compartments are contributing to the increase in cytosolic calcium and whether elevated calcium levels are directly linked to prion-mediated neurodegeneration.

Moreover, recent reports suggest that ultrastructural analyses of neurons from mice expressing the toxic $PrP_{\Delta 105\text{-}125}$ form are indicative of a Poly (ADP-ribose) polymerase 1 (PARP1)-regulated cell death (Christensen et al., 2010a). PARP enzymes are crucially involved in DNA repair and cell death (Gibson and Kraus, 2012), and morphological assessment of POM1 treated brain slices show chromatin condensation with features of PARP-dependent neuronal death exhibited by expression of $PrP_{\Delta 105\text{-}125}$. Congruently, we have found that in anti-PrP antibody- and prion-mediated cell death, neurotoxicity is blocked by selective PARP inhibitors (Badmavady Segarane). PARP enzymes are known players of caspase-independent cell death and an interplay between calpains and PARP enzymes has been described (Moubarak et al., 2007); however, the cascade of events in prion models still needs to be defined.

THE CONTRIBUTION OF AUTOPHAGY REMAINS TO BE ELUCIDATED

Autophagy is the intracellular degradation machinery for cytoplasmic material in order to generate new cellular components. During this process, cargo is taken up by autophagosomes that subsequently fuse with lysosomes, where degradation occurs (Mizushima and Komatsu, 2011).

There is evidence that induction of autophagy enhances PrP^{Sc} clearance *in vitro* (Heiseke et al., 2009; Heiseke et al., 2010), however *in vivo* studies do not support these data (Heiseke et al., 2010; Sarkar et al., 2007). On the other hand, induction of autophagy ameliorates the pathology of a genetic model of prion disease (GSS) (Cortes et al., 2012).

Ultrastructural morphological analyses of POM1-treated COCS (performed in collaboration with Prof Liberski) indicated the presence of autophagic vacuoles in axons (Sonati et al., 2013), similar to those found in infected-neuronal cells, prion-infected COCS, as well as human brain biopsies (Falsig et al., 2012; Heiseke et al., 2010; Liberski et al., 2008; Schatzl et al., 1997). The potential contribution of autophagy is still unexplored in antibody-mediated toxicity, and gene-knock down of authophagy-related genes (ATG proteins) responsible for authophagosome formation (Mizushima and Komatsu, 2011) *via* antisense oligonucleotides is ongoing (Dr. Daiji Sakata).

MAPK SIGNALLING MOLECULES AS MEDIATORS OF CELL DEATH

The MAPK family has been largely investigated and its involvement in prion pathology is well documented (LaCasse et al., 2008; Lee et al., 2005; Nixon, 2005; Schneider et al., 2003); however, despite confirming activation of ERK and other kinase members, it is still debated whether ERK is part of a neuroprotective pathway response or if it is contributing to cell death (Cheung and Slack, 2004). Both hypotheses are plausible, and activation of ERK1/2 and upregulation of immediate early genes were observed not only in antibody-treated, but also in prion-infected COCS (Hermann et al. unpublished). Remarkably, MEK1/2 inhibitor, which did not block POM1 toxicity, was neuroprotective against prion-mediated cell death (Hermann et al. unpublished) and this data crucially correlates ERK hyperactivation to prion-mediated toxicity.

SIGNALING CASCADE REMAINS TO BE UNCOVERED

Crucial molecular targets involved in prion-dependent neuronal death have been identified by pharmacological approach. Whereas neuroprotective compounds, calpain inhibitors, and antioxidants have highlighted novel effectors of prion-dependent cell death, negative results are less informative. For instance, inhibition of excitotoxic pathways or calcium stores (whose involvement has been documented in prion diseases, (Kristensson et al., 1993; Torres et al., 2010; You et al., 2012) can be attributed to ineffective concentrations or to the lack of specificity of the tool compounds used. Thus, we cannot exclude the contribution of certain pathways to prion-mediated neurotoxicity if they are not accompanied by functional read-outs, such as in the case of caspases.

Lastly, results from our group of a third model of prion-mediated neurotoxicity (above mentioned NGPI mice) supports the recent view in the prion field that the unfolded protein response pathways (UPR) contribute to prion-induced toxicity (Moreno et al., 2012), and the UPR pathway is currently being confirmed in POM1-mediated toxicity (Hermann unpublished).

More work is currently ongoing in our laboratory to elucidate the sequence of events including calpains, calcium release, ROS, PARP enzymes, ERK kinases, and UPR effector molecules (CHOP, PERK, eIF2α, ATF4) and all read-outs recently developed (i.e. calcium indicators, automated confocal microscopy, ROS assays, gene knock-down using antisense oligonucleotides) are being employed.

CONCLUDİNG REMARKS

SIGNIFICANCE OF THE MODEL

One may question the significance of the antibody model to study prion-mediated neurotoxicity since it does not contain infectivity. However, many modified PrP molecules are neurotoxic without PrP^{Sc} deposition, such as 1) PrP molecules carrying point or insertional mutations involved in human familial prion diseases, 2) altered topological variants of PrP (PrP^{Ctm} and PrP^{Ntm}) and, 3) toxic PrP mutants lacking the HC ($PrP_{\Delta 32\text{-}121}$, $PrP_{\Delta 32\text{-}134}$, $PrP_{\Delta 105\text{-}125}$ and $PrP_{\Delta 94\text{-}134}$). This suggests that PrP^{Sc} is not the exact cause of neuronal death, whereas neuronal PrP^{C} is essential to trigger prion-induced neurodegeneration (Brandner et al., 1996; Mallucci et al., 2003). Moreover, PrP^{Sc} replication and neurotoxicity have been proposed to be two distinct events, as infectivity propagates rapidly even in the presence of low amounts of PrP^{c}. In contrast, neurodegeneration is dependent on PrP^{c} expression levels and occurs at later stages of disease (Sandberg et al., 2011). Alternatively, a toxic conformer of PrP^{C} may be causal to the disease.

We found that GD antibody treatment and prion infections share many similarities, as neuronal death is dependent on PrP expression levels and neuronal PrP, is mediated by the flexible tail, and is accompanied by calpain activation and a ROS burst. Therefore, we believe that GD antibody neurotoxicity is a good surrogate model to study PrP-mediated neurotoxicity uncoupled from PrP^{Sc} replication/infectivity.

Studies of toxic effects exerted by ligands to PrP^{C} may have a major impact on understanding the development of other misfolded neurodegenerative disorders, as PrP^{c} has been reported to have a high affinity for amyloid beta (Aβ) oligomers and is a mediator of Aβ toxicity (Barry et al., 2011; Gimbel et al., 2010; Lauren et al., 2009) and likely of other β-sheet-rich aggregates (Resenberger et al., 2011). However, a requirement for PrP to mediate Aβ toxicity has not been confirmed by us and other groups (Balducci et al., 2010; Calella et al., 2010; Kessels et al., 2010). Zamponi and coworkers suggested that these controversial findings depend on different concentrations of copper and glycine used by the various groups since they showed a link between copper-dependent regulation of NMDA currents and neurotoxicity (You et al., 2012), however our results do not support a role for copper and NMDA and further investigations are required.

Furthermore, as anti-PrP antibodies trigger dramatic cerebellar neuronal loss, this may happen as well in humans. A screening of sera from patients with undiagnosed cerebellar

disorders to look for autoantibodies against the prion protein has already been started (Tory P. Johnson and Veronika Kana).

Establishment of the antibody model led us to novel discoveries and is a great advantage as it eliminates the need to work with infectious prions and enables us to study the progression of neurotoxicity in shorter timeframes than prion infections. Using a battery of anti-PrP antibodies targeting different epitopes in combination with transgenic mice expressing truncated variants of PrP, we identified two PrP modules, the GD as the receptor module of toxic ligands and the FT as the effector module of toxicity. We believe that therapeutic agents interfering with these domains may be a novel option for future drug development to treat prion-mediated neurodegeneration.

CHAPTER V
MATERIAL AND METHODS

This chapter contains unpublished data as well as parts that are adapted or reproduced from the following manuscript accepted by Nature on the 21st of June 2013 and assigned the DOI 10.1038/nature12402:

The toxicity of antiprion antibodies is mediated by the flexible tail of the prion protein

Tiziana Sonati[1,*], Regina R. Reimann[1,*], Jeppe Falsig[1,*], Pravas Kumar Baral[2], Tracy O'Connor[1], Simone Hornemann[1], Sine Yaganoglu[1], Bei Li[1], Uli S. Herrmann[1], Barbara Wieland[2], Mridula Swayampakula[2], Muhammad Hafizur Rahman[3], Dipankar Das[3], Nat Kav[3], Roland Riek[4], Pawel P. Liberski[5], Michael N. G. James[2], and Adriano Aguzzi[1†]

[1] Institute of Neuropathology, University Hospital Zurich, Switzerland
[2] Department of Biochemistry, University of Alberta, Canada
[3] Department of Agricultural, Food and Nutritional Science, University of Alberta, Canada
[4] ETH Zurich, Physical Chemistry, ETH Honggerberg, 8093 Zurich, Switzerland
[5] Laboratory of Electron Microscopy and Neuropathology, Department of Molecular Pathology and Neuropathology, Medical University of Lodz, Lodz, Poland.
[*] These authors contributed equally to this work

[†] Corresponding author: Adriano Aguzzi; Institute of Neuropathology, University Hospital of Zurich; Schmelzbergstrasse 12, CH-8091 Zurich, Switzerland; Tel: +41-44-255-2108, Email address: adriano.aguzzi@usz.ch

And reproduced or adapted from the following publication:

Falsig, J., Sonati, T., Herrmann, U.S., Saban, D., Li, B., Arroyo, K., Ballmer, B., Liberski, P.P., and Aguzzi, A. (2012). **Prion pathogenesis is faithfully reproduced in cerebellar organotypic slice cultures.** PLoS Pathog *8*, e1002985.

MICE

GABA-Aα6-CRE mice were generated on a C57BL/6xCBA background and back-crossed to a *Prnp*$^{o/o}$ background (Aller et al., 2003; Büeler et al., 1992). Tg37 mice allowing for conditional PrP deletion were generated on a *Prnp*$^{o/o}$ FVB background (Mallucci et al., 2002). GABA-A$_{\alpha 6}$-CRE^{-};loxPrP-tg37 littermates were used as negative controls (PrP^{CGC+}). B6.129S6-*Cybb*^{tm1Din}/J (NOX2)-deficient mice were generated on a mixed C57BL/6xSv129 background and backcrossed to C57BL/6 (Pollock et al., 1995). *Prnp*$^{o/o}$, *Prnp*$^{o/o}$;*tga20*$^{+/+}$ (*tga20*), *Prnp*$^{o/o}$;F35 (PrP $_{\Delta 32\text{-}134}$), *Prnp*$^{o/o}$;*C4/C4* (PrP$_{\Delta 32\text{-}93}$), *Prnp*$^{o/o}$;*1046* (PrP$_{\Delta 94\text{-}134}$), *Prnp*$^{o/o}$;*L52* (PrP$_{\Delta 94\text{-}110}$), *Prnp*$^{o/o}$;NSE-PrP$^{+/+}$ (*NSE-PrP*) and *Prnp*$^{o/o}$;MBP-PrP$^{+/+}$ (*MBP-PrP*) mice were on a mixed 129Sv/BL6 background, and *wt* mice on a C57BL/6 background (Baumann et al., 2007; Bremer et al., 2010; Büeler et al., 1992; Fischer et al., 1996; Flechsig et al., 2000; Prinz et al., 2004; Radovanovic et al., 2005; Shmerling et al., 1998). *Prnp*$^{o/o}$;*L52* (PrP$_{\Delta 94\text{-}110}$) was the second line previously reported by Bremer et al (Bremer et al., 2010). CD11b-HSVTK mice (Heppner et al., 2005) on a C57BL/6 background were crossed to *Prnp*$^{o/o}$;*tga20*$^{+/+}$. All offspring were *Prnp*$^{+/o}$;*tga20*$^{+}$ and CD11b-HSVTK positive offspring were referred to as *tga20*$^{TK+}$. All mouse experiments conformed to Swiss law and were approved by the Animal Experimentation Committee of the Canton of Zurich (permits 200/2007 and 130/2008).

CHEMICALS

All compounds were purchased from Sigma/Aldrich unless otherwise stated.

NEWBORN INJECTIONS

Newborn mice (P0) were injected with a thin Hamilton syringe into the lateral ventricle (2 uL of 2mg ml^{-1} IgG or POM2 solution into each hemisphere) according to previously reported protocols(Levites et al., 2006).

ORGANOTYPIC CEREBELLAR CULTURE PREPARATION

Organotypic cerebellar slice cultures, 350 µm thick, were prepared from 10-12 day-old pups according to a previously published protocol (Falsig and Aguzzi, 2008). Free-floating sections were cut in Gey's balanced salt solution (GBSS) (NaCl 8 g l^{-1}, KCl 0.37 g l^{-1}, Na_2HPO_4 0.12 g l^{-1}, $CaCl_2$ $2H_2O$ 0.22 g l^{-1}, KH_2PO_4 0.09 g l^{-1}, $MgSO_4$ $7H_2O$ 0.07 g l^{-1}, $MgCl_2$ $6H_2O$ 0.210 g l^{-1}, $NaHCO_3$ 0.227 g l^{-1}) supplemented with the glutamate receptor antagonist kynurenic acid (1 mM) (GBSSK) at 4°C. COCS were placed on a 6-well Millicell-CM Biopore PTFE membrane insert (Millipore).

For antibody treatment experiments, residual buffer was removed and the inserts were transferred to a cell culture plate and cultured in "slice-culture medium" (SCM) (50% vol/vol

MEM, 25% vol/vol basal medium Eagle and 25% vol/vol horse serum supplemented with 0.65% glucose (w/vol), penicillin/streptomycin and glutamax (Invitrogen)). Cultures were kept in a standard cell incubator (37°C, 5% CO_2, 95% humidity) and the culture medium was exchanged three times weekly.

For prion experiments, COCS were incubated with infectious brain homogenates as free-floating sections for 1h at 4°C. COCS were then washed twice in 6 ml GBSSK, and 5-10 COCS were placed on a 6-well Millicell-CM Biopore PTFE membrane insert (Millipore). After removing any residual buffer, inserts were transferred to a cell culture plate and cultured in standard slice culture medium.

LOW CALCIUM MEDIUM EXPERIMENTS

COCS were cultured for 14 days with SCM and then switched to LCM. To prepare LCM, 3.7g of MEM (Joklik medium US Biological cat C8010301, calcium-free) was dissolved in 300mL MQ water at pH 7.1, and mixed with 25% vol/vol of horse serum supplemented with 0.65% glucose (w/vol), penicillin/streptomycin, and glutamax (Invitrogen). This medium contains approximately 25% of the calcium contained in the horse serum.

ANTIBODY TREATMENT OF COCS

Antibody treatment was started after a 10-14 day recovery period, allowing the initial gliosis induced by tissue preparation to subside. The antibody was diluted in PBS at the desired concentration, spiked into the medium, and re-applied at every medium change. COCS were harvested for biochemical analyses or fixed for immunocytochemical analysis at various time points, mainly depending on the levels of PrP and read-outs used. *Tga20* COCS were treated with POM1 at 67nM for 10-14 days, the length of treatment at whichmost of the NeuN positive cells were lost. Most of the protein analyses were performed on COCS harvested after 3 days of treatment in *tga20* COCS. Experiments using mouse lines that had PrP expression levels similar to *wt* were conducted with 268nM of antibody for 21 days, the time when almost complete neuronal loss was achieved.

For the microglia depletion experiment, *tga20*$^{TK+}$ COCS were treated with ganciclovir (GCV, 5 µg ml^{-1}) for 14 days prior to antibody treatment. At this time point, less than 1% of microglia was left in the tissue (Falsig et al., 2008).

POM2 treatment (50 µg ml^{-1}, 335nM) in prion experiments was initiated after plating and re-supplied at every medium exchange.

PHARMACOLOGICAL TREATMENT OF COCS

For antibody treatment experiment, drug treatment was initiated at the time of antibody addition and drugs were re-added at every medium change.

For prion experiments, drug treatment was initiated at 21 dpi when PrP^{Sc} is detectable in the cultures and performed at every medium change till 44 dpi when almost complete loss occurs.

Appropriate drug concentrations were determined by literature search, assuming that slice culture uptake of compounds were similar to other cell culture systems. The toxicity of each compound was tested in parallel on IgG- and POM1-treated and in RML and NBH inoculated COCS (for prion experiments); if toxicity occurred, drugs were retested at a lower concentration.

Drug and concentration used were (+)-5-methyl-10,11-dihydro-5H-dibenzo[a,d] cyclohepten-5,10-imine maleate) (MK-801, 20 µM), 6-cyano-7-nitroquinoxaline-2,3-dione (CNQX, 20 µM), 4,5,6,7-tetrahydroisoxazolo[5,4-*c*]pyridin-3(2*H*)-one (gaboxadol, 100 µM), cyclosporine A (1 µM), ascorbate (1.5 mM), isoascorbate (1.5mM), N-(3-methyl-5-sulfamoyl-1,3,4-tiadiazol-2-ylidine)acetamide (methazolamide, 10 µM), MnTBAP (100 µM), benzyloxycarbonyl-Val-Ala-Asp (OMe) fluoromethylketone (zVAD-fmk, 40 µM), diphenyleneiodonium chloride (DPI, 5 µM), N-([3-(Aminomethyl)phenyl]methyl)-ethanimidamide dihydrochloride (1400W, 20 µM), N-benzyloxycarbonyl-L-leucylnorleucinal (calpeptin, 20 µM), N-acetylcystein (NaC, 1 mM). 1-[(5-(p-Nitrophenyl)furfurylidene)amino]-hydantoin sodium salt (dantrolene, 10 µM), ryanodine (10 µM), (9S,10S,12R)-2,3,9,10,11,12-Hexahydro-10-hydroxy-9-methyl-1-oxo-9,12-epoxy-1H-diindolo[1,2,3-fg:3',2',1'-kl]pyrrolo[3,4-i][1,6]benzodiazocine-10-carboxylic acid hexyl ester, (KT5720, 1 µM), 4-[(2S)-2-[(5-Isoquinolinylsulfonyl)methylamino]-3-oxo-3-(4-phenyl-1-piperazinyl)propyl] phenylisoquinolinesulfonic acid ester (KN62, 10 µM), 1-[6-[((17β)-3-Methoxyestra-1,3,5[10]-trien-17-yl)amino]hexyl]-1H-pyrrole-2,5-dione (U73122, 5 µM, Cayman), KB7943, 4-(4-Fluorophenyl)-2-(4-methylsulfinylphenyl)-5-(4-pyridyl)1H-imidazol (SB203580, 5µM, calbiochem), 1,9-pyrazoloanthrone (SP600125-JNK2, 10 µM, calbiochem), 1,4-diamino-2,3-dicyano-1,4-bis (2-aminophenylthio)butadiene (U0126, 20 µM, calbiochem), 4',5,7-Trihydroxyisoflavone, (genistein, 30 µM, calbiochem), 4-Amino-5-(4-chlorophenyl)-7-(*t*-butyl)pyrazolo[3,4-d]pyrimidine, (PP2, 5 µM, calbiochem), wortmannin (200 nM, calbiochem), apamin (100nM), endo-(±)-α-(Hydroxymethyl)benzeneacetic acid 8-methyl-8-azabicyclo[3.2.1]oct-3-yl ester (atropine, 10µM), 3,4',5-Trihydroxy-*trans*-stilbene, 5-[(1*E*)-2-

(4-Hydroxyphenyl)ethenyl]-1,3-benzenediol (resveratrol, 10 µM), pentosan polysulfate (PPS, 5 µM) a gift of Bene pharma company.

PROTEIN ANALYSIS

COCS were washed twice in PBS. Cerebellar tissue was then scraped off the membrane using 10 µl per slice of PBS with 0.5% DOC, 0.5% NP-40 supplemented with PMSF (1 µM) and complete mini protease inhibitor cocktail (Roche), and homogenized by trituration using a 30G syringe. For pospho-blots, the tissue was harvested in ice-cold PBS, 10 mM NaF (1:20) and 1 mM Na3VO4 (1:50). Protein concentration was determined using the bicinchoninic acid assay (Pierce). Samples were prepared in loading buffer (NuPAGE, Invitrogen) and boiled at 95°C for 5 min. Proteins (10 µg per lane) were separated on a 12% Bis-Tris polyacrylamide gel or for higher molecular weight proteins on a 4-12% gradient gel (NuPAGE, Invitrogen) and blotted onto a nitrocellulose membrane. For detection of PrP^{Sc}, samples were adjusted to 20 µg protein in 20 µl and digested with 25 µg ml^{-1} proteinase K in digestion buffer (0.5% wt/vol sodium deoxycholate and 0.5% vol/vol Nonidet P-40 in PBS) for 30 min at 37°C. This protocol allowed specific detection of PrP^{Sc} as shown previously (13). PK digestion was stopped by adding loading buffer (NuPAGE, Invitrogen) and boiling samples at 95°C for 5 min. Proteins were separated on a 12% Bis-Tris polyacrylamide gel and blotted onto a nitrocellulose membrane. Membranes were blocked with 5% w/vol Topblock (Fluka) in Tris-buffered saline supplemented with Tween (150 mM NaCl, 10 mM Tris HCl, 0.05% Tween 20 (vol/vol)) and incubated with primary antibodies in 1% Topblock. Primary mouse monoclonal antibodies used were: POM1, POM2 or POM11, mouse IgG_1 antibody raised against PrP^{C} (anti-PrP^{C}; 200 ng ml^{-1}), mouse anti-α-fodrin (AA6, 100 ng ml^{-1}, Millipore), anti-GAPDH (200 ng ml^{-1}, Millipore), and anti-actin (200 ng ml^{-1}, Chemicon). Secondary antibodies were horseradish peroxidase (HRP)-conjugated rabbit anti–mouse IgG_1 (1:10,000, Zymed), goat anti–rabbit IgG_1 (1:10,000, Zymed), and rabbit anti–goat IgG_1 (1:10,000, Zymed). Blots were developed using SuperSignal West Pico chemiluminescent substrate (Pierce) and visualized using the VersaDoc system (model 3000, Bio-Rad). PNGase treatment was performed using a commercially available kit, according to the manufacturer's protocol (New England Biolabs). In brief, 10 µg protein was treated with 2 µl denaturation buffer in a 20 µl reaction and incubated for 15 min at 95°C. A reaction mixture of 2.6 µl G7, 2.6 µl NP-40 (10%), as well as 0.5 µl PNGase was added and samples were incubated for 2h at 37°C. Samples were then mixed with loading dye, cooked and analysed by western blotting. Cerebella from 10 day-old pups were homogenized (10% w/v) in 0.32 M sucrose in 1x PBS

supplemented with 4-(2-Aminoethyl)-Benzene sulfonyl fluoride HCL (AEBSF, 1 mM) and complete mini protease inhibitor cocktail (Roche) using a tissue Ribolyser (Qiagen). PrP^C expression in the brains of PrP deletion mutants was analyzed by PrP-specific sandwich ELISA. Briefly, samples were incubated in POM1-coated ELISA plates (overnight at 4°C). Plates were then washed and incubated with biotinylated POM19 (1.6 ng ml^{-1}) for 1h at 37°C. Avidin-HRP (1:1000) (BD-Pharmigen) was used as detection antibody (1h, 37°C). After 3 washes, stabilized chromogen (Invitrogen) was added, incubated for 30 minutes at 37°C, and absorbance was read at 450 nm. All samples were analysed at dilutions falling within the logarithmic range of the calibration curve ($rmPrP_{23-230}$: 0.62-80 ng ml^{-1}).

IMMUNOCYTOCHEMISTRY

For immunocytochemistry, organotypic COCS were washed twice in PBS and fixed in 4% formalin overnight at 4°C. Membrane inserts were washed and incubated for 1 h in blocking buffer (0.05% vol/vol Triton X-100 and 3% vol/vol goat serum dissolved in PBS) and incubated with primary antibodies diluted in blocking buffer at 4°C for 3 d. Primary antibodies and concentrations used were mouse anti-Neuronal Nuclei (NeuN, 1 µg ml^{-1}, Serotec), rat anti-CD68 (1 µg ml^{-1}, Serotec), rabbit anti- glial fibrillary acidic protein (GFAP, 1 µg ml^{-1}, DAKO) and directly conjugated mouse anti-NeuN-$Alexa^{488}$ (0.5 µg ml^{-1}, Millipore). The primary antibodies were detected using Alexa-conjugated secondary antibodies (3 µg ml^{-1}, Molecular Probes) and counterstained with 4,6-diamidino-2-phenylindole (DAPI) (1 µg ml^{-1}). For NeuN morphometry images were recorded at 4x magnification on a fluorescence microscope (BX-61, Olympus) equipped with a cooled black/white CCD camera at identical exposure times. TUNEL imaging assay was performed according to manufacturer's protocol (Promega) and, images were taken and quantified like NeuN stainings. Confocal images were taken with a Leica SP5 confocal laser scanning microscope using a 40x oil immersion lens. The area of immunoreactivity was determined by morphometry with image analysis software analySIS vs5.0 using greyscale threshold settings for identifying positive pixels. Hematoxylin and eosin staining (H&E) of slices was performed on thin paraffin sections according to standard protocols.

PROTEOLYTIC ASSAYS

Slices were harvested in pools of 18 slices in PBS, 0.5% DOC, 0.5% NP-40 with 2% β-mercaptoethanol and homogenized by trituration. Homogenates were analyzed immediately for DEVDase activity using caspase 3 fluorometric detection kit (Enzo Life Sciences Caspase-3 Activity Assay kit) and normalized to protein concentration. Slices (pools

of 18) were homogenized and processed according to the manufacturer's instructions (Biovision Calpain Activity Assay kit). Cleavage of calpain substrate, Ac-LLVY-AFC was measured on a fluorescence plate reader (360-nm excitation filter, 440-nm emission filter) and normalized to protein amount.

ELECTRON MICROSCOPY

Slices were washed in Na-phosphate buffer, fixed in freshly prepared 2% PFA + 2.5% GA in 0.1 M Na-phosphate buffer 0.1 M pH 7.4, postfixed in 1% osmium tetroxide for 1-2 hours, dehydrated through a series of graded ethanol and propylene oxide, embedded in Epon and processed for electron microscopy using standard procedures. Grids were examined and photographed in JEOL JEM 100 CX and JEOL JEM 1011 transmission electron microscopes at 80 kV. Nuclear morphology (as presented in Supplementary Figure 10) was determined by counting 11 fields in IgG-treated COCS at 3, 7, and 10 dpe. For POM1-treated COCS, 10 fields at 3 dpe, 12 fields at 5 and 10 dpe, were analyzed. For assessing necrotic, apoptotic and normal POM1-treated slices at 7 dpe, 15, 16 and 20 fields were counted, respectively.

VIABILITY AND ROS ASSAYS

For propidium iodide (PI) incorporation, slices were incubated for 30 min with PI (5 µg ml^{-1}) and images were recorded in living tissue using a fluorescent microscope (Axiovert 200) equipped with a cooled CCD camera using a 5x objective and analysed by morphometry using the software analySIS vs5.0.

Lucigenin conversion assay was performed at room temperature as follows: Inserts containing 5-10 slices each were washed in PBS and harvested in Krebs-Ringer solution supplemented with complete mini protease inhibitor cocktail (Roche). Samples were triturated with a 30G syringe, and 50 µl of each sample was mixed with 175 µl assay buffer and 0.25 µl lucigenin (10 mM). Background activity was measured using a chemiluminescence reader. Subsequently, 50 µl NADPH (1 mM) was added to each well and the plate was read again. Background activity was subtracted from the NADPH dependent signal and data (each bar: average of 4 inserts ± s.d.) are presented as relative light unit mg^{-1} total protein.

STATISTICAL ANALYSIS OF COCS

One-way ANOVA with Tukey's post-test for multi-column comparison, or Dunnet's post-test for comparison of all columns to a control column, were used for statistical analysis of experiments involving the comparison of three or more samples. Paired Student's t-test was used for comparing two samples. Results are displayed as the average of replicas ± s.d.

F(AB)$_1$POM1 AND F(AB)$_2$POM1 GENERATION

F(ab)$_1$POM1 and F(ab)$_2$POM1 fragments were generated by ficin digestion and purified on a protein A column according to manufacturer's protocol (Pierce). Ficin is a non-specific sulfhydryl protease that cleaves antibodies into Fab and F(ab')$_2$ fragments in the presence of cysteine. The cleavage reaction leads mainly to monovalent Fab or divalent F(ab')$_2$ fragments depending on the concentration of cysteine and digestion times. By purification with protein A, Fc fragments and undigested IgG are retained in the column, while Fab and F(ab')$_2$ fragments are eluted. Protein A flow-through containing F(ab)$_1$POM1 was collected, concentrated by amicon ultra-15 centrifugal units (Millipore). F(ab)$_1$POM1 was further purified by size exclusion chromatography (Superdex75 10/300 GL, GE Healthcare) using PBS and a flow rate of 0.5 ml min^{-1}. Pure fractions were pooled, concentrated and stored at -20°C. The concentrations of the IgG and F(ab)$_1$POM fragments were determined by measuring their absorbance at 280 nm in a UV-VIS photometer using an extinction coefficient (E) 0.1% at 280nm of 1.35. Aldolase (158 kDa), conalbumin (75 kDa) and ovalbumin (43 kDa) were used as control molecular weight markers. The purity of the fragments was checked by Coomassie-stained SDS PAGE.

F(AB)$_1$POM FRAGMENTS GENERATION

For Kd determination, F(ab)$_1$POM fragments were generated from the POM antibodies using immobilized papain (10-20 mg of mAb ml^{-1} of immobilized papain as packed resin) activated in digestion buffer (20 mM sodium phosphate, 10 mM EDTA, 20 mM cysteine hydrochloride, pH 7.0) according to the manufacturer's instructions (Pierce, Rockfort, IL). The reaction mixture was incubated overnight with rigorous shaking at 37°C. The digest was separated from the immobilized papain with a resin separator. The immobilized papain was then washed with binding buffer (Protein A IgG Binding Buffer, Pierce) which was added to the digest. To remove undigested IgG and Fc fragments from the F(ab)$_1$ fragments, the digest was loaded onto a 2 ml Protein A plus Agarose column (Pierce), equilibrated in binding buffer, and washed with 6 ml binding buffer. The F(ab)$_1$-containing flow-through and wash fractions were pooled and further purified by size exclusion chromatography as described above.

PERIPLASMIC EXPRESSION AND PURIFICATION OF SCFVPOM1 AND SCFVPOM2

For periplasmic expression and purification of scFv^{POM2}, the pET-22b(+) vector (Novagen) was used, as it has both periplasmic localization and C-term 6xHis tag sequences. The scFvPOM2 gene, constructed previously using the phage display method (Polymenidou et al., 2008),

was inserted into the pET-22b(+) vector between the restriction sites- *Eco*RI and *Xho*I. The resulting plasmid was transformed into competent Rosetta^{TM} (DE3) pLysS cells by heat-shock.

A fresh, single colony of transformed Rosetta cells was inoculated in 2xYT media with 100 μg ml^{-1} Ampicillin and 34 μg ml^{-1} Chloramphenicol (2xYT-AC media) and grown overnight at 37°C at 250 rpm. The overnight culture was further propagated (1:1000) in fresh 2xYT-AC media until the OD_{600} reached ~0.4-0.5. The culture was then cooled down to 25°C in a cold water bath and induced with Isopropyl β-D-1-thiogalactopyranoside (IPTG) to a final concentration of 0.5 mM. The induction was allowed to continue overnight at 25°C and 250 rpm. The cells were harvested and resuspended in 50ml l^{-1} of the original culture volume of freshly prepared, pre-chilled periplasmic extraction buffer [200mM Tris-HCl, 20% (w/v) sucrose, 1 mM EDTA pH-8.0] and incubated on ice for 1 hour with occasional stirring. The suspension was spun down at 15,000xg for 30 min at 4°C and the supernatant was collected as the soluble protein extract. The extract was thoroughly dialyzed against 50 mM Tris-HCl, 100 mM NaCl, pH 7.0 at 4°C and further clarified by centrifugation at 15,000xg for 30 min at 4°C(Das et al., 2005).

The clarified soluble protein extract was loaded onto a Ni-NTA agarose (Qiagen) column equilibrated with 50 mM Tris and 100 mM NaCl, pH 7.0. The unbound protein and impurities were washed off with 50 mM Tris, 100 mM NaCl and 50 mM Imidazole pH 7.0 and the elution was performed with 50 mM Tris, 100 mM NaCl and 500 mM Imidazole pH 7.0. The purity of the eluates was checked using gel electrophoresis. Pure $scFV^{POM2}$ samples were dialyzed against 50 mM Tris, 100 mM NaCl and 50 mM Imidazole pH 7.0 and concentrated to ~3 mg ml^{-1}. The same procedures applied to expression and purification of periplasmic $scFv^{POM1}$ except the induction was at 17°C.

EXPRESSION AND PURIFICATION OF SCFVPOM1, VH AND VL FROM INCLUSION BODIES

Primers for light chain and heavy chain POM1 amplification were designed by Pravas Baral : Heavy chain forward primer sequence: 5'-CGA-CAT-GCC-ATG-GTC-CAG-CTC-CAG-CA-3'; Heavy chain reverse primer sequence: 5'-TAA-AAT-CCT-CGA-GAC-TAC-CGC-GTG-GC-3'; Light chain forward primer sequence: 5'-CGA-CAT-CCC-ATG-GAT-ATT-GTG-CTG-AC-3'; Light chain reverse primer sequence: 5'-TAA- AAT-CCT-CGA-GAC-TAC-CGC-GTG-GC-3'. Primers #1 and #2 were used to amplify the heavy chain whereas #3 and #4 were used to amplify the light chain. These amplified products were then inserted into the pET22b (+) (Novagen) vector using the NcoI and XhoI restriction sites.

For protein expression, the heavy and light chain plasmids were heat transformed into chemically competent Rosetta (DE3) pLysS cells (Novagen). As the periplasmic fraction yield was very low, all the protein was obtained from the inclusion bodies only. The harvested cells were resuspended in 50 mM Tris, 150 mM NaCl , pH 8.0 (5% of original culture volume) and cells were disrupted by sonication (amplitude 50%, 3x 30 seconds with 30 seconds intermediate cooling period). Inclusion bodies were obtained by spinning down the sonicated suspensionn at 27,000 x g for 30 minutes at 4^{o}C. The IBs were extensively washed, first with 2% sodiumdeoxycholate in 50 mM Tris-Cl, 200 mM NaCl, pH 8.0, followed by 6 washes with 50 mM Tris-Cl, 200 mM NaCl, pH8.0. Purified inclusion bodies were dissolved in 8M urea, 100 mM NaH_2PO_4, 10 mM Tris, 10 mM reduced Glutathione, 5 mM Imidazole, pH 8.0 by gently stirring over night at room temperature. After centrifugation at 15,000 rpm, the supernatant containing the denatured scFv (light chain-, heavy chain-)-POM1 fragments, was loaded onto Ni-NTA, equilibrated with denaturing buffer. After loading the column was washed with 5 CV denaturing buffer, followed by 2 CV 50 mM Imodazole in denaturing buffer and elution of scFv (light chain, heavy chain)-POM1 with 500 mM Imidazole in the same buffer; The elute was diluted with 50 mM KCl, 50 mM Tris-Cl, pH 8.0 to a final urea concentration of 4 M urea. Urea was totally removed by stepwise dialysis against 3M, 2M, 1M, 0.5 M and 0M urea in 50 mM KCl, 50 mM Tris-Cl, pH 8.0; samples were concentrated using filter devices from Amicon with a MWCO 10,000Da. Samples were dialysed against 50 mM Tris-Cl, 100 mM NaCl, 250 mM Imidazole, pH 7.0.

PERIPLASMIC EXPRESSION AND PURIFICATION OF RMPRP$_{23-230}$ AND RMPRP$_{90-230}$:

Recombinant mouse PrP was generated in bacteria and purified as reported elsewhere (Lysek and Wüthrich, 2004; Zahn et al., 1997).

PEPTIDES 1, 2 AND 3

Three anti-prion peptides (CQSNTWPYTC, CQWRSNPTYC and CDPSDSYC) were designed by P. Baral, based on the structural data from the crystal structures of POM1 F(ab)$_1$:huPrP (PDB ID:4DGI) and ICSM18 F(ab)$_1$:huPrP (PDB ID:2W9E). The terminal residues of the linear peptide fragment were changed to cysteine in order to make a disulphide bond joining the N-terminus and the C-terminus. Crude peptide fragments were synthesized and were purified using reversed-phase high-performance liquid chromatography (RP-HPLC). Afterwards the peptides were cyclized in a one-step oxidation reaction in ammonium bicarbonate (0.1 M, pH 8.5) and stirred for 24h at room temperature.

SPR MEASUREMENTS AND BINDING AFFINITY DETERMINATION

Amino-terminally truncated $rmPrP_{90-230}$ and full-length $rmPrP_{23-230}$ were immobilized on a carboxymethylated-dextran sensor chip (CM5, Biacore) by standard EDC/NHS chemistry, and active carboxyl groups were deactivated by adding ethanolamine. The amount of protein immobilized on the surface corresponded to 1000 Resonance Units (RU) of $rmPrP_{23-231}$ and 4600 RU of $rmPrP_{90-230}$ when comparing $F(ab)_1$POM1 binding in the absence of the OR.

When comparing different $F(ab)_1$ affinities, a density of 100 RU of $rmPrP_{23-230}$ was used (Table 3.1). Various concentration measurements of $F(ab)_1$ were performed on a Biacore T100 at 37°C. $F(ab)_1$ fragments, diluted in running buffer (HBS-EP+) and at a concentration range of 0.01-5.12 nM, were injected for 350s at a flow rate of 30 µl min^{-1}. The sensor surface was regenerated between each measurement with 20 mM NaOH. Binding affinity was determined using the instrument software (Biacore T100 Evaluation Software, version: 2.0.3).

Measurements of $F(ab)_1$ and scFvPOM1 ranging between 0.04-5.12nM were conducted at 37°C (reflecting the *in vitro* experiment conditions) with a lower density surface of $rmPrP_{23-230}$ (100 RU). Comparisons of the two measurements are reported in Table 3.2.

The affinity of small molecules (like peptides) was measured using a surface with an higher density of rmPrP. Fifty $\mu g ml^{-1}$ of $rmPrP_{23-230}$ in water.in a volume of 100µl were injected for 420s to achieve a surface of 5500 RU. PEP01, PEP02 and PEP03 were used at conc. of 10.24, 5.12, 2.56, 1.28, 0.64, 0.32, 0.16, 0.08, 0.04, and 0 nM.

BIACORE MEASUREMENTS IN SOLUTION

Full-length $rmPrP_{23-230}$ was immobilized on a carboxymethylated-dextran sensor chip (CM5, Biacore) by standard EDC/NHS chemistry. The amount of protein immobilized on the surface corresponded to 3380 RU of $rmPrP_{23-230}$.

In order to obtain the calibration curve, concentrations of antibody, ranging from 10.9 to 0.05nM (10.935, 3.645, 1.215, 0.405, 0.135, 0.405, 0.135, 0.045, 0.015, 0.05nM) were diluted in HBS-EP buffer and injected at a flow rate of 10µl ml^{-1}. Various concentrations of rmPrP (193.83, 65.61, 21.87, 7.29, 2.43, 0.81, 0.27, 0.09, 0.03, 0.01, 0.003 and 0 nM) were mixed with 0.5nM of POM1 and injected at a flow rate of 10µl ml^{-1}. The surface was regenerated with 20mM NaOH before each concentration was injected. This procedure was applied only to POM1 and POM19.

In a second set of experiments concentrations of $rmPrP_{23-230}$ in a range of 5.12-0 nM (5.12, 2.56, 1.28, 0.64, 0.32, 0.16, 0.08, 0.04, 0.02, 0.01, 0.005, 0 nM) were pre-incubated with 0.5nM of antibody. In addition, BSA 0.1mg/ml was supplemented to the buffer solution to diminish any aggregation. This procedure was applied to POM1, POM19, POM5, POM13, POM15, POM19 and POM6.

PROTEIN EXPRESSION

For the expression of uniform $^{2}H^{15}N$]-labeled $rmPrP_{23-230}$, M9 medium was produced from D_2O. M9 medium was supplemented with magnesium chloride, vitamins, ampicillin (final concentration: 100 µg ml^{-1}) and ammonium chloride (2g l^{-1}). The main culture was started by transferring cells from a 2l preculture of LB medium grown to an OD 1.6 at 37°C into 2 liter of M9 D_2O medium. Cells were further incubated for 1h at 37°C and induced by addition of 1 mM IPTG. After 6h, cells were harvested and $rmPrP_{23-230}$ was purified according to our standard protocol (Hornemann et al., 2009a; Zahn et al., 1997).

NMR EXPERIMENTS

The [^{15}N,^{1}H]-TROSY NMR(Pervushin et al., 1997) experiments of the ^{2}H,^{15}N-labeled $rmPrP_{23-231}$ free and in presence of $scFv^{POM1}$ complex were performed on a Bruker Avance 700 MHz spectrometer equipped with a 5 mm triple-resonance cryoprobe and a single pulsed field gradient in 10 mM sodium phosphate, pH 7.3, 20°C, and 5% (v/v) D_2O. The data were processed by the software XwinNMR, version 3.5 (Bruker, Germany) and further analysed by the program CARA (www.nmr.ch)(keller, 2004). The backbone assignment for mouse mPrP(23-230) is based on the assignment of residues 89-230 at pH 7, which is deposited in the BioMagResBank (accession numbers: rmPrP-(90–230), 16071, numeration according to human PrP (Hornemann et al., 2009b) and a tentative assignment for residues 23-88 was based on the available assignments at pH 4.5 (Riek, 1998).

DATA COLLECTION AND STRUCTURE DETERMINATION

Diffraction quality POM1 $F(ab)_1$:$rmPrP_{120-230}$ protein complex crystals were grown by the vapor diffusion method at room temperature as described by Baral et al (Baral et al., 2011). X ray diffraction data were measured at the Stanford Synchrotron Radiation Laboratory (SSRL), beamline 9-2(Cohen et al., 2002)'(Gonzalez et al., 2008)'(McPhillips et al., 2002). The data were processed in space group *C2* to a resolution of 1.9Å using the program HKL2000(Otwinowski and Minor, 1997). The data collection details as well as the refinement statistics are presented in Supplementary Table 5.1. The structure of POM1 $F(ab)_1$:$rmPrP_{120-230}$ protein complex was solved by the molecular replacement method using

the program MOLREP(Vagin and Teplyakov, 1997) of the CCP4 package (Winn et al., 2011). The coordinates of POM1 $F(ab)_1$:$huPrP_{120-230}$ protein complex, protein data bank (PDB ID: 4DGI), were used as the template. Solution from the molecular replacement was then refined by restrained refinement, implemented in the refinement program of the PHENIX package (Echols et al., 2012). The progress of the refinement process was monitored by a reduction in both the R_{work} and R_{free} factors to 19.9% and 23.4%, respectively. Solvent molecules are added to the model by an automated PHENIX program and those water molecules were accepted only when well defined positive peaks were present in both the $2|F_o|-|F_c|$ and $|F_o|-|F_c|$ electron density maps and there was a satisfactory hydrogen-bonding network with either protein atoms or other water molecules. Model building was performed with the program COOT(Emsley and Cowtan, 2004). The final structural coordinates for the POM1 $F(ab)_1$:$rmPrP_{120-230}$ complex were validated with MOLPROBITY(Chen et al., 2010) and deposited in the RSCB PDB (accession code 4H88) along with the structure factors. MOLPROBITY showed that 96.8% of the amino acid residues were in the most favored region of the Ramachandran plot.

Supplementary Table 5.1. Crystallographic analysis of the POM1-PrP complex: data collection and refinement statistics.

	POM1 $F(ab)_1$:PrP(120-230)
Data collection	
Space group	C2
Cell dimensions	
a, *b*, *c* (Å)	83.4, 107.3, 75.4
α, β, γ (°)	90.0, 95.2, 90.0
Resolution (Å)	50-1.90 (1.97-1.90) *
R_{merge}	0.08 (0.52)
$I/\sigma I$	4.2 (3.9)
Completeness (%)	96.0 (74.1)
Redundancy	4.2 (3.9)
Refinement	
Resolution (Å)	50.0-1.90
No. reflections	49,880

$R_{work/}$ R_{free}	0.19/0.23
No. atoms	
Protein	4153
Ligand/ion	1
Water	359
B-factors	
Protein	42.2
Ligand/ion	12.8
Water	43.7
R.m.s deviations	
Bond lengths (Å)	0.006
Bond angles (°)	0.956

Number of crystals =1.

*Highest resolution shell is shown in parenthesis.

ILLUSTRATIONS

All illustrations were created with the program Pymol (www.pymol.org).

SCRAPIE CELL ASSAY IN ENDPOINT FORMAT (SCEPA)

Prion-susceptible neuroblastoma cells (subclone N2aPK1)(Klohn et al., 2003) were exposed to 300-µl brain homogenates using 6 replicas per dilution in 96-well plates for 3 d. Cells were subsequently split three times 1:10 every 3 days. After the cells reached confluence, 25'000 cells from each well were filtered onto the membrane of ELISPOT plates, treated with PK (0.5 µg ml^{-1} for 90 min at 37°C), denatured, and infected (PrP^{Sc+}) cells were detected by immunocytochemistry using alkaline phosphatase-conjugated POM1 mouse anti-PrP and an alkaline phosphatase-conjugated substrate kit (Bio-Rad). We performed serial ten-fold dilutions of experimental samples in cell culture medium containing healthy mouse brain homogenate. Scrapie-susceptible PK1 cells were then exposed to dilutions of experimental samples ranging from 10^{-4} to 10^{-7} (corresponding to homogenate with a protein concentration of 10 µg ml^{-1} to 0.01 µg ml^{-1}), or to a 10-fold dilution of RML or healthy mouse brain homogenate. Samples were quantified in endpoint format by counting positive wells according to established methods(Klohn et al., 2003).

REFERENCES

Aarts, M., Iihara, K., Wei, W.L., Xiong, Z.G., Arundine, M., Cerwinski, W., MacDonald, J.F., and Tymianski, M. (2003). A key role for TRPM7 channels in anoxic neuronal death. Cell *115*, 863-877.

Abalos, G.C., Cruite, J.T., Bellon, A., Hemmers, S., Akagi, J., Mastrianni, J.A., Williamson, R.A., and Solforosi, L. (2008). Identifying Key Components of the PrP(C)-PrP(Sc) Replicative Interface. Journal of Biological Chemistry *283*, 34021-34028.

Abramov, A.Y., Scorziello, A., and Duchen, M.R. (2007). Three distinct mechanisms generate oxygen free radicals in neurons and contribute to cell death during anoxia and reoxygenation. J Neurosci *27*, 1129-1138.

Aguzzi, A., Baumann, F., and Bremer, J. (2008). The prion's elusive reason for being. Annu Rev Neurosci *31*, 439-477.

Aguzzi, A., and Calella, A.M. (2009). Prions: protein aggregation and infectious diseases. Physiol Rev *89*, 1105-1152.

Aguzzi, A., and Haass, C. (2003). Games played by rogue proteins in prion disorders and Alzheimer's disease. Science *302*, 814-818.

Aguzzi, A., Heikenwalder, M., and Polymenidou, M. (2007). Insights into prion strains and neurotoxicity. Nat Rev Mol Cell Biol *8*, 552-561.

Alfa Cisse, M., Sunyach, C., Slack, B.E., Fisher, A., Vincent, B., and Checler, F. (2007). M1 and M3 muscarinic receptors control physiological processing of cellular prion by modulating ADAM17 phosphorylation and activity. J Neurosci *27*, 4083-4092.

Aller, M.I., Jones, A., Merlo, D., Paterlini, M., Meyer, A.H., Amtmann, U., Brickley, S., Jolin, H.E., McKenzie, A.N., Monyer, H.*, et al.* (2003). Cerebellar granule cell Cre recombinase expression. Genesis *36*, 97-103.

Alper, T., Cramp, W.A., Haig, D.A., and Clarke, M.C. (1967). Does the agent of scrapie replicate without nucleic acid? Nature *214*, 764-766.

Alper, T., Haig, D.A., and Clarke, M.C. (1966). The exceptionally small size of the scrapie agent. Biochem Biophys Res Commun *22*, 278-284.

Aronoff-Spencer, E., Burns, C.S., Avdievich, N.I., Gerfen, G.J., Peisach, J., Antholine, W.E., Ball, H.L., Cohen, F.E., Prusiner, S.B., and Millhauser, G.L. (2000). Identification of the Cu2+ binding sites in the N-terminal domain of the prion protein by EPR and CD spectroscopy. Biochemistry *39*, 13760-13771.

Avshalumov, M.V., Chen, B.T., and Rice, M.E. (2000). Mechanisms underlying H(2)O(2)-mediated inhibition of synaptic transmission in rat hippocampal slices. Brain Res *882*, 86-94.

Avshalumov, M.V., and Rice, M.E. (2002). NMDA receptor activation mediates hydrogen peroxide-induced pathophysiology in rat hippocampal slices. J Neurophysiol *87*, 2896-2903.

Balducci, C., Beeg, M., Stravalaci, M., Bastone, A., Sclip, A., Biasini, E., Tapella, L., Colombo, L., Manzoni, C., Borsello, T.*, et al.* (2010). Synthetic amyloid-beta oligomers impair long-term memory independently of cellular prion protein. Proc Natl Acad Sci U S A *107*, 2295-2300.

Bano, D., Young, K.W., Guerin, C.J., Lefeuvre, R., Rothwell, N.J., Naldini, L., Rizzuto, R., Carafoli, E., and Nicotera, P. (2005). Cleavage of the plasma membrane Na+/Ca2+ exchanger in excitotoxicity. Cell *120*, 275-285.

Baral, P.K., Wieland, B., Swayampakula, M., Polymenidou, M., Aguzzi, A., Kav, N.N., and James, M.N. (2011). Crystallization and preliminary X-ray diffraction analysis of prion protein bound to the Fab fragment of the POM1 antibody. Acta Crystallogr Sect F Struct Biol Cryst Commun *67*, 1211-1213.

Baron, G.S., and Caughey, B. (2003). Effect of glycosylphosphatidylinositol anchor-dependent and -independent prion protein association with model raft membranes on conversion to the protease-resistant isoform. J Biol Chem *278*, 14883-14892.

Barry, A.E., Klyubin, I., Mc Donald, J.M., Mably, A.J., Farrell, M.A., Scott, M., Walsh, D.M., and Rowan, M.J. (2011). Alzheimer's disease brain-derived amyloid-beta-mediated inhibition of LTP in vivo is prevented by immunotargeting cellular prion protein. J Neurosci *31*, 7259-7263.

Basler, K., Oesch, B., Scott, M., Westaway, D., Walchli, M., Groth, D.F., McKinley, M.P., Prusiner, S.B., and Weissmann, C. (1986). Scrapie and cellular PrP isoforms are encoded by the same chromosomal gene. Cell *46*, 417-428.

Baumann, F., Pahnke, J., Radovanovic, I., Rulicke, T., Bremer, J., Tolnay, M., and Aguzzi, A. (2009). Functionally relevant domains of the prion protein identified in vivo. PLoS ONE *4*, e6707.

Baumann, F., Tolnay, M., Brabeck, C., Pahnke, J., Kloz, U., Niemann, H.H., Heikenwalder, M., Rulicke, T., Burkle, A., and Aguzzi, A. (2007). Lethal recessive myelin toxicity of prion protein lacking its central domain. Embo J *26*, 538-547.

Beland, M., and Roucou, X. (2012). The prion protein unstructured N-terminal region is a broad-spectrum molecular sensor with diverse and contrasting potential functions. J Neurochem *120*, 853-868.

Bell, J.U., Lopez, J.M., and Bartos, K.D. (1987). The postnatal development of serum zinc, copper and ceruloplasmin in the horse. Comp Biochem Physiol A Comp Physiol *87*, 561-564.

Bennett, B.L., Sasaki, D.T., Murray, B.W., O'Leary, E.C., Sakata, S.T., Xu, W., Leisten, J.C., Motiwala, A., Pierce, S., Satoh, Y.*, et al.* (2001). SP600125, an anthrapyrazolone inhibitor of Jun N-terminal kinase. Proc Natl Acad Sci U S A *98*, 13681-13686.

Berdichevsky, Y., Dryer, A.M., Saponjian, Y., Mahoney, M.M., Pimentel, C.A., Lucini, C.A., Usenovic, M., and Staley, K.J. (2013). PI3K-Akt signaling activates mTOR-mediated epileptogenesis in organotypic hippocampal culture model of post-traumatic epilepsy. J Neurosci *33*, 9056-9067.

Boland, M.P., Hatty, C.R., Separovic, F., Hill, A.F., Tew, D.J., Barnham, K.J., Haigh, C.L., James, M., Masters, C.L., and Collins, S.J. (2010). Anionic phospholipid interactions of the prion protein N terminus are minimally perturbing and not driven solely by the octapeptide repeat domain. J Biol Chem *285*, 32282-32292.

Bolton, D.C., McKinley, M.P., and Prusiner, S.B. (1982). Identification of a protein that purifies with the scrapie prion. Science *218*, 1309-1311.

Brandner, S., Isenmann, S., Raeber, A., Fischer, M., Sailer, A., Kobayashi, Y., Marino, S., Weissmann, C., and Aguzzi, A. (1996). Normal host prion protein necessary for scrapie-induced neurotoxicity. Nature *379*, 339-343.

Bremer, J., Baumann, F., Tiberi, C., Wessig, C., Fischer, H., Schwarz, P., Steele, A.D., Toyka, K.V., Nave, K.A., Weis, J.*, et al.* (2010). Axonal prion protein is required for peripheral myelin maintenance. Nat Neurosci *13*, 310-318.

Brennan, A.M., Suh, S.W., Won, S.J., Narasimhan, P., Kauppinen, T.M., Lee, H., Edling, Y., Chan, P.H., Swanson, R.A. (2009). NADPH oxidase is the primary source of superoxide induced by NMDA receptor activation. Nat Neurosci *12*, 857-863.

Brown, D.R., Herms, J., and Kretzschmar, H.A. (1994). Mouse cortical cells lacking cellular PrP survive in culture with a neurotoxic PrP fragment. Neuroreport *5*, 2057-2060.

Brown, D.R., Schmidt, B., and Kretzschmar, H.A. (1996). Role of microglia and host prion protein in neurotoxicity of a prion protein fragment. Nature *380*, 345-347.

Brown, D.R., Schmidt, B., and Kretzschmar, H.A. (1997a). Effects of oxidative stress on prion protein expression in PC12 cells. Int J Dev Neurosci *15*, 961-972.

Brown, D.R., Schulz-Schaeffer, W.J., Schmidt, B., and Kretzschmar, H.A. (1997b). Prion protein-deficient cells show altered response to oxidative stress due to decreased SOD-1 activity. Exp Neurol *146*, 104-112.

Brown, D.R., Wong, B.S., Hafiz, F., Clive, C., Haswell, S.J., and Jones, I.M. (1999). Normal prion protein has an activity like that of superoxide dismutase. Biochem J *344 Pt 1*, 1-5.

Budka, H., Aguzzi, A., Brown, P., Brucher, J.M., Bugiani, O., Gullotta, F., Haltia, M., Hauw, J.J., Ironside, J.W., Jellinger, K.*, et al.* (1995). Neuropathological diagnostic criteria for Creutzfeldt-Jakob disease (CJD) and other human spongiform encephalopathies (prion diseases). Brain Pathol *5*, 459-466.

Bueler, H., Aguzzi, A., Sailer, A., Greiner, R.A., Autenried, P., Aguet, M., and Weissmann, C. (1993). Mice devoid of PrP are resistant to scrapie. Cell *73*, 1339-1347.

Büeler, H.R., Fischer, M., Lang, Y., Bluethmann, H., Lipp, H.P., DeArmond, S.J., Prusiner, S.B., Aguet, M., and Weissmann, C. (1992). Normal development and behaviour of mice lacking the neuronal cell-surface PrP protein. Nature *356*, 577-582.

Burns, C.S., Aronoff-Spencer, E., Dunham, C.M., Lario, P., Avdievich, N.I., Antholine, W.E., Olmstead, M.M., Vrielink, A., Gerfen, G.J., Peisach, J.*, et al.* (2002). Molecular features of the copper binding sites in the octarepeat domain of the prion protein. Biochemistry *41*, 3991-4001.

Calella, A.M., Farinelli, M., Nuvolone, M., Mirante, O., Moos, R., Falsig, J., Mansuy, I.M., and Aguzzi, A. (2010). Prion protein and Abeta-related synaptic toxicity impairment. EMBO Mol Med *2*, 306-314.

Chen, S., Mange, A., Dong, L., Lehmann, S., and Schachner, M. (2003). Prion protein as trans-interacting partner for neurons is involved in neurite outgrowth and neuronal survival. Mol Cell Neurosci *22*, 227-233.

Chen, S.G., Teplow, D.B., Parchi, P., Teller, J.K., Gambetti, P., and Autilio-Gambetti, L. (1995). Truncated forms of the human prion protein in normal brain and in prion diseases. J Biol Chem *270*, 19173-19180.

Chen, V.B., Arendall, W.B., III, Headd, J.J., Keedy, D.A., Immormino, R.M., Kapral, G.J., Murray, L.W., Richardson, J.S., and Richardson, D.C. (2010). MolProbity: all-atom structure validation for macromolecular crystallography. Acta Crystallographica Section D *66*, 12-21.

Chesebro, B., Trifilo, M., Race, R., Meade-White, K., Teng, C., LaCasse, R., Raymond, L., Favara, C., Baron, G., Priola, S.*, et al.* (2005). Anchorless prion protein results in infectious amyloid disease without clinical scrapie. Science *308*, 1435-1439.

Cheung, E.C., and Slack, R.S. (2004). Emerging role for ERK as a key regulator of neuronal apoptosis. Sci STKE *2004*, PE45.

Chiarini, L.B., Freitas, A.R., Zanata, S.M., Brentani, R.R., Martins, V.R., and Linden, R. (2002). Cellular prion protein transduces neuroprotective signals. Embo J *21*, 3317-3326.

Chiesa, R., Piccardo, P., Dossena, S., Nowoslawski, L., Roth, K.A., Ghetti, B., and Harris, D.A. (2005). Bax deletion prevents neuronal loss but not neurological symptoms in a transgenic model of inherited prion disease. Proc Natl Acad Sci U S A *102*, 238-243.

Chiesa, R., Piccardo, P., Ghetti, B., and Harris, D.A. (1998). Neurological illness in transgenic mice expressing a prion protein with an insertional mutation. Neuron *21*, 1339-1351.

Choi, H.S., Kim, J.W., Cha, Y.N., and Kim, C. (2006). A quantitative nitroblue tetrazolium assay for determining intracellular superoxide anion production in phagocytic cells. J Immunoassay Immunochem *27*, 31-44.

Christensen, H.M., Dikranian, K., Li, A., Baysac, K.C., Walls, K.C., Olney, J.W., Roth, K.A., and Harris, D.A. (2010a). A highly toxic cellular prion protein induces a novel, nonapoptotic form of neuronal death. Am J Pathol *176*, 2695-2706.

Christensen, H.M., Dikranian, K., Li, A., Baysac, K.C., Walls, K.C., Olney, J.W., Roth, K.A., and Harris, D.A. (2010b). A highly toxic cellular prion protein induces a novel, nonapoptotic form of

neuronal death. Am J Pathol *176*, 2695-2706.

Cohen, A.E., Ellis, P.J., Miller, M.D., Deacon, A.M., and Phizackerley, R.P. (2002). An automated system to mount cryo-cooled protein crystals on a synchrotron beamline, using compact sample cassettes and a small-scale robot. Journal of Applied Crystallography *35*, 720-726.

Coitinho, A.S., Freitas, A.R., Lopes, M.H., Hajj, G.N., Roesler, R., Walz, R., Rossato, J.I., Cammarota, M., Izquierdo, I., Martins, V.R.*, et al.* (2006). The interaction between prion protein and laminin modulates memory consolidation. Eur J Neurosci *24*, 3255-3264.

Collinge, J., Palmer, M.S., and Dryden, A.J. (1991). Genetic predisposition to iatrogenic Creutzfeldt-Jakob disease. Lancet *337*, 1441-1442.

Collinge, J., Sidle, K.C., Meads, J., Ironside, J., and Hill, A.F. (1996). Molecular analysis of prion strain variation and the aetiology of 'new variant' CJD. Nature *383*, 685-690.

Collins, S., McLean, C.A., and Masters, C.L. (2001). Gerstmann-Straussler-Scheinker syndrome,fatal familial insomnia, and kuru: a review of these less common human transmissible spongiform encephalopathies. J Clin Neurosci *8*, 387-397.

Cortes, C.J., Qin, K., Cook, J., Solanki, A., and Mastrianni, J.A. (2012). Rapamycin delays disease onset and prevents PrP plaque deposition in a mouse model of Gerstmann-Straussler-Scheinker disease. J Neurosci *32*, 12396-12405.

Das, D., Allen, T.M., and Suresh, M.R. (2005). Comparative evaluation of two purification methods of anti-CD19-c-myc-His6-Cys scFv. Protein Expr Purif *39*, 199-208.

De Gioia, L., Selvaggini, C., Ghibaudi, E., Diomede, L., Bugiani, O., Forloni, G., Tagliavini, F., and Salmona, M. (1994). Conformational polymorphism of the amyloidogenic and neurotoxic peptide homologous to residues 106-126 of the prion protein. J Biol Chem *269*, 7859-7862.

DeArmond, S.J. (1993). Alzheimer's disease and Creutzfeldt-Jakob disease: overlap of pathogenic mechanisms. Curr Opin Neurol *6*, 872-881.

DeArmond, S.J., Mobley, W.C., DeMott, D.L., Barry, R.A., Beckstead, J.H., and Prusiner, S.B. (1987). Changes in the localization of brain prion proteins during scrapie infection [published erratum appears in Neurology 1987 Nov;37(11):1770]. Neurology *37*, 1271-1280.

Doh-ura, K., Ishikawa, K., Murakami-Kubo, I., Sasaki, K., Mohri, S., Race, R., and Iwaki, T. (2004). Treatment of transmissible spongiform encephalopathy by intraventricular drug infusion in animal models. J Virol *78*, 4999-5006.

Duffy, P., Wolf, J., Collins, G., DeVoe, A.G., Streeten, B., and Cowen, D. (1974). Letter: Possible person-to-person transmission of Creutzfeldt-Jakob disease. N Engl J Med *290*, 692-693.

Echols, N., Grosse-Kunstleve, R.W., Afonine, P.V., Bunkoczi, G., Chen, V.B., Headd, J.J., McCoy, A.J., Moriarty, N.W., Read, R.J., Richardson, D.C*., et al.* (2012). Graphical tools for macromolecular crystallography in PHENIX. Journal of Applied Crystallography *45*, 581-586.

Emsley, P., and Cowtan, K. (2004). Coot: model-building tools for molecular graphics. Acta Crystallographica Section D *60*, 2126-2132.

Falsig, J., and Aguzzi, A. (2008). The prion organotypic slice culture assay - POSCA. Nat Protoc *3*, 555-562.

Falsig, J., Julius, C., Margalith, I., Schwarz, P., Heppner, F., and Aguzzi, A. (2008). A versatile prion replication assay in organotypic brain slices. Nat Neurosci *11*, 109-117.

Falsig, J., Sonati, T., Herrmann, U.S., Saban, D., Li, B., Arroyo, K., Ballmer, B., Liberski, P.P., and Aguzzi, A. (2012). Prion pathogenesis is faithfully reproduced in cerebellar organotypic slice cultures. PLoS Pathog *8*, e1002985.

Fatokun, A.A., Stone, T.W., and Smith, R.A. (2008). Oxidative stress in neurodegeneration and available means of protection. Front Biosci *13*, 3288-3311.

Favata, M.F., Horiuchi, K.Y., Manos, E.J., Daulerio, A.J., Stradley, D.A., Feeser, W.S., Van Dyk, D.E., Pitts, W.J., Earl, R.A., Hobbs, F*., et al.* (1998). Identification of a novel inhibitor of mitogen-activated protein kinase kinase. J Biol Chem *273*, 18623-18632.

Fischer, M., Rülicke, T., Raeber, A., Sailer, A., Moser, M., Oesch, B., Brandner, S., Aguzzi, A., and Weissmann, C. (1996). Prion protein (PrP) with amino-proximal deletions restoring susceptibility of PrP knockout mice to scrapie. Embo J *15*, 1255-1264.

Flechsig, E., Shmerling, D., Hegyi, I., Raeber, A.J., Fischer, M., Cozzio, A., von Mering, C., Aguzzi, A., and Weissmann, C. (2000). Prion protein devoid of the octapeptide repeat region restores susceptibility to scrapie in PrP knockout mice. Neuron *27*, 399-408.

Forloni, G., Angeretti, N., Chiesa, R., Monzani, E., Salmona, M., Bugiani, O., and Tagliavini, F. (1993). Neurotoxicity of a prion protein fragment. Nature *362*, 543-546.

Fournier, J.G. (2000). Introduction to histological localization of prion proteins. Microsc Res Tech *50*, 1.

Fox, J.E., Austin, C.D., Reynolds, C.C., and Steffen, P.K. (1991). Evidence that agonist-induced activation of calpain causes the shedding of procoagulant-containing

microvesicles from the membrane of aggregating platelets. J Biol Chem *266*, 13289-13295.

Fuhrmann, M., Bittner, T., Mitteregger, G., Haider, N., Moosmang, S., Kretzschmar, H., and Herms, J. (2006). Loss of the cellular prion protein affects the Ca2+ homeostasis in hippocampal CA1 neurons. J Neurochem *98*, 1876-1885.

Fukui, M., Choi, H.J., and Zhu, B.T. (2010). Mechanism for the protective effect of resveratrol against oxidative stress-induced neuronal death. Free Radic Biol Med *49*, 800-813.

Gajdusek, D.C., and Zigas, V. (1957). Degenerative disease of the central nervous system in New Guinea; the endemic occurrence of kuru in the native population. N Engl J Med *257*, 974-978.

Gambetti, P., Parchi, P., Petersen, R.B., Chen, S.G., and Lugaresi, E. (1995). Fatal familial insomnia and familial Creutzfeldt-Jakob disease: clinical, pathological and molecular features. Brain Pathol *5*, 43-51.

Gerencser, A.A., Mark, K.A., Hubbard, A.E., Divakaruni, A.S., Mehrabian, Z., Nicholls, D.G., and Polster, B.M. (2009). Real-time visualization of cytoplasmic calpain activation and calcium deregulation in acute glutamate excitotoxicity. J Neurochem *110*, 990-1004.

Gibson, B.A., and Kraus, W.L. (2012). New insights into the molecular and cellular functions of poly(ADP-ribose) and PARPs. Nat Rev Mol Cell Biol *13*, 411-424.

Gimbel, D.A., Nygaard, H.B., Coffey, E.E., Gunther, E.C., Lauren, J., Gimbel, Z.A., and Strittmatter, S.M. (2010). Memory impairment in transgenic Alzheimer mice requires cellular prion protein. J Neurosci *30*, 6367-6374.

Gonzalez, A., Moorhead, P., McPhillips, S.E., Song, J., Sharp, K., Taylor, J.R., Adams, P.D., Sauter, N.K., and Soltis, S.M. (2008). Web-Ice: integrated data collection and analysis for macromolecular crystallography. Journal of Applied Crystallography *41*, 176-184.

Gordon, W.S. (1946). Advances in veterinary research. Vet Rec *58*, 516-525.

Graner, E., Mercadante, A.F., Zanata, S.M., Forlenza, O.V., Cabral, A.L., Veiga, S.S., Juliano, M.A., Roesler, R., Walz, R., Minetti, A.*, et al.* (2000). Cellular prion protein binds laminin and mediates neuritogenesis. Brain Res Mol Brain Res *76*, 85-92.

Gray, B.C., Skipp, P., O'Connor, V.M., Perry, V.H. (2006). Increased expression of glial fibrillary acidic protein fragments and mu-calpain activation within the hippocampus of prion-infected mice. Biochem Soc Trans *34*, 51-54.

Griffith, J.S. (1967). Self-replication and scrapie. Nature *215*, 1043-1044.

Guillot-Sestier, M.V., Sunyach, C., Druon, C., Scarzello, S., and Checler, F. (2009). The alpha-secretase-derived N-terminal product of cellular prion, N1, displays neuroprotective function in vitro and in vivo. J Biol Chem *284*, 35973-35986.

Gulledge, A.T., and Stuart, G.J. (2005). Cholinergic inhibition of neocortical pyramidal neurons. J Neurosci *25*, 10308-10320.

Hainfellner, J.A., Brantner Inthaler, S., Cervenakova, L., Brown, P., Kitamoto, T., Tateishi, J., Diringer, H., Liberski, P.P., Regele, H., and Feucht, M. (1995). The original Gerstmann-Straussler-Scheinker family of Austria: divergent clinicopathological phenotypes but constant PrP genotype. Brain Pathol

5, 201-211.

Harris, D.A. (2003). Trafficking, turnover and membrane topology of PrP. Br Med Bull *66*, 71-85.

Hegde, R.S., Mastrianni, J.A., Scott, M.R., DeFea, K.A., Tremblay, P., Torchia, M., DeArmond, S.J., Prusiner, S.B., and Lingappa, V.R. (1998). A transmembrane form of the prion protein in neurodegenerative disease. Science *279*, 827-834.

Hegde, R.S., Tremblay, P., Groth, D., DeArmond, S.J., Prusiner, S.B., and Lingappa, V.R. (1999). Transmissible and genetic prion diseases share a common pathway of neurodegeneration. Nature *402*, 822-826.

Heiseke, A., Aguib, Y., Riemer, C., Baier, M., and Schatzl, H.M. (2009). Lithium induces clearance of protease resistant prion protein in prion-infected cells by induction of autophagy. J Neurochem *109*, 25-34.

Heiseke, A., Aguib, Y., and Schatzl, H.M. (2010). Autophagy, prion infection and their mutual interactions. Curr Issues Mol Biol *12*, 87-97.

Heppner, F.L., Greter, M., Marino, D., Falsig, J., Raivich, G., Hovelmeyer, N., Waisman, A., Rulicke, T., Prinz, M., Priller, J*., et al.* (2005). Experimental autoimmune encephalomyelitis repressed by microglial paralysis. Nat Med *11*, 146-152.

Heppner, F.L., Musahl, C., Arrighi, I., Klein, M.A., Rulicke, T., Oesch, B., Zinkernagel, R.M., Kalinke, U., and Aguzzi, A. (2001). Prevention of Scrapie Pathogenesis by Transgenic Expression of Anti-Prion Protein Antibodies. Science *294*, 178-182.

Herms, J.W., Korte, S., Gall, S., Schneider, I., Dunker, S., and Kretzschmar, H.A. (2000). Altered intracellular calcium homeostasis in cerebellar granule cells of prion protein-deficient mice. J Neurochem *75*, 1487-1492.

Hetz, C., Russelakis-Carneiro, M., Maundrell, K., Castilla, J., and Soto, C. (2003). Caspase-12 and endoplasmic reticulum stress mediate neurotoxicity of pathological prion protein. EMBO J *22*, 5435-5445.

Hodak, M., Chisnell, R., Lu, W., and Bernholc, J. (2009). Functional implications of multistage copper binding to the prion protein. Proc Natl Acad Sci U S A *106*, 11576-11581.

Hornemann, S., Christen, B., von Schroetter, C., Perez, D.R., and Wuthrich, K. (2009a). Prion protein library of recombinant constructs for structural biology. FEBS J *276*, 2359-2367.

Hornemann, S., Korth, C., Oesch, B., Riek, R., Wider, G., Wuthrich, K., and Glockshuber, R. (1997). Recombinant full-length murine prion protein, mPrP(23-231): purification and spectroscopic characterization. FEBS Lett *413*, 277-281.

Hornemann, S., von Schroetter, C., Damberger, F.F., and Wuthrich, K. (2009b). Prion protein-detergent micelle interactions studied by NMR in solution. J Biol Chem *284*, 22713-22721.

Hsiao, K., Baker, H.F., Crow, T.J., Poulter, M., Owen, F., Terwilliger, J.D., Westaway, D., Ott, J., and Prusiner, S.B. (1989). Linkage of a prion protein missense variant to Gerstmann-Sträussler syndrome. Nature *338*, 342-345.

Hsiao, K., and Prusiner, S.B. (1991). Molecular genetics and transgenic model of Gertsmann-Straussler-Scheinker disease. Alzheimer Dis Assoc Disord *5*, 155-162.

Hsiao, K.K., Cass, C., Schellenberg, G.D., Bird, T., Devine Gage, E., Wisniewski, H., and Prusiner, S.B. (1991). A prion protein variant in a family with the telencephalic form of Gerstmann-Straussler-Scheinker syndrome. Neurology *41*, 681-684.

Hsiao, Y.H., Chen, P.S., Yeh, S.H., Lin, C.H., and Gean, P.W. (2008). N-acetylcysteine prevents beta-amyloid toxicity by a stimulatory effect on p35/cyclin-dependent kinase 5 activity in cultured cortical neurons. J Neurosci Res *86*, 2685-2695.

Jackson, G.S., Murray, I., Hosszu, L.L., Gibbs, N., Waltho, J.P., Clarke, A.R., and Collinge, J. (2001). Location and properties of metal-binding sites on the human prion protein. Proc Natl Acad Sci U S A *98*, 8531-8535.

Jason-Moller, L., Murphy, M., and Bruno, J. (2006). Overview of Biacore systems and their applications. Curr Protoc Protein Sci *Chapter 19*, Unit 19 13.

Jobling, M.F., Stewart, L.R., White, A.R., McLean, C., Friedhuber, A., Maher, F., Beyreuther, K., Masters, C.L., Barrow, C.J., Collins, S.J.*, et al.* (1999). The hydrophobic core sequence modulates the neurotoxic and secondary structure properties of the prion peptide 106-126. J Neurochem *73*, 1557-1565.

Jomova, K., Vondrakova, D., Lawson, M., and Valko, M. (2010). Metals, oxidative stress and neurodegenerative disorders. Mol Cell Biochem *345*, 91-104.

Kanaani, J., Prusiner, S.B., Diacovo, J., Baekkeskov, S., and Legname, G. (2005). Recombinant prion protein induces rapid polarization and development of synapses in embryonic rat hippocampal neurons in vitro. J Neurochem *95*, 1373-1386.

keller, R. (2004). The Computer-aided Resonance Assignment Tutorial CARA G. Cantina Verlag, Switzerland, ed.

Kessels, H.W., Nguyen, L.N., Nabavi, S., and Malinow, R. (2010). The prion protein as a receptor for amyloid-beta. Nature *466*, E3-4; discussion E4-5.

Klöhn, P.C., Farmer, M., Linehan, J.M., O'Malley, C., Fernandez de Marco, M., Taylor, W., Farrow, M., Khalili-Shirazi, A., Brandner, S., and Collinge, J. (2012). PrP antibodies do not trigger mouse hippocampal neuron apoptosis. Science *335*, 52.

Klohn, P.C., Stoltze, L., Flechsig, E., Enari, M., and Weissmann, C. (2003). A quantitative, highly sensitive cell-based infectivity assay for mouse scrapie prions. Proc Natl Acad Sci U S A *100*, 11666-11671.

Kovacs, G.G., and Budka, H. (2010). Distribution of apoptosis-related proteins in sporadic Creutzfeldt-Jakob disease. Brain Res *1323*, 192-199.

Krasemann, S., Zerr, I., Weber, T., Poser, S., Kretzschmar, H., Hunsmann, G., and Bodemer, W. (1995). Prion disease associated with a novel nine octapeptide repeat insertion in the PRNP gene. Brain Res Mol Brain Res *34*, 173-176.

Krebs, B., Dorner-Ciossek, C., Schmalzbauer, R., Vassallo, N., Herms, J., and Kretzschmar, H.A. (2006). Prion protein induced signaling cascades in monocytes. Biochem Biophys Res Commun *340*, 13-22.

Kristensson, K., Feuerstein, B., Taraboulos, A., Hyun, W.C., Prusiner, S.B., and DeArmond, S.J. (1993). Scrapie prions alter receptor-mediated calcium responses in cultured cells. Neurology *43*, 2335-2341.

Kunz, B., Sandmeier, E., and Christen, P. (1999). Neurotoxicity of prion peptide 106-126 not confirmed. FEBS Lett *458*, 65-68.

LaCasse, R.A., Striebel, J.F., Favara, C., Kercher, L., and Chesebro, B. (2008). Role of Erk1/2 activation in prion disease pathogenesis: absence of CCR1 leads to increased Erk1/2 activation and accelerated disease progression. Journal of neuroimmunology *196*, 16-26.

Lampert, P.W., Gajdusek, D.C., and Gibbs, C.J., Jr. (1972). Subacute spongiform virus encephalopathies. Scrapie, Kuru and Creutzfeldt-Jakob disease: a review. Am J Pathol *68*, 626-652.

Lauren, J., Gimbel, D.A., Nygaard, H.B., Gilbert, J.W., and Strittmatter, S.M. (2009). Cellular prion protein mediates impairment of synaptic plasticity by amyloid-beta oligomers. Nature *457*, 1128-1132.

Lee, H.P., Jun, Y.C., Choi, J.K., Kim, J.I., Carp, R.I., and Kim, Y.S. (2005). Activation of mitogen-activated protein kinases in hamster brains infected with 263K scrapie agent. J Neurochem *95*, 584-593.

Lee, K.S., Magalhaes, A.C., Zanata, S.M., Brentani, R.R., Martins, V.R., and Prado, M.A. (2001). Internalization of mammalian fluorescent cellular prion protein and N-terminal deletion mutants in living cells. J Neurochem *79*, 79-87.

Lefebvre-Roque, M., Kremmer, E., Gilch, S., Zou, W.Q., Feraudet, C., Gilles, C.M., Sales, N., Grassi, J., Gambetti, P., Baron, T.*, et al.* (2007). Toxic effects of intracerebral PrP antibody administration during the course of BSE infection in mice. Prion *1*, 198-206.

Leski, M.L., Valentine, S.L., and Coyle, J.T. (1999). L-type voltage-gated calcium channels modulate kainic acid neurotoxicity in cerebellar granule cells. Brain Res *828*, 27-40.

Levites, Y., Jansen, K., Smithson, L.A., Dakin, R., Holloway, V.M., Das, P., and Golde, T.E. (2006). Intracranial adeno-associated virus-mediated delivery of anti-pan amyloid beta, amyloid beta40, and amyloid beta42 single-chain variable fragments attenuates plaque pathology in amyloid precursor protein mice. J Neurosci *26*, 11923-11928.

Li, A., Christensen, H., Stewart, L., Roth, K., Chiesa, R., and Harris, D. (2007). Neonatal lethality in transgenic mice expressing prion protein with a deletion of residues 105-125. Embo J *26*, 548-558.

Li, Z., Ji, G., and Neugebauer, V. (2011). Mitochondrial reactive oxygen species are activated by mGluR5 through IP3 and activate ERK and PKA to increase excitability of amygdala neurons and pain behavior. J Neurosci *31*, 1114-1127.

Liberski, P.P., Brown, D.R., Sikorska, B., Caughey, B., and Brown, P. (2008). Cell death and autophagy in prion diseases (transmissible spongiform encephalopathies). Folia Neuropathol *46*, 1-25.

Liberski, P.P., Sikorska, B., Bratosiewicz-Wasik, J., Gajdusek, D.C., and Brown, P. (2004). Neuronal cell death in transmissible spongiform encephalopathies (prion diseases) revisited: from apoptosis to autophagy. Int J Biochem Cell Biol *36*, 2473-2490.

Liu, J., Liu, M.C., and Wang, K.K. (2008). Calpain in the CNS: from synaptic function to neurotoxicity. Sci Signal *1*, re1.

Lopes, M.H., Hajj, G.N., Muras, A.G., Mancini, G.L., Castro, R.M., Ribeiro, K.C., Brentani, R.R., Linden, R., and Martins, V.R. (2005). Interaction of cellular prion and stress-inducible protein 1 promotes neuritogenesis and neuroprotection by distinct signaling pathways. J Neurosci *25*, 11330-11339.

Lopez Garcia, F., Zahn, R., Riek, R., and Wuthrich, K. (2000). NMR structure of the bovine prion protein. Proc Natl Acad Sci U S A *97*, 8334-8339.

Lugaresi, E., Medori, R., Montagna, P., Baruzzi, A., Cortelli, P., Lugaresi, A., Tinuper, P., Zucconi, M., and Gambetti, P. (1986). Fatal familial insomnia and dysautonomia with selective degeneration of thalamic nuclei. N Engl J Med *315*, 997-1003.

Lysek, D.A., and Wüthrich, K. (2004). Prion protein interaction with the C-terminal SH3 domain of Grb2 studied using NMR and optical spectroscopy. Biochemistry *43*, 10393–10399.

Macmillan, D., and McCarron, J.G. (2010). The phospholipase C inhibitor U-73122 inhibits Ca(2+) release from the intracellular sarcoplasmic reticulum Ca(2+) store by inhibiting Ca(2+) pumps in smooth muscle. Br J Pharmacol *160*, 1295-1301.

Mallucci, G., Dickinson, A., Linehan, J., Klohn, P.C., Brandner, S., and Collinge, J. (2003). Depleting neuronal PrP in prion infection prevents disease and reverses spongiosis. Science *302*, 871-874.

Mallucci, G.R., Ratte, S., Asante, E.A., Linehan, J., Gowland, I., Jefferys, J.G., and Collinge, J. (2002). Post-natal knockout of prion protein alters hippocampal CA1 properties, but does not result in neurodegeneration. Embo J *21*, 202-210.

Malouitre, S., Dube, H., Selwood, D., and Crompton, M. (2009). Mitochondrial targeting of cyclosporin A enables selective inhibition of cyclophilin-D and enhanced cytoprotection after glucose and oxygen deprivation. Biochem J *425*, 137-148.

Mander, P., and Brown, G.C. (2005). Activation of microglial NADPH oxidase is synergistic with glial iNOS expression in inducing neuronal death: a dual-key mechanism of inflammatory neurodegeneration. J Neuroinflammation *2*, 20.

Mange, A., Beranger, F., Peoc'h, K., Onodera, T., Frobert, Y., and Lehmann, S. (2004). Alpha- and beta- cleavages of the amino-terminus of the cellular prion protein. Biol Cell *96*, 125-132.

Martins, V.R., Beraldo, F.H., Hajj, G.N., Lopes, M.H., Lee, K.S., Prado, M.A., and Linden, R. (2010). Prion protein: orchestrating neurotrophic activities. Curr Issues Mol Biol *12*, 63-86.

Massignan, T., Biasini, E., and Harris, D.A. (2011). A Drug-Based Cellular Assay (DBCA) for studying cytotoxic and cytoprotective activities of the prion protein: A practical guide. Methods *53*, 214-219.

Massignan, T., Stewart, R.S., Biasini, E., Solomon, I.H., Bonetto, V., Chiesa, R., and Harris, D.A. (2010). A novel, drug-based, cellular assay for the activity of neurotoxic mutants of the prion protein. J Biol Chem *285*, 7752-7765.

Masters, C.L., Gajdusek, D.C., and Gibbs, C.J. (1981). Creutzfeldt-Jakob disease virus isolations from the Gerstmann-Straussler syndrome with an analysis of the various forms of amyloid plaque deposition in the virus-induced spongiform encephalopathies. Brain *104*, 559-588.

Mastrianni, J.A., Nixon, R., Layzer, R., Telling, G.C., Han, D., DeArmond, S.J., and Prusiner, S.B. (1999). Prion protein conformation in a patient with sporadic fatal insomnia. N Engl J Med *340*, 1630-1638.

McMahon, H.E., Mange, A., Nishida, N., Creminon, C., Casanova, D., and Lehmann, S. (2001). Cleavage of the amino terminus of the prion protein by reactive oxygen species. J Biol Chem *276*, 2286-2291.

McPhillips, T.M., McPhillips, S.E., Chiu, H.J., Cohen, A.E., Deacon, A.M., Ellis, P.J., Garman, E., Gonzalez, A., Sauter, N.K., Phizackerley, R.P*., et al.* (2002). Blu-Ice and

the Distributed Control System: software for data acquisition and instrument control at macromolecular crystallography beamlines. J Synchrotron Radiat *9*, 401-406.

Mead, S., Poulter, M., Beck, J., Webb, T.E., Campbell, T.A., Linehan, J.M., Desbruslais, M., Joiner, S., Wadsworth, J.D., King, A.*, et al.* (2006). Inherited prion disease with six octapeptide repeat insertional mutation--molecular analysis of phenotypic heterogeneity. Brain *129*, 2297-2317.

Medori, R., Tritschler, H.J., LeBlanc, A., Villare, F., Manetto, V., Chen, H.Y., Xue, R., Leal, S., Montagna, P., Cortelli, P.*, et al.* (1992). Fatal familial insomnia, a prion disease with a mutation at codon 178 of the prion protein gene. N Engl J Med *326*, 444-449.

Mitteregger, G., Korte, S., Shakarami, M., Herms, J., and Kretzschmar, H.A. (2009). Role of copper and manganese in prion disease progression. Brain Res *1292*, 155-164.

Miura, S., Ishida, A., Nakajima, W., Ohmura, A., Kawamura, M., and Takada, G. (2006). Intraventricular ascorbic acid administration decreases hypoxic-ischemic brain injury in newborn rats. Brain Res *1095*, 159-166.

Mizushima, N., and Komatsu, M. (2011). Autophagy: renovation of cells and tissues. Cell *147*, 728-741.

Monnet, C., Gavard, J., Mege, R.M., and Sobel, A. (2004). Clustering of cellular prion protein induces ERK1/2 and stathmin phosphorylation in GT1-7 neuronal cells. FEBS Lett *576*, 114-118.

Moreno, J.A., Radford, H., Peretti, D., Steinert, J.R., Verity, N., Martin, M.G., Halliday, M., Morgan, J., Dinsdale, D., Ortori, C.A.*, et al.* (2012). Sustained translational repression by eIF2alpha-P mediates prion neurodegeneration. Nature *485*, 507-511.

Moubarak, R.S., Yuste, V.J., Artus, C., Bouharrour, A., Greer, P.A., Menissier-de Murcia, J., and Susin, S.A. (2007). Sequential activation of poly(ADP-ribose) polymerase 1, calpains, and Bax is essential in apoptosis-inducing factor-mediated programmed necrosis. Mol Cell Biol *27*, 4844-4862.

Mouillet-Richard, S., Ermonval, M., Chebassier, C., Laplanche, J.L., Lehmann, S., Launay, J.M., and Kellermann, O. (2000). Signal transduction through prion protein. Science *289*, 1925-1928.

Muramoto, T., DeArmond, S.J., Scott, M., Telling, G.C., Cohen, F.E., and Prusiner, S.B. (1997). Heritable disorder resembling neuronal storage disease in mice expressing prion protein with deletion of an alpha-helix. Nat Med *3*, 750-755.

Muramoto, T., Scott, M., Cohen, F.E., and Prusiner, S.B. (1996). Recombinant scrapie-like prion protein of 106 amino acids is soluble. Proc Natl Acad Sci U S A *93*, 15457-15462.

Nicolas, O., Gavin, R., Braun, N., Urena, J.M., Fontana, X., Soriano, E., Aguzzi, A., and del Rio, J.A. (2007). Bcl-2 overexpression delays caspase-3 activation and rescues cerebellar degeneration in prion-deficient mice that overexpress amino-terminally truncated prion. FASEB J *21*, 3107-3117.

Nixon, R.R. (2005). Prion-associated increases in Src-family kinases. J Biol Chem *280*, 2455-2462.

Oesch, B., Westaway, D., Walchli, M., McKinley, M.P., Kent, S.B., Aebersold, R., Barry, R.A., Tempst, P., Teplow, D.B., Hood, L.E*., et al.* (1985). A cellular gene encodes scrapie PrP 27-30 protein. Cell *40*, 735-746.

Oliveira-Martins, J.B., Yusa, S., Calella, A.M., Bridel, C., Baumann, F., Dametto, P., and Aguzzi, A. (2010). Unexpected tolerance of alpha-cleavage of the prion protein to sequence variations. PLoS ONE *5*, e9107.

Otwinowski, Z., and Minor, W. (1997). Processing of X-ray Diffraction Data Collected in Oscillation Mode. Methods in Enzymology *276*, 307-326.

Palmer, M.S., Dryden, A.J., Hughes, J.T., and Collinge, J. (1991). Homozygous prion protein genotype predisposes to sporadic Creutzfeldt-Jakob disease. Nature *352*, 340-342.

Parchi, P., Capellari, S., Chin, S., Schwarz, H.B., Schecter, N.P., Butts, J.D., Hudkins, P., Burns, D.K., Powers, J.M., and Gambetti, P. (1999). A subtype of sporadic prion disease mimicking fatal familial insomnia. Neurology *52*, 1757-1763.

Pauly, P.C., and Harris, D.A. (1998). Copper stimulates endocytosis of the prion protein. J Biol Chem *273*, 33107-33110.

Perera, W.S., and Hooper, N.M. (2001). Ablation of the metal ion-induced endocytosis of the prion protein by disease-associated mutation of the octarepeat region. Curr Biol *11*, 519-523.

Pervushin, K., Riek, R., Wider, G., and Wuthrich, K. (1997). Attenuated T2 relaxation by mutual cancellation of dipole-dipole coupling and chemical shift anisotropy indicates an avenue to NMR structures of very large biological macromolecules in solution. Proc Natl Acad Sci U S A *94*, 12366-12371.

Peshavariya, H.M., Dusting, G.J., and Selemidis, S. (2007). Analysis of dihydroethidium fluorescence for the detection of intracellular and extracellular superoxide produced by NADPH oxidase. Free Radic Res *41*, 699-712.

Pietri, M., Caprini, A., Mouillet-Richard, S., Pradines, E., Ermonval, M., Grassi, J., Kellermann, O., and Schneider, B. (2006). Overstimulation of PrPC signaling pathways by prion peptide 106-126 causes oxidative injury of bioaminergic neuronal cells. J Biol Chem *281*, 28470-28479.

Pollock, J.D., Williams, D.A., Gifford, M.A., Li, L.L., Du, X., Fisherman, J., Orkin, S.H., Doerschuk, C.M., and Dinauer, M.C. (1995). Mouse model of X-linked chronic granulomatous disease, an inherited defect in phagocyte superoxide production. Nat Genet *9*, 202-209.

Polymenidou, M., Moos, R., Scott, M., Sigurdson, C., Shi, Y.Z., Yajima, B., Hafner-Bratkovic, I., Jerala, R., Hornemann, S., Wuthrich, K.*, et al.* (2008). The POM monoclonals: a comprehensive set of antibodies to non-overlapping prion protein epitopes. PLoS One *3*, e3872.

Prinz, M., Montrasio, F., Furukawa, H., van der Haar, M.E., Schwarz, P., Rülicke, T., Giger, O., Häusler, K.G., Glatzel, M., and Aguzzi, A. (2004). Intrinsic resistance of oligodendrocytes to prion infection. J Neurosci *24*, 5974-5981.

Prusiner, S.B. (1982). Novel proteinaceous infectious particles cause scrapie. Science *216*, 136-144.

Prusiner, S.B., Scott, M.R., DeArmond, S.J., and Cohen, F.E. (1998). Prion protein biology. Cell *93*, 337-348.

Qin, K., Yang, Y., Mastrangelo, P., and Westaway, D. (2002). Mapping Cu(II) binding sites in prion proteins by diethyl pyrocarbonate modification and matrix-assisted laser desorption ionization-time of flight (MALDI-TOF) mass spectrometric footprinting. J Biol Chem *277*, 1981-1990.

Radovanovic, I., Braun, N., Giger, O.T., Mertz, K., Miele, G., Prinz, M., Navarro, B., and Aguzzi, A. (2005). Truncated Prion Protein and Doppel Are Myelinotoxic in the Absence of Oligodendrocytic PrPC. J Neurosci *25*, 4879-4888.

Rane, N.S., Kang, S.W., Chakrabarti, O., Feigenbaum, L., and Hegde, R.S. (2008). Reduced translocation of nascent prion protein during ER stress contributes to neurodegeneration. Dev Cell *15*, 359-370.

Rangel, A., Burgaya, F., Gavin, R., Soriano, E., Aguzzi, A., and Del Rio, J.A. (2007). Enhanced susceptibility of Prnp-deficient mice to kainate-induced seizures, neuronal

apoptosis, and death: Role of AMPA/kainate receptors. J Neurosci Res *85*, 2741-2755.

Resenberger, U.K., Harmeier, A., Woerner, A.C., Goodman, J.L., Muller, V., Krishnan, R., Vabulas, R.M., Kretzschmar, H.A., Lindquist, S., Hartl, F.U.*, et al.* (2011). The cellular prion protein mediates neurotoxic signalling of beta-sheet-rich conformers independent of prion replication. EMBO J *30*, 2057-2070.

Riek, R. (1998). NMR of the mouse prion protein, Diss. Naturwiss. Nr. 12759, (ETH Zürich).

Riek, R., Hornemann, S., Wider, G., Billeter, M., Glockshuber, R., and Wüthrich, K. (1996). NMR structure of the mouse prion protein domain PrP(121-231). Nature *382*, 180-182.

Riek, R., Hornemann, S., Wider, G., Glockshuber, R., and Wüthrich, K. (1997). NMR characterization of the full-length recombinant murine prion protein, mPrP(23-231). FEBS Lett *413*, 282-288.

Rivera-Milla, E., Oidtmann, B., Panagiotidis, C.H., Baier, M., Sklaviadis, T., Hoffmann, R., Zhou, Y., Solis, G.P., Stuermer, C.A., and Malaga-Trillo, E. (2006). Disparate evolution of prion protein domains and the distinct origin of Doppel- and prion-related loci revealed by fish-to-mammal comparisons. FASEB J *20*, 317-319.

Ross, C.A., and Poirier, M.A. (2005). Opinion: What is the role of protein aggregation in neurodegeneration? Nat Rev Mol Cell Biol *6*, 891-898.

Sales, N., Rodolfo, K., Hassig, R., Faucheux, B., Di Giamberardino, L., and Moya, K.L. (1998). Cellular prion protein localization in rodent and primate brain. Eur J Neurosci *10*, 2464-2471.

Salmona, M., Malesani, P., De Gioia, L., Gorla, S., Bruschi, M., Molinari, A., Della Vedova, F., Pedrotti, B., Marrari, M.A., Awan, T.*, et al.* (1999). Molecular determinants of the physicochemical properties of a critical prion protein region comprising residues 106-126. Biochem J *342 (Pt 1)*, 207-214.

Sandberg, M.K., Al-Doujaily, H., Sharps, B., Clarke, A.R., and Collinge, J. (2011). Prion propagation and toxicity in vivo occur in two distinct mechanistic phases. Nature *470*, 540-542.

Santuccione, A., Sytnyk, V., Leshchyns'ka, I., and Schachner, M. (2005). Prion protein recruits its neuronal receptor NCAM to lipid rafts to activate p59fyn and to enhance neurite outgrowth. J Cell Biol *169*, 341-354.

Sarkar, S., Davies, J.E., Huang, Z., Tunnacliffe, A., and Rubinsztein, D.C. (2007). Trehalose, a novel mTOR-independent autophagy enhancer, accelerates the clearance of mutant huntingtin and alpha-synuclein. J Biol Chem *282*, 5641-5652.

Satoh, J., Obayashi, S., Misawa, T., Sumiyoshi, K., Oosumi, K., and Tabunoki, H. (2009). Protein microarray analysis identifies human cellular prion protein interactors. Neuropathol Appl Neurobiol *35*, 16-35.

Schatzl, H.M., Laszlo, L., Holtzman, D.M., Tatzelt, J., DeArmond, S.J., Weiner, R.I., Mobley, W.C., and Prusiner, S.B. (1997). A hypothalamic neuronal cell line persistently infected with scrapie prions exhibits apoptosis. J Virol *71*, 8821-8831.

Schneider, B., Mutel, V., Pietri, M., Ermonval, M., Mouillet-Richard, S., and Kellermann, O. (2003). NADPH oxidase and extracellular regulated kinases 1/2 are targets of prion protein signaling in neuronal and nonneuronal cells. Proc Natl Acad Sci U S A *100*, 13326-13331.

Schneider, B., Pietri, M., Pradines, E., Loubet, D., Launay, J.M., Kellermann, O., and Mouillet-Richard, S. (2011). Understanding the neurospecificity of Prion protein signaling. Front Biosci *16*, 169-186.

Selvaggini, C., De Gioia, L., Cantu, L., Ghibaudi, E., Diomede, L., Passerini, F., Forloni, G., Bugiani, O., Tagliavini, F., and Salmona, M. (1993). Molecular characteristics of a protease-resistant, amyloidogenic and neurotoxic peptide homologous to residues 106-126 of the prion protein. Biochem Biophys Res Commun *194*, 1380-1386.

Shakkottai, V.G., Chou, C.H., Oddo, S., Sailer, C.A., Knaus, H.G., Gutman, G.A., Barish, M.E., LaFerla, F.M., and Chandy, K.G. (2004). Enhanced neuronal excitability in the absence of neurodegeneration induces cerebellar ataxia. J Clin Invest *113*, 582-590.

Shehata, M., Matsumura, H., Okubo-Suzuki, R., Ohkawa, N., and Inokuchi, K. (2012). Neuronal stimulation induces autophagy in hippocampal neurons that is involved in AMPA receptor degradation after chemical long-term depression. J Neurosci *32*, 10413-10422.

Shmerling, D., Hegyi, I., Fischer, M., Blattler, T., Brandner, S., Gotz, J., Rulicke, T., Flechsig, E., Cozzio, A., von Mering, C.*, et al.* (1998). Expression of amino-terminally truncated PrP in the mouse leading to ataxia and specific cerebellar lesions. Cell *93*, 203-214.

Sigurdson, C.J. (2008). A prion disease of cervids: chronic wasting disease. Vet Res *39*, 41.

Sigurdson, C.J., and Aguzzi, A. (2007). Chronic wasting disease. Biochim Biophys Acta *1772*, 610-618.

Sigurdsson, E.M., Brown, D.R., Alim, M.A., Scholtzova, H., Carp, R., Meeker, H.C., Prelli, F., Frangione, B., and Wisniewski, T. (2003). Copper chelation delays the onset of prion disease. J Biol Chem *278*, 46199-46202.

Solforosi, L., Criado, J.R., McGavern, D.B., Wirz, S., Sanchez-Alavez, M., Sugama, S., DeGiorgio, L.A., Volpe, B.T., Wiseman, E., Abalos, G.*, et al.* (2004). Cross-linking cellular prion protein triggers neuronal apoptosis in vivo. Science *303*, 1514-1516.

Solomon, I.H., Huettner, J.E., and Harris, D.A. (2010). Neurotoxic mutants of the prion protein induce spontaneous ionic currents in cultured cells. J Biol Chem *285*, 26719-26726.

Solomon, I.H., Khatri, N., Biasini, E., Massignan, T., Huettner, J.E., and Harris, D.A. (2011). An N-terminal polybasic domain and cell surface localization are required for mutant prion protein toxicity. J Biol Chem *286*, 14724-14736.

Sonati, T., Reimann, R.R., Falsig, J., Baral, P.K., O'Connor, T., Hornemann, S., Yaganoglu, S., Li, B., Herrmann, U.S., Wieland, B.*, et al.* (2013). The toxicity of antiprion antibodies is mediated by the flexible tail of the prion protein

Nature.

Sorce, S., and Krause, K.H. (2009). NOX enzymes in the central nervous system: from signaling to disease. Antioxid Redox Signal *11*, 2481-2504.

Soto, C., and Satani, N. (2010). The intricate mechanisms of neurodegeneration in prion diseases. Trends Mol Med.

Sponarova, J., Nystrom, S.N., and Westermark, G.T. (2008). AA-amyloidosis can be transferred by peripheral blood monocytes. PLoS ONE *3*, e3308.

Spudich, A., Frigg, R., Kilic, E., Kilic, U., Oesch, B., Raeber, A., Bassetti, C.L., and Hermann, D.M. (2005). Aggravation of ischemic brain injury by prion protein deficiency: Role of ERK-1/-2 and STAT-1. Neurobiol Dis *20*, 442-449.

Stahl, N., Baldwin, M.A., Teplow, D.B., Hood, L., Gibson, B.W., Burlingame, A.L., and Prusiner, S.B. (1993). Structural studies of the scrapie prion protein using mass spectrometry and amino acid sequencing. Biochemistry *32*, 1991-2002.

Steele, A.D., Emsley, J.G., Ozdinler, P.H., Lindquist, S., and Macklis, J.D. (2006). Prion protein (PrPc) positively regulates neural precursor proliferation during

developmental and adult mammalian neurogenesis. Proc Natl Acad Sci U S A *103*, 3416-3421.

Steele, A.D., King, O.D., Jackson, W.S., Hetz, C.A., Borkowski, A.W., Thielen, P., Wollmann, R., and Lindquist, S. (2007). Diminishing apoptosis by deletion of Bax or overexpression of Bcl-2 does not protect against infectious prion toxicity in vivo. J Neurosci *27*, 13022-13027.

Supattapone, S., Muramoto, T., Legname, G., Mehlhorn, I., Cohen, F.E., DeArmond, S.J., Prusiner, S.B., and Scott, M.R. (2001). Identification of two prion protein regions that modify scrapie incubation time. J Virol *75*, 1408-1413.

Suzuki, K., Hata, S., Kawabata, Y., and Sorimachi, H. (2004). Structure, activation, and biology of calpain. Diabetes *53 Suppl 1*, S12-18.

Suzuki, K.G., Kasai, R.S., Hirosawa, K.M., Nemoto, Y.L., Ishibashi, M., Miwa, Y., Fujiwara, T.K., and Kusumi, A. (2012). Transient GPI-anchored protein homodimers are units for raft organization and function. Nat Chem Biol *8*, 774-783.

Tagliavini, F., Prelli, F., Verga, L., Giaccone, G., Sarma, R., Gorevic, P., Ghetti, B., Passerini, F., Ghibaudi, E., Forloni, G*., et al.* (1993). Synthetic peptides homologous to prion protein residues 106-147 form amyloid-like fibrils in vitro. Proc Natl Acad Sci U S A *90*, 9678-9682.

Takenouchi, T., Iwamaru, Y., Imamura, M., Fukuhara, S., Sugama, S., Sato, M., Mochizuki, N., Hashimoto, M., Yokoyama, T., Mohri, S*., et al.* (2012). Cytochalasin D enhances the accumulation of a protease-resistant form of prion protein in ScN2a cells: involvement of PI3 kinase/Akt signalling pathway. Cell Biol Int *36*, 1223-1231.

Tateishi, J., Brown, P., Kitamoto, T., Hoque, Z.M., Roos, R., Wollman, R., Cervenakova, L., and Gajdusek, D.C. (1995). First experimental transmission of fatal familial insomnia. Nature *376*, 434-435.

Taubner, L.M., Bienkiewicz, E.A., Copie, V., and Caughey, B. (2010). Structure of the flexible amino-terminal domain of prion protein bound to a sulfated glycan. J Mol Biol *395*, 475-490.

Taylor, D.R., Watt, N.T., Perera, W.S., and Hooper, N.M. (2005). Assigning functions to distinct regions of the N-terminus of the prion protein that are involved in its copper-stimulated, clathrin-dependent endocytosis. J Cell Sci *118*, 5141-5153.

Torres, M., Castillo, K., Armisen, R., Stutzin, A., Soto, C., and Hetz, C. (2010). Prion protein misfolding affects calcium homeostasis and sensitizes cells to endoplasmic reticulum stress. PLoS One *5*, e15658.

Turnbaugh, J.A., Unterberger, U., Saa, P., Massignan, T., Fluharty, B.R., Bowman, F.P., Miller, M.B., Supattapone, S., Biasini, E., and Harris, D.A. (2012). The N-terminal, polybasic region of PrP(C) dictates the efficiency of prion propagation by binding to PrP(Sc). J Neurosci *32*, 8817-8830.

Turnbaugh, J.A., Westergard, L., Unterberger, U., Biasini, E., and Harris, D.A. (2011). The N-terminal, polybasic region is critical for prion protein neuroprotective activity. PLoS ONE *6*, e25675.

Uppington, K.M., and Brown, D.R. (2008). Resistance of cell lines to prion toxicity aided by phospho-ERK expression. J Neurochem *105*, 842-852.

Vagin, A., and Teplyakov, A. (1997). MOLREP: an Automated Program for Molecular Replacement. Journal of Applied Crystallography *30*, 1022-1025.

Vest, R.S., O'Leary, H., Coultrap, S.J., Kindy, M.S., and Bayer, K.U. (2010). Effective post-insult neuroprotection by a novel Ca(2+)/ calmodulin-dependent protein kinase II (CaMKII) inhibitor. J Biol Chem *285*, 20675-20682.

Vital, C., Gray, F., Vital, A., Ferrer, X., and Julien, J. (1999). Prion disease with octapeptide repeat insertion. Clin Exp Pathol *47*, 153-159.

Vosler, P.S., Brennan, C.S., and Chen, J. (2008). Calpain-mediated signaling mechanisms in neuronal injury and neurodegeneration. Mol Neurobiol *38*, 78-100.

Walmsley, A.R., Zeng, F., and Hooper, N.M. (2003). The N-terminal region of the prion protein ectodomain contains a lipid raft targeting determinant. J Biol Chem *278*, 37241-37248.

Wang, K.K. (2000). Calpain and caspase: can you tell the difference? Trends Neurosci *23*, 20-26.

Wang, X., Zhu, S., Pei, Z., Drozda, M., Stavrovskaya, I.G., Del Signore, S.J., Cormier, K., Shimony, E.M., Wang, H., Ferrante, R.J.*, et al.* (2008). Inhibitors of cytochrome c release with therapeutic potential for Huntington's disease. J Neurosci *28*, 9473-9485.

Weise, J., Sandau, R., Schwarting, S., Crome, O., Wrede, A., Schulz-Schaeffer, W., Zerr, I., and Bahr, M. (2006). Deletion of cellular prion protein results in reduced Akt activation, enhanced postischemic caspase-3 activation, and exacerbation of ischemic brain injury. Stroke *37*, 1296-1300.

Weissmann, C. (1991a). Spongiform encephalopathies. The prion's progress. Nature *349*, 569-571.

Weissmann, C. (1991b). A 'unified theory' of prion propagation. Nature *352*, 679-683.

Weissmann, C. (1999). Molecular genetics of transmissible spongiform encephalopathies. J Biol Chem *274*, 3-6.

Wells, G.A., Scott, A.C., Johnson, C.T., Gunning, R.F., Hancock, R.D., Jeffrey, M., Dawson, M., and Bradley, R. (1987). A novel progressive spongiform encephalopathy in cattle. Vet Rec *121*, 419-420.

Westergard, L., Turnbaugh, J.A., and Harris, D.A. (2011). A nine amino acid domain is essential for mutant prion protein toxicity. J Neurosci *31*, 14005-14017.

Westermark, G.T., and Westermark, P. (2010). Prion-like aggregates: infectious agents in human disease. Trends Mol Med *16*, 501-507.

White, A.R., Enever, P., Tayebi, M., Mushens, R., Linehan, J., Brandner, S., Anstee, D., Collinge, J., and Hawke, S. (2003). Monoclonal antibodies inhibit prion replication and delay the development of prion disease. Nature *422*, 80-83.

Whitmarsh, A.J., and Davis, R.J. (1999). Signal transduction by MAP kinases: regulation by phosphorylation-dependent switches. Sci STKE *1999*, PE1.

Will, R.G. (2003). Acquired prion disease: iatrogenic CJD, variant CJD, kuru. Br Med Bull *66*, 255-265.

Windelborn, J.A., Lipton, P (2008). Lysosomal release of cathepsins causes ischemic damage in the rat hippocampal slice and depends on NMDA-mediated calcium influx, arachidonic acid metabolism, and free radical production. J Neurochem *106*, 56-69.

Winn, M.D., Ballard, C.C., Cowtan, K.D., Dodson, E.J., Emsley, P., Evans, P.R., Keegan, R.M., Krissinel, E.B., Leslie, A.G.W., McCoy, A.*, et al.* (2011). Overview of the CCP4 suite and current developments. Acta Crystallographica Section D *67*, 235-242.

Wopfner, F., Weidenhofer, G., Schneider, R., von Brunn, A., Gilch, S., Schwarz, T.F., Werner, T., and Schatzl, H.M. (1999). Analysis of 27 mammalian and 9 avian PrPs reveals high conservation of flexible regions of the prion protein. J Mol Biol *289*, 1163-1178.

Wu, W., Sun, H.Y., Deng, X.L., and Li, G.R. (2013). EGFR tyrosine kinase regulates human small-conductance Ca2+-activated K+ (hSKCa1) channels expressed in HEK-293 cells. Biochem J *452*, 121-129.

Yadavalli, R., Guttmann, R.P., Seward, T., Centers, A.P., Williamson, R.A., and Telling, G.C. (2004). Calpain-dependent endoproteolytic cleavage of PrPSc modulates scrapie prion propagation. J Biol Chem.

Yamaguchi, Y., Miyata, H., Uchiyama, K., Ootsuyama, A., Inubushi, S., Mori, T., Muramatsu, N., Katamine, S., and Sakaguchi, S. (2012). Biological and biochemical characterization of mice expressing prion protein devoid of the octapeptide repeat region after infection with prions. PLoS ONE *7*, e43540.

Yoshikawa, D., Yamaguchi, N., Ishibashi, D., Yamanaka, H., Okimura, N., Yamaguchi, Y., Mori, T., Miyata, H., Shigematsu, K., Katamine, S*., et al.* (2008). Dominant-negative effects of the N-terminal half of prion protein on neurotoxicity of prion protein-like protein/doppel in mice. J Biol Chem *283*, 24202-24211.

You, H., Tsutsui, S., Hameed, S., Kannanayakal, T.J., Chen, L., Xia, P., Engbers, J.D., Lipton, S.A., Stys, P.K., and Zamponi, G.W. (2012). Abeta neurotoxicity depends on interactions between copper ions, prion protein, and N-methyl-D-aspartate receptors. Proc Natl Acad Sci U S A *109*, 1737-1742.

Yuan, J., Lipinski, M., and Degterev, A. (2003). Diversity in the mechanisms of neuronal cell death. Neuron *40*, 401-413.

Zahn, R. (2003). The octapeptide repeats in mammalian prion protein constitute a pH-dependent folding and aggregation site. J Mol Biol *334*, 477-488.

Zahn, R., Liu, A., Luhrs, T., Riek, R., von Schroetter, C., Lopez Garcia, F., Billeter, M., Calzolai, L., Wider, G., and Wuthrich, K. (2000). NMR solution structure of the human prion protein. Proc Natl Acad Sci U S A *97*, 145-150.

Zahn, R., von Schroetter, C., and Wüthrich, K. (1997). Human prion proteins expressed in Escherichia coli and purified by high- affinity column refolding. FEBS Lett *417*, 400–404.

Zhao, M., New, L., Kravchenko, V.V., Kato, Y., Gram, H., di Padova, F., Olson, E.N., Ulevitch, R.J., and Han, J. (1999). Regulation of the MEF2 family of transcription factors by p38. Mol Cell Biol *19*, 21-30.

Zielonka, J., Hardy, M., and Kalyanaraman, B. (2009). HPLC study of oxidation products of hydroethidine in chemical and biological systems: ramifications in superoxide measurements. Free Radic Biol Med *46*, 329-338.

Zielonka, J., Srinivasan, S., Hardy, M., Ouari, O., Lopez, M., Vasquez-Vivar, J., Avadhani, N.G., and Kalyanaraman, B. (2008a). Cytochrome c-mediated oxidation of

hydroethidine and mito-hydroethidine in mitochondria: identification of homo- and heterodimers. Free Radic Biol Med *44*, 835-846.

Zielonka, J., Vasquez-Vivar, J., and Kalyanaraman, B. (2008b). Detection of 2-hydroxyethidium in cellular systems: a unique marker product of superoxide and hydroethidine. Nat Protoc *3*, 8-21.

ACKNOWLEDGEMENTS

I would like to thank all people that have helped me during these years, for making the way challenging, enjoyable and unforgettable.

Prof. Adriano Aguzzi for the excellent guidance, for keeping the motivation high when it dropped, for the time he has invested with us writing the papers and in supervising this project. I am very grateful for all the challenges I have been given not only project-wise but also in collaborations, supervising students, attending meetings, writing reports and so on, because all of that made this journey a great experience.

Prof. Dr. Christian Münz and Prof. Lawrence Rajendran for generously agreeing to take part in my PhD Committee and for their support during these years.

My deepest gratitude to my collaborators:

- Dr. Jeppe Falsig for the years we have worked together, for the fruitful discussions, and for representing one of the people I have learned the most from.
- Regina Reimann for her crucial contribution to this project and for being of great support until the end.
- Dr. Tracy O'Connor for believing in and supporting this project, for her critical revisions and for her charismatic personality.
- Dr. Simone Hornemann for her fundamental expertise for this research and for helpful discussions.
- Sine Yaganoglu for her contribution to the project during her master thesis and afterwards, for being a great help any time I have needed, for the pleasant discussions about the project, for giving me many critical insights while writing this thesis, for her friendship and the enjoyable moments.
- Dr. Pravas Baral, Barbara Wieland, Mridula Swayampakula, Prof. Nat Kav, Prof. Pawel P. Liberski and Prof. Michael James, Bei Li and Uli S. Herrmann for their positive encouragements and their collaboration.

I am indebted to Dr. Agnes Lau for correcting and revising this thesis, for productive discussions and for the good laughs.

I would like to acknowledge the current and former members of the lab who I have gotten to know as outstanding scientists with great personalities and who have definitely made my years here even more valuable. In particular I would like to thank Dr. Veronika Kana, Paolo Dametto, Dino Saban, Heike Fischer, Dr. Jana Sponarova, Dr. Alzbeta Trancikova, Badmavady Segarane, Mario Hermann and Dr. Gitta Seleznik for their help in the lab and productive discussions, for their friendship, the wonderful travels together and the great fun. Dr. Cinzia Tiberi and Dr. Daiji Sakata for creating a positive atmosphere in the office. Dr. Tory Johnson, Alexander Küffer and Arlind Adili for their sharp humor. Mario Nuvolone, Dr. Frank Baumann, Dr. Anna Maria Calella, Dr. Annika Keller, Dr. Sergey Yakushev, Dr. Silvia Sorce and

Dr. Caihong Zhu for valuable discussions and constructive criticisms. Flavio Vasella, Samuel Nobs and Erlend Hansen for their short internships working with me and the good times. Karl Frontzek for translating the summary of my thesis.

I would like to express my warmest thanks to Ahmet Varol, Petra Schwarz, Clemence Tournaire, Delic Mirzet and Rita Moos for their excellent technical and animal assistance and their support; especially Karina Arroyo for a lot of enjoyable moments also outside the lab and Laura Varrica and Jay Tracy for keeping me happy with many little surprises. Also, Norbert Wey for his computer technical support.

My most sincere thanks to Dr. Stefan Schauer from the Functional Genomics Center of Zürich (FGCZ) for helping me with the SPR measurements and for significant inputs.

I would like to express my appreciation to the PhD program of neuroscience of Zürich (ZNZ) and the University of Zürich for the large offer of high-standard educational events.

I am very grateful to Prof. Andrea Vasella for guiding my steps from chemistry to biology and for his enthusiastic and inspirational mentoring.

Finally, I should not forget to thank my friends Anna Devigili, Marco Devigili, Dr. Katja Chiesa, Dr. Cecilia Mondelli and Dr. Oliver Floegel that have represented my family here in Zürich and my friends in Sicily that even after so many years are still so close and caring.

I would like to dedicate the work of this thesis to my mother, my father and my sister for their support and unconditioned love, for all their efforts and they encouragements. Finally, I am profoundly grateful to Dr. Gildas Deniau for his patience, his love, his great support, for having accompanied me over these years, and because I don’t remember an unhappy day he did not turn into a happy one or a difficult moment when he was not there.

CURRİCULUM VİTAE

Personal Data

First name: *Tiziana*
Last name: *Sonati*
Date of birth: *21.04.1982*
Citizenship: *Italian*

Education and Training

2008-present	**Institute of Neuropathology, University Hospital, Zürich, Switzerland** PhD thesis. Research Advisor: Professor Adriano Aguzzi Research Title: Structural and molecular determinants of prion pathogenesis
2007	**Swiss Federal Institute of Technology (ETH), Zürich, Switzerland** Post-graduate research associate. Research Advisor: Prof. Andrea Vasella
January-June	Research Title: New Method for the Synthesis of 6-substituted Pteridinones, *via* 1, 3-dipolar nitrone cycloadditions. Italian State scholarship "*corso di perfezionamento all'estero*".
July-December	Research Title: Synthesis of backbone-base-integrating oligonucleotides. Financially supported by ETH.
July 2006	**Pharmacist qualification**

March 2006	**Master's degree in Pharmaceutical Chemistry and Technology**. **University of Palermo**, Faculty of Pharmacy, Italy (*with Highest Honours*). Thesis title: Synthesis of bis(3-*N*-methylindolyl) pyrroles, similar to marine alkaloid *Nortopsentina*. (in the medical chemistry laboratory at University of Palermo)
2005	Professional training, Pharmacy S. Michele, Palermo
1995-2000	**Scientific secondary school G.Galilei, Palermo**. (Final mark: 96 /100).

Publications

Steinlin T, **Sonati T**, Vasella A. **Synthesis and Reactivity in [3+2] Cycloadditions of Isoxanthopterin *N(5)*-Oxides –A New Synthesis of 6-Substituted Pteridinediones.** Helvetica Chimica Acta, 91, 10, 1879-1887, (2008).

Margalith I, Suter C, Ballmer B, Schwarz P, Tiberi C, **Sonati T**, Falsig J, Nyström S, Hammarström P, Aslund A, Nilsson KP, Yam A, Whitters E, Hornemann S, Aguzzi A. **Polythiophenes inhibit prion propagation by stabilizing prion protein (PrP) aggregates.** J Biol Chem. (2012) 287(23):18872-87.

Falsig, J, **Sonati, T,** Herrmann, US, Saban, D, Li, B, Arroyo, K, Ballmer, B, Liberski, PP, and Aguzzi, A (2012). **Prion pathogenesis is faithfully reproduced in cerebellar organotypic slice cultures.** PLoS Pathog *8*, e1002985.

Sonati T*, Reimann RR*, Falsig J*, Baral PK, O'Connor T, Hornemann S, Yaganoglu S, Sorce S, Li B, Herrmann US, Wieland B, Swayampakula M, Rahman MH, Das D, Kav N, Riek R, Liberski PP, James MNG, Aguzzi A. **The toxicity of antiprion antibodies is mediated by the flexible tail of the prion protein.** *Nature In press* (2013).

Reimann R*, **Sonati T***, Hornemann S, and Aguzzi A. Comment on "PrP Antibodies Do Not Trigger Mouse Hippocampal Neuron Apoptosis". *Submitted* (2013).

**equal contribution*